Identifying Regulators of Tumor Vascular Morphology

Identifizierung von Regulatoren der Tumorgefäßmorphologie

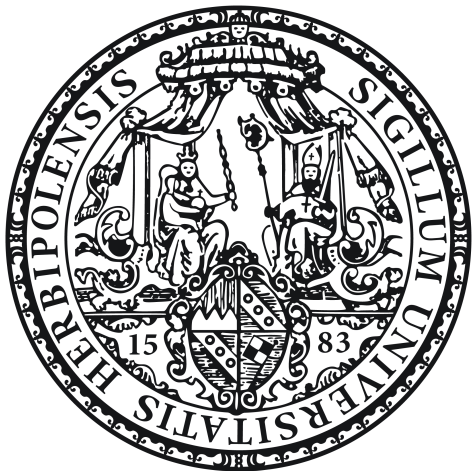

Doctoral thesis for a doctoral degree
at the Graduate School of Life Sciences,
Julius-Maximilians-Universität Würzburg,
Section Biomedicine

submitted by
Helene Hoffmann

from
Nürnberg

Würzburg 2016

Mitglieder des Promotionskomitees

Vorsitzender:	Prof. Dr. Thomas Hünig
Erster Betreuer:	Dr. Erik Henke
Zweiter Betreuer:	Prof. Dr. Manfred Gessler
Dritter Betreuer:	Prof. Dr. Alexander Buchberger

Eingereicht am: _____

Bürostempel

Tag des Promotionskolloquiums:

Doktorurkunden ausgehändigt am:

Contents

List of Figures

List of Tables

List of Abbreviations

AB-complex	Avidin-biotin complex
ACTB	Beta-actin
ALK	Activin receptor-like kinase
Angpt	Angiopoietin
bHLH	Basic helix-loop-helix
B2M	β-2-microglobulin
BSA	Bovine serum albumin
BW	Body weight
CAIX	Carbonic anhydrase IX
CAF	Carcinoma-associated fibroblast
CD	Cluster of differentiation
CDH1	E-cadherin
CDH2	N-cadherin
DAB	3,3'-Diaminobenzidine
Dll4	Delta-like-4
DMEM	Dulbecco's Modified Eagle's Medium
DMSO	Dimethylsulfoxide
EBM	Endothelial basal Medium
EC	Endothelial cell
EDTA	Ethylenediaminetetraacetic acid
EGF	Epidermal growth factor
EGFR	Epidermal growth factor receptor
EGM	Endothelial growth Medium
EMT	Epithelial to mesenchymal transition
EndMT	Endothelial to mesenchymal transition
EPC	Endothelial progenitor cells
ER	Estrogen receptor

FCS	Fetal calf serum
FDA	Food and Drug Administration
FF	Flash frozen
FGF	Fibroblast growth factor
FFPE	Formalin fixed paraffin embedded
fl	Floxed
FSP	Fibroblast secreted protein
fwd	Forward
GLUT-1	Glucose transporter-1
GSK	Glycogen-synthase kinase
HER	Human epidermal growth factor receptor
HGF	Hepatocyte growth factor
HIF	Hypoxia-inducible factor
HRP	Horseradish Peroxidase
HUVEC	Human umbilical cord endothelial cells
ID	Inhibitor of DNA binding
IDC	Infiltrating ductal carcinoma
IFN	Interferon
IGF	Insulin-like growth factor
IL	Interleukin
IRS	Immunoreactive score
IVT	In vitro transcription
LEF	Lymphoid enhancer factor
LLC	Lewis lung carcinoma
LMD	Laser microdissection
MESEC	Mouse embryonic stem cell-derived endothelial cell
MVD	Microvessel density
NES	Nuclear export signal
NGS	Normal goat serum
PAP	Peroxidase-antiperoxidase
PBS	Phosphate buffered saline
PCR	Polymerase chain reaction
PDGF	Platelet-derived growth factor
PDGFR	Platelet-derived growth factor receptor

PlGF	Placental growth factor
PPS	Polyphenylene sulfide
PR	Progesterone receptor
P/S	Penicillin/Streptomycin
SDS	Sodium dodecyl sulfate
RT	Room temperature
RTK	Receptor tyrosine kinase
RTKI	Receptor tyrosine kinase inhibitors
rv	Reverse
SEM	Standard error the of mean
SD	Standard deviation
SDF	Stromal-cell derived derived growth factor
SERM	Selective estrogen-receptor modulator
SMA	Smooth muscle actin
TCF	T-cell factor
TGF	Transforming growth factor
Th1	Type 1 T helper
TME	Tumor microenvironment
TSP	Thrombospondin
VE	Vascular endothelial
VEGF	Vascular endothelial growth factor
wt	Wild-type
ZEMM	Center for experimental molecular medicine
ZO	Zona occludens

1 Introduction

1.1 Structure and formation of the vasculature

1.1.1 Structure of blood vessels

Blood vessels are essential for the supply of organs with nutrients and oxygen while removing waste products and carbon dioxide. Larger veins and arteries are made up of three layers or tunics. The *tunica intima*, which is composed of endothelial cells (ECs), is the innermost layer and surrounds the lumen. The *tunica media* is a muscular and connective tissue layer, which consists of smooth muscle cells and elastic fibers (Popescu et al., 2013). The outside of vessels is covered by the *tunica adventitia*, which consists of fibrous connective tissue, adipose tissue and cells such as fibroblasts and macrophages (Grant and Twigg, 2013). As shown in Fig. 1.1, in microvessels (capillaries, venules and arterioles) the layer of endothelial cells is covered by a layer of perivascular cells, such as pericytes and smooth muscle cells (reviewed in Armulik et al., 2011).

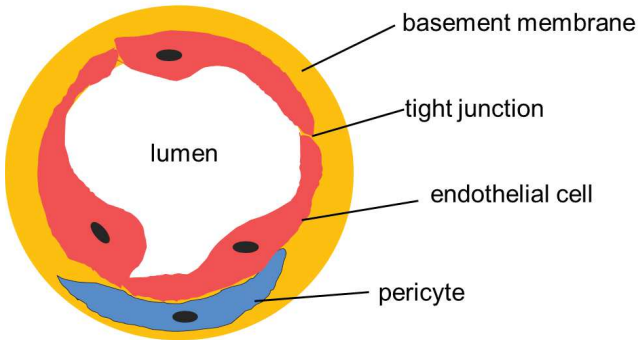

Figure 1.1: Cross-sectional diagram of a blood vessel. *The lumen is lined by a single layer of endothelial cells, which interact with pericytes within the basement membrane.*

1.1.2 Pericytes

Pericytes are essential for the structure and development of microvessels. Embedded within the vascular basement membrane (Fig. 1.1), they are able to establish focal contacts with endothelial cells via different mechanisms (reviewed in Armulik, 2005). The term pericyte denotes a very diverse cell type. While several markers for the detection of pericytes exist, none of them is specific or recognizes all types or states of pericytes (reviewed in Armulik et al., 2011). The proximity of endothelial cells and pericytes suggest an interaction among them. Various molecules, such as platelet-derived growth factor (PDGF) B, transforming growth factor β (TGFβ) and angiopoietins (Angpt1 and Angpt2) are involved in this interplay (Boscolo et al., 2013). Recruitment of pericytes to sites of sprouting is induced via PDGF-B/PDGFR-β signaling. Pericytes express the PDGF-β receptor, which detects PDGF-B released by endothelial cells during angiogenesis (Lindahl et al., 1997).
Perivascular cells express the angiogenic factor Angpt1 which is the ligand of the Tie2 receptor (Davis et al., 1996). The receptor tyrosine kinase Tie2 is primarily found on endothelial cells and is necessary for normal development of the vasculature (Dumont et al., 1992, 1994).
Transforming growth factor β is thought to play a key role in perciyte differentiation and proliferation (reviewed in Armulik et al., 2011). This growth factor signals via complexes of type I and type II receptors (reviewed in Lebrin et al., 2005). Endothelial cells express two different type I receptors, activin receptor-like kinase 1 and 5 (ALK1 and 5). Whereas ALK5 is broadly expressed, ALK1 is restricted to endothelial cells (Valdimarsdottir et al., 2006). Interestingly these two receptors trigger opposite events. In endothelial cells activation of ALK5 inhibits migration and proliferation, while activation of ALK1 increases migration and proliferation (Goumans et al., 2002).

1.1.3 Formation of blood vessels

There are two different mechanisms of blood vessel formation. Vasculogenesis usually occurs early during embryonic development and denotes the formation of new blood vessels from mesoderm-derived endothelial precursor cells, called angioblasts (reviewed in Ferguson et al., 2005 and Eilken and Adams, 2010). The second mechanism is angiogenesis. Here the vascular network expands from pre-existing small vessels by sprouting (reviewed in Eilken and Adams, 2010). In this complex process, vascular endothelial

growth factor A (VEGF-A), plays a major role (Ferrara and Henzel, 1989; Leung et al., 1989). Tip cells lead the growing sprout towards a spatial VEGF-A gradient (Gerhardt et al., 2003). Tip cell formation is regulated by the Delta-like-4 (Dll4)-Notch signaling pathway (Hellström et al., 2007; Siekmann and Lawson, 2007). Elongation of the sprout is then either achieved via proliferation (Gerhardt et al., 2003) or migration of endothelial cells (Siekmann and Lawson, 2007). Once tip cells encounter existing capillaries, migration stops and contacts between endothelial cells need to be established. Finally a vascular lumen is formed to enable blood flow (reviewed in Adams and Alitalo, 2007).
Sprouting angiogenesis is regulated by a balance of pro- and anti-angiogenic signals (Gerhardt et al., 2003). Inducers of angiogenesis are VEGF, fibroblast growth factor-2 (FGF-2), TGFβ, PDGF and Interleukin-8 (IL-8) (reviewed in Hanahan and Folkman, 1996). These elicitors are opposed by endogenous inhibitors of angiogenesis. Thrombospondin-1 (TSP-1) was found to inhibit neovascularization by blocking endothelial cell migration (Good et al., 1990). Another inhibitor derived from the extracellular matrix is endostatin, a fragment of type 18 collagen (O'Reilly et al., 1997). Angiostatin, which inhibits proliferation of endothelial cells, contains a fragment of Plasminogen, a blood coagulation factor, and is released by proteolysis (O'Reilly et al., 1994).

1.1.4 Vascular endothelial growth factor

VEGF-A, often only referred to as VEGF, belongs to a protein family, which consists of VEGF-A, VEGF-B, VEGF-C, VEGF-D, VEGF-E and placental growth factor (PlGF) (Meyer et al., 1999). Ferrara provides an overview of the VEGF protein family, focusing on VEGF-A (Ferrara, 2004, 2009). The members of this family bind to three different tyrosine kinase receptors (RTKs), termed VEGFR-1, VEGFR-2 and VEGFR-3 (Fig. 1.2). RTKs are transmembrane proteins with extracellular ligand binding domains and intracellular kinase domains. Once the ligand binds, the RTKs undergo dimerization and autophosphorylation, initiating a cascade of downstream signaling. VEGFR-1 and VEGFR-2 are primarily located on vascular endothelial cells, monocytes, macrophages and hematopoietic stem cells, while VEGFR-3 is found on the lymphatic endothelium (reviewed in Ferrara, 2009). As VEGF-C and -D are the primary ligands for VEGFR-3 they regulate lymphatic angiogenesis (Kukk et al., 1996;

Achen et al., 1998). While VEGF-A binds both VEGFR-1 and VEGFR-2, its affinity for VEGFR-1 is higher (Terman et al., 1992; Vries et al., 1992). Since it mediates signaling in ECs, VEGFR-2 plays an important role in angiogenesis, mitogenesis and vascular permeability (reviewed in Ferrara, 2004).

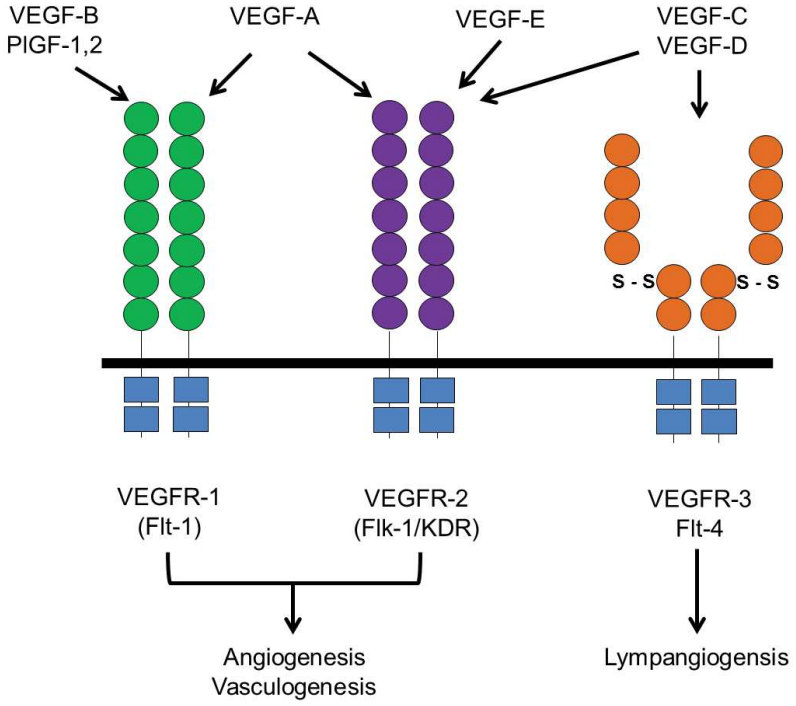

Figure 1.2: The VEGF family and their receptors. *This family consists of VEGF-A, VEGF-B, VEGF-C, VEGF-D, VEGF-E and PlGF. Each signaling molecule binds to its associated receptors, which then dimerize and are autophosphorylated. VEGF: vascular endothelial growth factor; PlGF: placental growth factor; (Adapted from Hicklin and Ellis, 2005)*

In case of hypoxia the intracellular concentration of hypoxia-inducible factor 1α (HIF-1α) increases. This oxygen-sensitive transcription factor is a key regulator of angiogenesis. HIF-1 activates the transcription of multiple angiogenic growth factors such as Angpt1 and Angpt2, PlGF, PDGFB and also VEGF-A (Kelly et al., 2003). The released VEGF-A attracts endothelial progenitor cells needed for vessel growth (Forsythe et al., 1996; Ozaki et al., 1999). VEGFR-1 is mainly involved in hematopoiesis and the recruitment of bone-marrow derived cells such as monocytes (Gerber et al., 2002; Hattori et al., 2002). PlGF and VEGF-B bind selectively to this receptor (Olofsson et al., 1998; Park et al., 1994). VEGF-E (VEGF-ORFV) is a homolog to VEGF-A and was found in the NZ2 strain of the parapoxvirus orf virus (Lyttle et al., 1994). VEGF-E has

some features similar to VEGF-A. It is able to induce angiogenesis, vascular permeability and proliferation and chemotactic migration of ECs. VEGF-E binds exclusively to VEGFR-2 (Wise et al., 1999; Meyer et al., 1999). In many human tumors, including those of the breast, high levels of VEGF-A mRNA are found. However, VEGF-A expression seems to differ not only between tumor types but is also heterogeneous within a single tumor (Brown et al., 1995; reviewed in Ferrara, 2004). Thereby, expression of VEGF-A appears to be upregulated in regions which are presumably hypoxic as they are close to sites of necrosis (Shweiki et al., 1992).

1.2 Tumor vasculature

1.2.1 Structure of vessels in tumors

Tumors, like normal tissues, depend on angiogenesis to survive and grow (Folkman, 1971). Gimbrone et al. examined angiogenesis in tumors implanted in the cornea of rabbits, which is an avascular tissue. They observed neovascularization originating from the limbus of the host, that started once tumors expanded (Gimbrone et al., 1974). The hypothesis that diffusible angiogenic molecules are involved in sprouting angiogenesis, was further supported by studies in transgenic mouse models. These studies led to the assumption that angiogenesis is triggered early during tumorigenesis by a mechanism named angiogenic switch (reviewed in Hanahan and Folkman, 1996). This switch might be activated by an increased production of inducers of angiogenesis such as VEGF, FGF-2, TGFβ, PDGF and IL-8, leading to a shift in the former balance of pro- and anti-angiogenic factors (Fig. 1.3). Downregulation of endogenous inhibitors of angiogenesis might also lead to an imbalance (reviewed in Ribatti et al., 2006 and in Hanahan and Folkman, 1996). The vasculature observed in tumors differs greatly from that of normal tissues. In solid tumors, vessels do not branch hierarchically and the vasculature is considered chaotic. The vessels are heterogeneous in shape and size, tortuous with excessive branching, arterio-venous shunts and blind ends (Baluk et al., 2005; Brown and Giaccia, 1998). In addition, vessels are dilated and micro vessel density is reduced (Dewhirst et al., 1989). Consequently, tumor blood flow is variable and leads to hypoxia (Brown and Giaccia, 1998). Another characteristic of tumor vessels is their leakiness. This is due to openings in the EC mono layer in which many of the ECs appear abnormal (Hashizume et al., 2000).

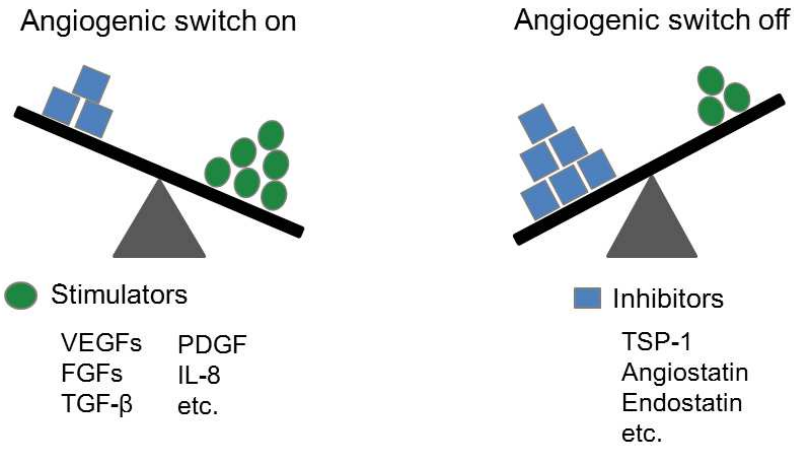

Figure 1.3: The angiogenic switch is regulated by a balance of pro- and anti-angiogenic factors. *Tumor angiogenesis is triggered by an increased production of angiogenic stimulators or a decrease in inhibitors. VEGF: Vascular endothelial growth factor; FGF: Fibroblast growth factor; TGFβ: Transforming growth factor-β; IL-8: Interleukin-8; TSP-1: Thrombospondin-1; (Adapted from Hanahan and Folkman, 1996)*

In addition, pericytes found on tumor vessels differ from those on vessels in other tissues. Studies show varying pericyte coverage, depending on tumor type and marker used for pericyte detection (Benjamin et al., 1999; Eberhard et al., 2000; Morikawa et al., 2002). Pericytes on tumor vessels show morphological abnormalities and are only loosely associated with ECs (Morikawa et al., 2002). These abnormalities seem to be related to PDGF signaling, which is important for pericyte recruitment and their integration into the vessel wall (Abramsson et al., 2003). Interestingly, VEGF-A seems to inhibit vessel maturation by ablation of pericyte coverage of nascent vascular sprouts (Greenberg et al., 2008). Finally, Angpt2, an endogenous inhibitor of the Angpt1/Tie2 angiogenic axis, was shown to interfere with pericyte-EC interactions (Mazzieri et al., 2011).

1.2.2 Mechanisms of tumor vascularization

Tumor vascularization, however, is not restricted to sprouting angiogenesis. Vessels in tumors may originate from a variety of sources, such as vasculogenesis, co-option of pre-exsisting vessels, vasculogenic mimicry, mosaic vessels and intussusception (reviewed in Seftor et al., 2012). To date little is known about the importance and occurrence of each of these mechanisms. If tumors originate in vascularized tissues they may co-opt

host microvessels and grow along these (Holash et al., 1999; Döme et al., 2002). Under normal as well as pathologic conditions vessels can remodel fast via intussusceptive microvascular growth. Thereby columns of interstitial tissue are inserted into the lumen of pre-exisiting vessels, subdividing them (Caduff et al., 1986). This mechanism, through which the tumor can increase the density and complexity of its vascular network, has recently been elucidated in experimental tumors and termed inverse sprouting (Paku et al., 2011). Mosaic vessels may be formed if cancer cells become exposed to the vascular lumen either because ECs are shed or if proliferation of ECs cannot keep up with rapid vessels growth. Endothelial cells might also simply just loose their typical markers such as CD31/CD105 (Chang et al., 2000).

In 1997, Asahara et al. isolated bone marrow derived endothelial progenitor cells (EPCs) from human peripheral blood (Asahara et al., 1997). The differentiation of EPCs into ECs is called postnatal vasculogenesis. During this process EPCs are recruited to angiogenic sites and incorporate into evolving vessels, where they proliferate and differentiate into ECs (reviewed in Ribatti, 2004). It is hypothesized that once EPCs have been recruited, they also contribute to the tumor endothelium by paracrine secretion of angiogenic factors (reviewed in Urbich and Dimmeler, 2004). However, it remains controversial to which extent EPCs contribute to postnatal vasculogenesis. Lyden et al. used Id-mutant mice, which are unable to perform neo-angiogenesis, and transplanted them with wild-type bone marrow or VEGF-mobilized stem cells. They found a high incorporation of EPCs into tumor vessels (Lyden et al., 1999, 2001). Other researchers, such as Rajantie et al., found only a low integration of EPCs into the tumor's vasculature. They investigated the incorporation of EPCs using chimeric mice reconstituted with genetically marked bone marrow(Rajantie et al., 2004). These discrepancies might be caused by the use of different methods for the quantification of EPCs and the lack of specific markers for the detection of this particular cell population (reviewed in Moschetta et al., 2014 and in Patenaude et al., 2010).

An alternate way of generating a blood supply is vascular mimicry, which was first discovered in aggressive melanoma. In this process cancer cells make up perfusable, patterned vessels which are not lined by endothelium (Maniotis et al., 1999). Later vascular mimicry was discovered in carcinomas, sarcomas and gliomas (reviewed in Hendrix et al., 2003).

1.3 Breast cancer

Of the 14.1 million cases of cancer worldwide 6.7 million cases occurred in women in 2012. With 1.7 million cases, breast cancer was the most frequently diagnosed cancer in women. Due to improvements in breast cancer treatment and early detection, there has been a decline in mortality of about 34% from 1990 to 2010 (American Cancer Society, 2013). Yet 522,000 breast cancer related deaths occurred in 2012 (Ferlay et al., 2013). Because of its cellular and molecular heterogeneity breast cancer is no longer considered as one disease but is classified into subgroups. This division is based on biological markers, such as the presence or absence of estrogen receptor (ER+ / ER-), progesterone receptor (PR+ / PR-) and human epidermal growth factor receptor (HER2+ / HER2-). Differences in gene expression patterns between different breast cancers have also been identified. Thus at least five major subtypes have been established: luminal A, luminal B, basal-like, HER2-enriched and normal-like (Tab. 1.1) (Sørlie et al., 2001; Perou et al., 2000).

Table 1.1: Major breast cancer subtypes (American Cancer Society, 2013). *ER: estrogen receptor, HER2: human epidermal growth factor receptor 2, PR: progesterone receptor*

Subtype	Tumors tend to be	prevalence (approx.)
Luminal A	ER+, PR+, HER2-	40%
Luminal B	ER+, PR+, HER2+	10% - 20%
Triple negative / Basal-like	ER-, PR-, HER2-	10% - 20%
HER2-enriched	ER-, PR-, HER2+	10%

Perou and Børresen-Dale provides an overview of the intrinsic subtypes of breast cancer (Perou and Børresen-Dale, 2011). The majority of breast cancers are ER+, showing an expression pattern that reminds of the luminal epithelial components of the breast (Perou et al., 2000). ER positive tumors make up the two luminal subtypes with luminal A being the most common (about 40%). These tumors generally have a high expression of ER and PR, and a low expression of HER2. They tend to grow slowly and are less aggressive than other subtypes (American Cancer Society, 2013; reviewed in Perou and Børresen-Dale, 2011).

About 10% to 20% of breast cancers are classified as luminal B (Carey et al., 2006). Most of them are ER and / or PR positive. The expression of HER2 or of the prolif-

erative biomarker Ki67 distinguishes them from the luminal A subtype (Cheang et al., 2009).
The majority of ER-negative tumors are either basal-like (10%-20%) or HER2 enriched (about 10%) (Carey et al., 2006). Basal-like breast cancers are also called triple-negative as most of them are ER, PR and HER2 negative. The term basal-like is based on the expression of cytokeratins 5, 6, 14 and 17, which are expressed within basal epithelial cells of the skin and airways. This type of breast cancer is more common in women carrying a mutation in *BRCA1* (reviewed in Perou and Børresen-Dale, 2011). As there is no targeted therapy for basal-like tumors, patients have a poorer short-term prognosis (American Cancer Society, 2013).
HER2 enriched breast tumors do not express hormone receptors but produce excess HER2 also known as HER2/neu or ErbB2. This subtype is characterized by low expression of the luminal and the basal-like gene clusters (reviewed in Perou and Børresen-Dale, 2011).

1.4 Breast cancer therapy

Conducting surgery is the standard procedure in breast cancer patients. In the US, 93% of women diagnosed with early stage breast cancer have either breast conserving surgery or mastectomy. At later stages the rate of surgery declines to 75% and the number of patients having mastectomy rises from 36% to 60%. Both types of surgery are usually accompanied by removal of regional lymph nodes to detect metastasis. In about 50% of cases surgery is followed by radiotherapy, which has been shown to reduce the risk of recurrence and of breast cancer related death (American Cancer Society, 2013). Systemic therapy such as endocrine therapy, chemotherapy and targeted therapy can be administered either before surgery (neoadjuvant) to shrink the tumor, or afterward (adjuvant) to remove remaining cancer cells.

1.4.1 Endocrine therapy

As the majority of breast cancers are ER positive, antiestrogen therapy is of great importance in breast cancer treatment. Today the standard treatment for this subgroup of patients involves either the estrogen inhibitor tamoxifen (Novaldex®, AstraZeneca) or aromatase inhibitors (reviewed in Chumsri et al., 2011 and in Jordan, 2003). Tamoxifen

is a selective estrogen-receptor modulator (SERM), which competes with estrogen for its receptors and inhibits the expression of estrogen regulated genes, eventually slowing cell proliferation (reviewed in Osborne, 1998). A newer estrogen receptor antagonist is fulvestrant (Faslodex®, AstraZeneca). This pure antiestrogen down-regulates the ER and shows no agonistic activity (Wakeling et al., 1991; Robertson et al., 2001). Fulvestrant may also serve as a second line treatment for patients who have developed tamoxifen resistence, as it lacks cross-resistence with tamoxifen (Wakeling et al., 1991; Howell et al., 2005). An alternative to SERMs are aromatase inhibitors such as anastrozole (Arimidex®, AstraZeneca), letrozole (Femara®, Novartis) and exemestane (Aromasin®, Pfizer). These drugs inhibit estrogen biosynthesis by binding the enzyme aromatase while exhibiting a greater efficacy compared to tamoxifen and showing less side effects (reviewed in Goss and Strasser-Weippl, 2004).

1.4.2 HER2 targeted therapy

The *HER2* gene, which has been found to be amplified in some mammary carcinomas, encodes an epidermal growth factor receptor-(EGFR)-related tyrosine kinase. This gene is a marker of overall survival as well as of relapse (Slamon et al., 1987). A monoclonal antibody, trastuzumab (Herceptin®, Genentech), is targeted directly at the HER2 extracellular domain (Carter et al., 1992). Trastuzumab acts via different molecular mechanisms. It suppresses growth and proliferation of cancer cells by reducing signaling via the PI3K/AKT and MAP kinase pathways, causes internalization and degradation of HER2, and attracts immune cells via antibody-dependent cellular toxicity (reviewed in Vu and Claret, 2012). A second monoclonal antibody to treat patients with HER2 positive breast cancer is pertuzumab (Perjeta®, Genentech). By binding a different part of HER2, pertuzumab inhibits receptor heterodimerization with other members of the EGFR family and thus restrains HER2 from functioning as a coreceptor (Franklin 2004).

1.4.3 Anti-angiogenic therapy

Folkman was the first to introduce the concept of anti-angiogenesis as he suggested starving a tumor by interfering with its blood supply (Folkman, 1971). The subsequent discovery and characterization of VEGF-A provided a potential target for this approach (Leung et al., 1989). In 2004, these discoveries led to the approval of the first

anti-angiogenic drug, bevacizumab (Avastin®, Genentech), a recombinant humanized anti-VEGF monoclonal antibody by the Food and Drug Administration (FDA). The approval was based on a phase III trial, which combined bevacizumab with the standard therapy for metastatic colorectal cancer, increasing overall survival from a median of 15.6 months to 20.3 months (Hurwitz et al., 2004). Four years later bevacizumab was approved for the treatment of HER2 negative metastatic breast cancer. Ductal mammary carcinomas show high VEGF expression, and the amount of VEGF protein is correlated with tumor micro vessel density (Toi et al., 1996). The first phase III trial for metastatic breast cancer compared treatment with either the chemotherapeutic capecitabine alone or in combination with bevacizumab in previously treated patients. While the objective response rate was increased, no effect on progression free survival or overall survival was observed (Miller et al., 2005). A later trial compared paclitaxel alone with paclitaxel plus bevacizumab as initial therapy. Combination therapy significantly prolonged progression free survival (11.8 months vs. 5.9 month) but not overall survival (Miller et al., 2007). In 2011 the FDA revoked the approval of the breast cancer indication for bevacizumab. While phase III trials showed a benefit for progression free survival, no improvement in overall survival or quality of life was observed (reviewed in Kümler et al., 2014). Another way to inhibit VEGF signaling is the use of receptor tyrosine kinase inhibitors (RTKIs) such as sunitinib (Sutent®, Pfizer), sorafenib (Nexavar®, Bayer), pazopanib (Votrient®, GlaxoSmithKline) and axitinib (Inlyta®, Pfizer). These small molecules target multiple RTKs including VEGFR-2, which is the major signaling receptor for VEGF mediated angiogenesis (reviewed in Ferrara, 2004). So far these RTKIs, whether combined with chemotherapy or used alone, did not improve overall survival in breast cancer (reviewed in Fakhrejahani and Toi, 2014).

In 2001, Jain gave an additional explanation for the effects of a blockade of VEGF, proposing a "normalization" of the tumor vasculature. Accordingly, pruning immature vessels by eliminating the excess VEGF could improve the delivery of therapeutics into the tumor (Jain, 2001). As described in Section 1.2, tumor blood vessels are functionally abnormal. Blood flow is chaotic, showing spatial and temporal heterogeneity, and thus preventing optimal drug delivery (Jain, 1998). It was observed that the inhibition of VEGF signaling not only impeded the growth of tumors and led to a decrease in vessel density but caused changes in vessel morphology, reducing vascular permeability and vessel diameter (Kim et al., 1993; Yuan et al., 1996). Vessels responding to

anti-VEGF treatment showed less endothelial fenestrations, disappearance of vascular sprouts and a cease of blood flow. Altogether, the phenotype of the remaining vessels appeared less abnormal (Inai et al., 2004). Interestingly this "normalization" seems to be temporal. During this period, oxygenation in tumor tissue improved as well as the tumor's response to radiation and chemotherapy (Winkler et al., 2004).
Dosing and type of chemotherapeutic, as well as molecular heterogeneity in breast cancer may have been involved in the failure to show an overall survival benefit for anti-angiogenic therapy. Selection of patients is challenging, as no reliable biomarkers predicting success of therapy are known. Furthermore angiogenesis is a complex process and inhibition of VEGF may trigger the production of other pro-angiogenic factors (reviewed in Kümler et al., 2014 and in Rugo, 2004). Thus tumors might rapidly become resistant to VEGF-ablation (reviewed in Bergers and Hanahan, 2008). Studies investigating use of bevacizumab in combination with other therapeutics are ongoing (NCT00625898, NCT01663727 and NCT00433511).

1.5 Metastasis

The majority of breast cancer deaths are not due to the primary tumor but to metastasis in distant organs. Within three years after detection of the primary tumor 10% to 15% of patients develop metastasis (reviewed in Weigelt et al., 2005). Common sites of metastasis in breast cancer patients are lungs, bones, lymph nodes or liver (Lee, 1983). Many years after resection of the primary tumor, metastasis at other distant sites might become apparent (Tarin, 2006).

1.5.1 Epithelial to mesenchymal transition

Metastasis is a multistep process, during which tumor cells have to invade the surrounding host tissue to reach the circulation and to be transported to distant sites. There they adhere to the capillary bed and extravasate into the surrounding parenchyma to form micrometastasis (reviewed in Weigelt et al., 2005). During invasion and intravasation, a process termed epithelial to mesenchymal transition (EMT) might play an important role. During this process polarized, adherent epithelial cells acquire a mesenchymal phenotype as they experience multiple biochemical changes (Fig. 1.4). These cells show enhanced migratory capacity and invasiveness and become resistant to apoptosis (reviewed in Lee et al., 2006). Originally the term EMT described a process occurring during embryogenesis (Type I EMT). For example, EMT is observed during the formation of the neural crest from the neural tube. Cells from the neural crest may then migrate and differentiate further (reviewed in Gumbiner, 2005). Type II EMT describes the transition of secondary epithelial cells to resident tissue fibroblasts due to inflammatory signals. This process is associated with organ fibrosis, wound healing and tissue regeneration (reviewed in Kalluri and Weinberg, 2009). Type III EMT appears in neoplastic cells, in which mutations in tumor suppressor genes and oncogenes occurred, enabling them to metastasize (reviewed in Kalluri and Weinberg, 2009). Interestingly, secondary tumors have a histopathology similar to the primary tumor. This indicates that EMT is followed by loss of mesenchymal characteristics in a reverse event termed mesenchymal to epithelial transition (Brabletz et al., 2001).

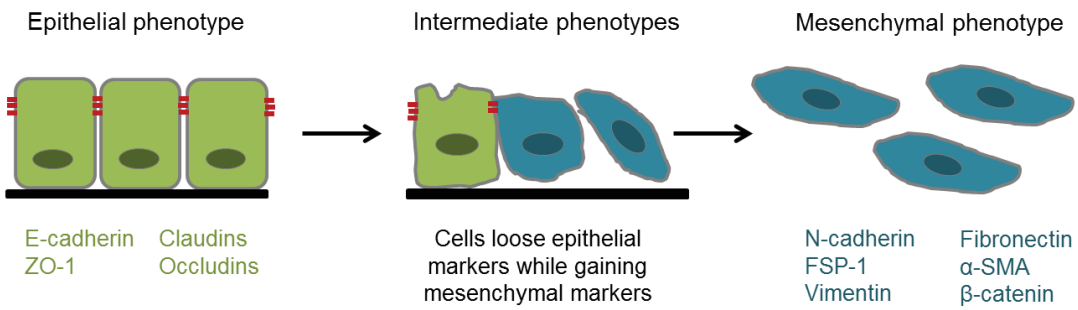

Figure 1.4: Epithelial to mesenchymal transition (EMT). *During EMT polarized, adherent epithelial cells experience multiple biochemical changes and acquire a mobile, mesenchymal phenotype. Common markers to identify both cells types are listed. ZO-1: Zona occludens-1; FSP-1: Fibroblast secreted protein-1; SMA: Smooth muscle actin. (Adapted from Kalluri and Weinberg, 2009).*

1.5.2 Biomarkers of EMT

Typically epithelia consist of a sheet of cells held together by cell-cell-junctions and cell-adhesions. E-cadherin (CDH1), which forms adherens junctions, is a prototypical surface marker of epithelial cells (Gumbiner et al., 1988). Loss of E-cadherin enhances invasiveness in human carcinoma cell lines (Frixen et al., 1991). Parallel to loss of E-cadherin, N-cadherin (CDH2) a marker for mesenchymal cells, is upregulated (reviewed in Hazan et al., 2004). This change has been termed cadherin switch and can be used to monitor the progress of EMT.

There are also a number of cytoskeletal markers of EMT, such as fibroblast secreted protein (FSP-1), vimentin, α-smooth muscle actin (SMA) and β-catenin. FSP-1 is a calcium-binding protein, which is expressed on carcinoma-associated fibroblasts (CAFs) and metastatic carcinoma cells (Xue et al., 2003; Egeblad et al., 2005). α-SMA is a member of the actin family and a marker for pericytes and smooth muscle cells (reviewed in Armulik, 2005). Vimentin, an intermediate filament, is expressed in various cells. In cancer cells its expression is positively correlated with increased invasiveness and metastasis (Raymond and Leong, 1989; Thompson et al., 1992; Hendrix et al., 1997). β-catenin is part of cell-cell adherens junctions, where it links cadherins to the cytoskeleton. If E-cadherin is downregulated, β-catenin is released, accumulates in the cytoplasm and can reach the nucleus. Here it functions as a regulatory protein, binding to a complex of lymphoid enhancer factor (LEF-1) and T-cell factor (TCF). The LEF-1/TCF complex stimulates the transcription of Wnt target genes and promotes

EMT (Behrens et al., 1996, Gilles et al., 2003, reviewed in Gottardi and Gumbiner, 2001). Fibronectin, a glycoprotein of the extracellular matrix, is also up-regulated during EMT (Park and Schwarzbauer, 2014).

1.5.3 Regulation of EMT/ the Snail family

There is an increasing number of known EMT inducers such as growth factors, constituents of the extracellular matrix, proteases and hypoxia (Zeisberg and Neilson, 2009). A key regulator of EMT is the SNAI1 transcriptional repressor, as it is a central convergence point for EMT-inducing factors. Nieto describes the organization of the Snail superfamily, to which SNAI1 belongs (Nieto, 2002). The Snail superfamily is subdivided into the two independent families Snail and Scratch. Vertebrates have three Snail members: SNAI1 (previously SNAIL), SNAI2 (previously SLUG) and SNAI3 (previously Smuc). The Snail family members encode transcription factors of the zinc-finger type (Fig. 1.5). Their highly conserved carboxy region contains

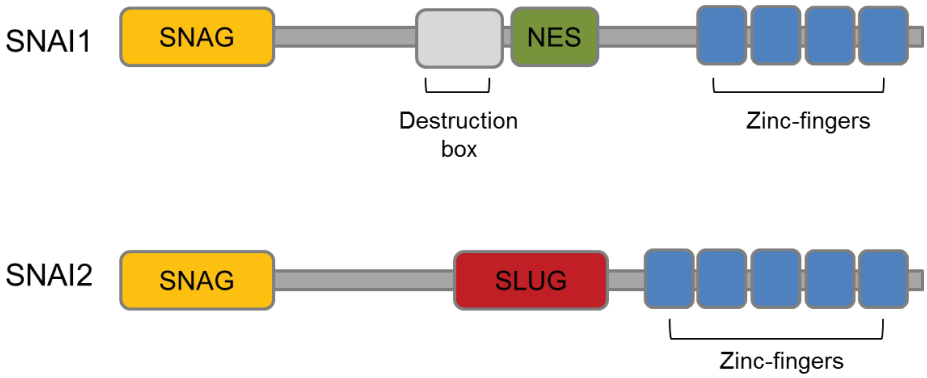

Figure 1.5: Scheme of the main structural domains in mammalian SNAI1 and SNAI2. *The SNAG repressor domain is located at the N-terminus, the C-terminal region contains four or five zinc-finger elements respectively. NES: nuclear export signal. (Adapted from Peinado et al., 2007).*

four to six zinc-finger elements, which serve as sequence specific DNA binding motifs (Barrallo-Gimeno and Nieto, 2005; reviewed in Nieto, 2002). Thus they are able to bind a motif identical to the E-box, which is also the consensus sequence of the binding site of basic-helix-loop-helix (bHLH) transcription factors (Mauhin et al., 1993). Another motif important for repressor activity is the highly conserved SNAG domain located at the N-terminus (reviewed in Nieto, 2002). SNAI2 contains an additional con-

served domain (SLUG), important for efficient repression (Molina-Ortiz et al., 2012). *Snai1* is a mesodermal determinant gene and in general regulates cell movement, adhesion, proliferation and death. It is also able to repress epithelial markers and to upregulate mesenchymal markers (Barrallo-Gimeno and Nieto, 2005). Activity and localization of SNAI1 are controlled via phosphorylation. One of the kinases involved is glycogen-synthase kinase 3β (GSK-3β), which maintains SNAI1 in an inactive state (Zhou et al., 2004; Yook et al., 2005), suggesting a cooperation between Snail-induced signaling pathways and Wnt-signaling (Barrallo-Gimeno and Nieto, 2005). SNAI1 and 2 are able to repress the transcription of E-cadherin via the E-box elements in the proximal E-cadherin-promotor and thus are direct repressors of E-cadherin (Batlle et al., 2000; Cano et al., 2000; Hajra et al., 2002). Consequently E-cadherin is not able to bind β-catenin and to form adherens junctions. SNAI1 is also able to down regulate other tight junction proteins such as Claudin-1, Occludin and Zona occludens (ZO-1) (Ohkubo and Ozawa, 2004; Ikenouchi et al., 2003). Specifically in breast cancer, repression of transcription of E-cadherin via SNAI2 seems of greater importance than via SNAI1 (Hajra et al., 2002). *Snai1* is expressed in all infiltrating ductal carcinomas (IDCs) with lymph node metastasis. Yet its expression is inversely correlated with the grade of differentiation of IDCs (Blanco et al., 2002). In contrast expression of *Snai2* increases with tumor grade (Martin et al., 2005).
Another elicitor of EMT is TWIST1 (Yang et al., 2004), a bHLH transcription factor, important for normal development and embryological morphogenesis. Twist1 can form dimers with other members of the HLH superfamily, which then bind to the E-cadherin promotor and repress E-cadherin transcription (Vesuna et al., 2008). In invasive breast carcinomas a higher *Twist1* expression than in normal breast tissue has been observed (Mironchik et al., 2005).

1.5.4 Endothelial to mesenchymal transition

Endothelial to mesenchymal transition (EndMT) was first observed during the development of the heart valves and is now considered a specialized form of EMT (Markwald et al., 1977). While both processes give rise to similar mesenchymal phenotypes and even seem to utilize common signaling pathways such as Notch and TGF-β, endothelial cells differ from epithelial cells. In the endothelium adherens junctions are formed by vascular endothelial (VE)-cadherin and a typical endothelial marker is CD31 (PECAM-

1). In addition the intermediate filament protein vimentin is abundant in endothelial cells (reviewed in Potenta et al., 2008). Recently it was revealed that EndMT also occurs in cancer and is an important source for the accumulation of cancer promoting carcinoma-associated fibroblasts (CAFs) (Zeisberg et al., 2007a). CAFs within the tumor stroma are thought to be involved in tumor progression, yet it was not clear where this type of fibroblast originates from (reviewed in Kalluri and Zeisberg, 2006). Interestingly there are hints that transcription factors of the Snail family are also involved in EndMT. For the formation of the endocardial cushion tissue in the chicken heart the transcription factor SNAI2, which is regulated via TGF-β2 signaling, is necessary (Romano and Runyan, 1999, 2000). Via Notch signaling, SNAI1 also seems to be involved in embryonic heart development by repressing the VE-cadherin promotor (Timmerman et al., 2004). In vitro knockdown of *Snai1* prevented EndMT induced by TGF-β2. Yet *Snai1* over expression was not sufficient to induce EndMT. While additional inhibition of GSK-3β allowed EndMT initiation (Medici et al., 2011).

1.6 Research aims

Tumor angiogenesis is stimulated by a multitude of growth factors and chemokines and is also influenced by the inflammatory microenvironment of the tumor. Variations in the tumor microenvironment result in diverse profiles of angiogenic factors and in differences in the stimulation of ECs, leading to diverse vessel phenotypes. Our research group hypothesized that the spectrum of vascular abnormalities observed in tumors is reflected in the expression profile of endothelial transcription factors. Inhibiting these transcription factors might be a promising way for angiogenic intervention and vascular re-engineering. Therefore we wanted to investigate the interdependence of tumor,-stroma- and immune cell-derived angiogenic factors, transcription factors and resulting vessel phenotypes. The objective of this thesis was to establish expression profiles of angiogenic factors in mammary carcinomas using a multi-step systemic approach. We also analyzed whether vessel phenotypes differ between subtypes (HER2-enriched, basal-like, luminal A and luminal B) of ductal mammary carcinomas. The acquired expression data of tumor cells was combined with the vessel phenotypes for correlation. Additionally we evaluated whether transcription factors that regulate EMT are interesting targets for vascular remodeling. As the SNAI1 transcriptional repressor is a key regulator of EMT, we examined the effect of vascular knockdown of *Snai1* in

murine cancer models.

2 Material

2.1 Primer

Primers were designed using Primer-Blast [1] and produced by Integrated DNA Technologies, Leuven, Belgium. In order to detect amplicons using the GenomeLab^{TM}GeXP Genetic Analysis System each primer contained a universal sequence (reverse: GTACGACTCACTATAGGGA, forward: AGGTGACACTATAGAATA).

Table 2.1: Primer for human genes.

Gene	Accession number	Primer	Sequence
ACTB	NM_333333	forward	5‘-CGAGCACAGAGCCTCGCCTTT-3’
		reverse	5‘-ACGAGCGCGGCGATATCATCA-3’
ANGPT1	NM_001146.3	forward	5‘-GACTGGGAAGGGAACCGAGCC-3’
		reverse	5‘-TCCTGCTGTCCCAGTGTGACCTT-3’
ANGPT2	NM_001118888.1	forward	5‘-AAAGACTGGGAAGGGAATGAGGCT-3’
		reverse	5‘-TCATTTCCTGGTTGGCTGATGCTGC-3’
B2M	NM_555555	forward	5‘-ACTTGTCTTTCAGCAAGGACTGGTC-3’
		reverse	5‘-TCCAATCCAAATGCGGCATCTTCA-3’
CD11B	NM_000632.3	forward	5‘-AGAAGAGCACACGGGATCGGCT-3’
		reverse	5‘-AAGACGGCGCGGGAATGTGG-3’
CD34	NM_001025109	forward	5‘-ACCGCGCTTTGCTTGCTGAGT-3’
		reverse	5‘-GTGCAGGCTGGTACTTCCAAGGG-3’
CD3D	NM_001040651.1	forward	5‘-CTCTCTGGCCTGGTACTGGCTACC-3’
		reverse	5‘-CCACCGTTCCCTCTACCCATGTGA-3’

Continued on next page

[1] http://www.ncbi.nlm.nih.gov/tools/primer-blast/

Table 2.1 – *Continued from previous page*

Gene	Accession number	Primer	Sequence
CD45	NM_080921.2	forward	5‘-CTTAGGGACACGGCTGACTTCCAGA-3’
		reverse	5‘-AGGCATCAGTGGGGGAAGGTGTTG-3’
CD68	NM_001040059.1	forward	5‘-TGCTCAGCTGCCCCACACAG-3’
		reverse	5‘-CCAGGGCGAGGAGGCCAAGAA-3’
CDH1	NM_004360.3	forward	5‘-CGCCCTGCCAATCCCGATG-3’
		reverse	5‘-GCAGCTTCGGAACCGCTTCCT-3’
CDH2	NM_001792.3	forward	5‘-CCCAAGGGGCTGAGCGGC-3’
		reverse	5‘-GCGGAGCCCCGTGATCTTGTT-3’
CDH5	NM_001795.3	forward	5‘-GACAAACCCCGCCCACAACG-3’
		reverse	5‘-GGGGTCTGTGGCCTCGACGAT-3’
COL6A1	NM_001848.2	forward	5‘-CCTGGAGACCCGGGGCTGAT-3’
		reverse	5‘-CTTGAGGCCGGGGTAGCCCT-3’
COL18A1	NM_030582.3	forward	5‘-GCCGGGAGATGCCAGCCTTG-3’
		reverse	5‘-GGGCGGCTGGACTCAGCAAA-3’
COUPTFII	NM_001145155.1	forward	5‘-CTCAGCCGAGTACAGCTGCCT-3’‘
		reverse	5‘-TCCGAATCTCGTCGGCTGGTT-3’‘
CTNNA1	NM_001903.2	forward	5‘-AAGCTTGGCCGCACCATTGC-3’
		reverse	5‘-CCTCGGCCTTGACCTTGCTGC-3’
EGF	NM_005429.2	forward	5‘-GATGTGAGGAGTCGCAGGCCT-3’‘
		reverse	5‘-CCCATCTGCTGCCTGGCCAT-3’‘
ERG	NM_182918.3	forward	5‘-GTCTCAACCCCCAGCCAGGGT-3’‘
		reverse	5‘-CGCCTTTGGCCACACTGCATT-3’‘
ESR1	NM_000125.3	forward	5‘-GGAAGAGCTGCCAGGCCTGC-3’
		reverse	5‘-CACCCCTGCCCTCCCCATCA-3’
ETS1	NM_001143820.1	forward	5‘-TCTCGAGCTGGCCCCAGACTT-3’
		reverse	5‘-CGGGATTCTGGATAGGCTGGGTT-3’‘
ETV1	NM_004956.4	forward	5‘-GGTCACCAATAGTCAGCGTGGGA-3’
		reverse	5‘-ACCTGAGCTTCTGCAAGCCATGT-3‘

Continued on next page

Table 2.1 – *Continued from previous page*

Gene	Accession number	Primer	Sequence
ETV4	NM_001986.2	forward	5‘-CCCTGTATGAACAGGCGGGCC-3‘
		reverse	5‘-ATTGATGCGCACCCGGTGACA-3‘
FGF-1	NM_000800.3	forward	5‘-TGAGGATCCTTCCGGATGGCA-3
		reverse	5‘-CGTCGGTGTCCATGGCCAAGTA-3
FGF-2	NM_002608.2	forward	5‘-CTTCCTGCGCATCCACCCCG-3‘
		reverse	5‘-AGCCAGGTAACGGTTAGCACACA-3‘
FLI1	NM_002017.3	forward	5‘-CCCCTTGGAGGGGCACAAACG-3‘
		reverse	5‘-CTGCCCGCTTCCAGGGTTGG-3‘
FN1	NM_002026.2	forward	5‘-CGCCCTGGTGTCACAGAGGCTA-3’
		reverse	5‘-TGGGGTGTGGAAGGGTTACCAG-3’
FOXC1	NM_001453.2	forward	5‘-ACTTCCACTCGGTGCGGGAGA-3‘
		reverse	5‘-GCTCCGGACGTGCGGTACAG-3‘
FOXC2	NM_005251.2	forward	5‘-CCGTCTCGGAAGCAGCATGCAGG-3‘
		reverse	5‘-CTGCCCGCAGCCCGGTAGT-3‘
FOXF1	NM_001451.2	forward	5‘-CGGCGCCTCTTATATCAAGCAGC-3‘
		reverse	5‘-CTGCGAGTGATACCGCGGGATG-3‘
FOXO1	NM_002015.3	forward	5‘-CAGCAACAGCTCGGCGGGCT-3‘
		reverse	5‘-CCCGCTCTTGCCACCCTCTGGAT
FOXO3	NM_201559.2	forward	5‘-TGGTGCGTTGCGTGCCCTAC-3‘
		reverse	5‘-GTTCCCTCATTCTGGACCCGCA-3‘
GATA1	NM_002049.3	forward	5‘-ATCCCCAAGGCGGCCGAAC-3‘
		reverse	5‘-TGGGGGAGGGGCTCTGAGGTC-3‘
GATA2	NM_032638.4	forward	5‘-CACCCCTAAGCAGCGCAGCAA-3‘
		reverse	5‘-GTAGTGGCCGGTGCCGTCCC-3‘
GATA3	NM_001002295.1	forward	5‘-GCCCCTCATTAAGCCCAAGCGA-3’
		reverse	5‘-GTCCCCATTGGCATTCCTCCTCC-3’
G-CSF	NM_000759.3	forward	5‘-GTGCCACCTACAAGCTGTGCCA-3’
		reverse	5‘-AGTTGGCTCAAGCAGCCTGC-3’

Continued on next page

Table 2.1 – *Continued from previous page*

Gene	Accession number	Primer	Sequence
GM-CSF	NM_00078.2	forward	5‘-GCCACTACAAGCAGCACTGCC-3’
		reverse	5‘-GGGGATGACAAGCAGAAAGTCCTTC-3’
GROb	NM_002089.3	forward	5‘-TCCTCCTTCCTTCTGGTCAGTTGGA-3’
		reverse	5‘-CCTGTAAGGGCAGGGCCTCCT-3’
GTF2I	NM_032999.2	forward	5‘-CGTTCCCTTCAAGCCACGAGGG-3‘
		reverse	5‘-ACGCGAACGGCACCTTCACA-3‘
HEY1	NM_012258.3	forward	5‘-GCTGCATACGGCAGGAGGGAAAG-3‘
		reverse	5‘-AGCGGGTCAGAGGCATCTAGTCC-3‘
HEY2	NM_012259.2	forward	5‘-AGAGAAAAGGCGTCGGGATCGGA-3‘
		reverse	5‘-ACCCCCTGTTGCCTGAAGCAT-3‘
HGF	NM_000601.4	forward	5‘-CAGCCCTGGAGTTCCATGATACCA-3‘
		reverse	5‘-GTCCCCCTTCTTCCCCTCGAGG-3‘
HOXA9	NM_152739.3	forward	5‘-GAGAAAAACAACCCAGCGAAGGCG-3‘
		reverse	5‘-GAGCGCGCATGAAGCCAGTT-3‘
HOXB3	NM_002146.4	forward	5‘-TGGGATCTGCAGAGTTCGGGCG-3‘
		reverse	5‘-CTTAGCCACCGACGAGGGGAGAA-3‘
HOXB5	NM_002147.3	forward	5‘-TCCCCTGGATGAGGAAGCTTCACAT-3‘
		reverse	5‘-GGCGATCTCGATGCGCCGTC-3‘
HOXD3	NM_006898.4	forward	5‘-GCTCCTCAGCCACCATCAGCAAG-3‘
		reverse	5‘-GTATGCCGTGCGTACCCGCTT-3‘
ID1	NM_002165.2	forward	5‘-GACCTTCAGTTGGAGCTGAACTCGG-3‘
		reverse	5‘-CCGCAGGAACGCATGCCGC-3‘
ID3	NM_002167.3	forward	5‘-CCACCCTGACTCGTTACCCCAGA-3‘
		reverse	5‘-GCAACCGTGCCGTCCCGTTG-3‘
IGJ	NM_144646.3	forward	5‘-GCTTTTCTGGGGAGTCCTGGCG-3’
		reverse	5‘-TGATCCTGGAAGTAATCCGGGCAC-3’
IL-2	NM_000586.3	forward	5‘-TCCCAAACTCACCAGGATGCTCAC-3’
		reverse	5‘-TAGCACTTCCTCCAGAGGTTTGAGT-3’

Continued on next page

Table 2.1 – *Continued from previous page*

Gene	Accession number	Primer	Sequence
IL-6	NM_000600.3	forward	5‘-ACAAGCCAGAGCTGTGCAGATGAG-3’
		reverse	5‘-GCTTCGTCAGCAGGCTGGCAT-3’
IL-8	NM_000584.3	forward	5‘-GTAAACATGACTTCCAAGCTGGCCG-3’
		reverse	5‘-TTAGCACTCCTTGGCAAAACTGCA-3’
IL-12A	NM_000882.3	forward	5‘-CCCAAAACCTGCTGAGGGCCG-3’
		reverse	5‘-AACAGGCCTCCACTGTGCTGG-3’
IP-10	NM_001565.3	forward	5‘-TTGTCCACGTGTTGAGATCATTGCT-3’
		reverse	5‘-GCACTGCATCGATTTTGCTCCCC-3’
KRT5	NM_000424.3	forward	5‘-GCTCATGAACACCAAGCTGGCC-3’
		reverse	5‘-TCCAGAGGAAACACTGCTTGTGACA-3’
KRT8	NM_002273.3	forward	5‘-CTGGAGGCGGAGCTTGGCA-3’
		reverse	5‘-GGCGAGACTCCAGCTCTACCTTGT-3’
KRT17	NM_000422.2	forward	5‘-GGTACCAGAGGCAGGCCCC-3’
		reverse	5‘-GTTGGCATTGTCCACGGTGGC-3’
KRT18	NM_000224.2	forward	5‘-AGATCATCGAGGACCTGAGGGCTCA-3’
		reverse	5‘-TGCGGAGCCCATGGATGTCGTT-3’
MCP-1	NM_002982.3	forward	5‘-TCATTCCCCAAGGGCTCGCTCA-3’
		reverse	5‘-TCGCGAGCCTCTGCACTGAGAT-3’
MEF2C	NM_002397.4	forward	5‘-AGCAACCCTGTCAGCTCACTGG-3’
		reverse	5‘-GGTGCCTGCACCAGACGTGAG-3‘
PBX1	NM_002585.2	forward	5‘-TTCTGGAGGGGCAGGTTCAGACAA-3‘
		reverse	5‘-CGTGGGTGGTGAACTCGTTGCA-3‘
PDGF-A	NM_002607.5	forward	5‘-GGACGCGATGAGGACCTTGGC-3‘
		reverse	5‘-CTCGATCACCTCGCGGGGGA-3‘
PDGF-B	NM_002608.2	forward	5‘-TCCCACTCTGGAGGCGAGCTG-3‘
		reverse	5‘-GGCGCCGGGAGATCTCGAAC-3‘
PDGFRB	NM_002609.3	forward	5‘-AGGGCCCACTGGAGGGTTCC-3‘
		reverse	5‘-TGGGGCTCTGGCTCTGGTTCG-3‘

Continued on next page

Table 2.1 – *Continued from previous page*

Gene	Accession number	Primer	Sequence
PLGF	NM_002632.4	forward	5‘-GCTTCCTGCAGCTCCTGGCC-3‘
		reverse	5‘-CTGCGGCCCCACACTTCCTG-3‘
RUNX1	NM_001122607.1	forward	5‘-TGAGCTGAGAAATGCTACCGCAGC-3‘
		reverse	5‘-GTGGTAGGTGGCGACTTGCGG-3‘
SDF1	NM_199168.3	forward	5‘-AACGCCAAGGTCGTGGTCGTG-3’
		reverse	5‘-GATGCTTGACGTTGGCTCTGGCAA-3’
SMA	NM_001141945.1	forward	5‘-GACGATGCTCCCAGGGCTGT-3’
		reverse	5‘-TGTGCTTCGTCACCCACGTAGC-3’
SNAI1	NM_005985.3	forward	5‘-CAGTGCCTCGACCACTATGCCG-3‘
		reverse	5‘-GATCTCCGGAGGTGGGATGGCT-3‘
SNAI2	NM_003068.3	forward	5‘-AGCCAAACTACAGCGAACTGGACAC-3‘
		reverse	5‘-TGGAGCAGCGGTAGTCCACACA-3‘
SOX17	NM_022454.3	forward	5‘-CGAGCCAAGGGCGAGTCCCGTAT-3‘
		reverse	5‘-GCGTCAGCGCCTTCCACGACT-3‘
SOX18	NM_018419.2	forward	5‘-GCAAAGGACGAGCGCAAGC-3‘
		reverse	5‘-CTCCGCCGCGTTCAGCT-3‘
TGFB1	NM_000660.4	forward	5‘-GCTGGAGAGGGCCCAGCATC-3‘
		reverse	5‘-ATGTACAGCTGCCGCACGCA-3‘
TSP1	NM_003246.2	forward	5‘-AGGAATGGACTGTTGATAGCTGCAC-3’
		reverse	5‘-TGTGGCATTGGAGCAGGGCA-3’
TWIST1	NM_000474.3	forward	5‘-TGCAGCTATGTGGCTCACGAG-3‘
		reverse	5‘-CTCTGGAAACAATGACATCTAGGTC-3‘
VEGF-A	NM_003376.5	forward	5‘-ATGCGGGGGCTGCTGCAATG-3‘
		reverse	5‘-TGTGCTGGCCTTGGTGAGGTTT-3‘
VEGF-B	NM_003377.3	forward	5‘-CGGGCACCATGAGCCCTCTG-3‘
		reverse	5‘-AGGGGCATCAGGCTGGGAGAC-3‘
VEGF-C	NM_005429.2	forward	5‘-ACCTGCCCCAGAAATCAACCCCT-3‘
		reverse	5‘-TGGCGGTTCGTACATGGCCG-3‘

Continued on next page

Table 2.1 – *Continued from previous page*

Gene	Accession number	Primer	Sequence
VEZF1	NM_007146.2	forward	5‘-GTGACAAGCTGGCCAGGGAAGC-3‘
		reverse	5‘-GTAGCAGCCGTGGAGGTTTGGC-3‘
VIM	NM_003380.3	forward	5‘-TGCCAAGAACCTGCAGGAGGCA-3’
		reverse	5‘-AGGTGAGGGACTGCACCTGTCT-3’
VWF	NM_000552.3	forward	5‘-GGGCTGCGATGTGTGCACCT-3’
		reverse	5‘-GGCAGGCACCTTCCACAGCA-3’
YB1	NM_004559.3	forward	5‘-TCGCAACGAAGGTTTTGGGAACA-3’
		reverse	5‘-TGCGAAGGTACTTCCTGGGGT-3‘
ZO-1	NM_175610.2	forward	5‘-GCCTGTCACCAGCGCGTCTC-3’
		reverse	5‘-GGAGGTGGGTCTGGTTTGGACA-3’

Table 2.2: Primer for mouse genes.

Gene	Accession number	Primer	Sequence
Ca9	NM_139305.2	forward	5‘-TTCCTTTCTCCTCGTTGGGC-3’
		reverse	5‘-TCCATTCAAGGTCGCTTAGTCC-3’
Glut-1	NM_011400.3	forward	5’-ATA GTT ACA GCG CGT CCG TT-3’
		reverse	5’TA GCC GAA CTG CAG TGA TCC-3’
Rsp29	NM_009093.2	forward	5’-GGTGCACCTCAGTACTGCTT-3’
		reverse	5’-ATGGGACAGCAACTGTTCGT-3’
Vegfa	NM_001287056.1	forward	5’-GGC CTC CGA AAC CAT GAA CT-3’
		reverse	5’-GT CCA CCA GGG TCT CAA TCG-3’

Table 2.3: Primer for genotyping.

Target	Primer	Sequence
Floxed Snai1	10079	5‘-CGGGCTTAGGTGTTTTCAGA-3’
	10080	5‘-CTTGCTTGGTACCTGCCTTC-3’
Cre transgene	oIMR1084	5’-GCGGTCTGGTAAAAACTATC-3‘
	oIMR1085	5’-GTGAAACAGCATTGCTGTCACTT-3‘

2.2 Antibodies

Table 2.4: Primary antibodies.

Name	Type	Dilution	Manufacturer
CD34	monoclonal, mouse	1:1000	Dako Deutschland GmbH, Hamburg, Germany
CD34	monoclonal, rat	1:50	Abcam, Cambridge, UK
Cre recombinase	monoclonal, mouse	1:250	Abcam, Cambridge, UK
PAP-complex	polyclonal, mouse	1:250	Dianova GmbH, Hamburg, Germany

Table 2.5: Secondary antibodies.

Name	Label	Dilution	Manufacturer
Goat-anti-mouse IgG	HRP	1:250	Jackson ImmunoResearch, Suffolk, UK
Goat-anti-rat IgG	HRP	1:2500	VECTOR Laboratories, Burlingame, CA, USA

2.3 Cell culture

Table 2.6: Human cell lines.

Name	Tissue	Manufacturer
HEK293T	kidney	ATCC, Wesel, Germany
HUVEC	umbilical vein/vascular endothelium	BD, Heidelberg, Germany
MCF-7	adenocarcinoma of mammary gland, breast	ATCC, Wesel, Germany
MDA-MB-231	adenocarcinoma of mammary gland/breast	ATCC, Wesel, Germany
MDA-MB-435s	previously described as: ductal carcinoma of mammary gland/breast	ATCC, Wesel, Germany

Table 2.7: Murine cell lines.

Name	Tissue	Manufacturer
B16-F10	melanoma of the skin	ATCC, Wesel, Germany
E0771	medullary breast adenocarcinoma	CH3 BioSystems, Amherst, NY, USA
LLC	lewis lung carcinoma	ATCC, Wesel, Germany

Table 2.8: Media, solutions and buffers for cell culture.

Name	Manufacturer
DMEM	Life Technologies, Darmstadt, Germany
EGM^{TM}-2 BulletKit^{TM}	LONZA, Basel, Switzerland
Fetal calf Serum	Life Technologies, Darmstadt, Germany
Penicillin/Streptomycin	Sigma-Aldrich,Munich, Germany
Phosphate Buffered Saline	Life Technologies, Darmstadt, Germany
Trypsin-EDTA-solution	Sigma-Aldrich, Munich, Germany
VascuLife® EnGS	Lifeline Cell Technology, Carlsbad, CA, USA

2.4 Mice

Table 2.9: Mice strains.

Strain	Manufacturer
C57BL/6	Provided by ZEMM
B6;129S-Snai1^{tm2Grid}/J	The Jackson Labratory, Bar Harbor, ME USA
B6.Cg-Tg(Cdh5-cre)7Mlia/J	The Jackson Labratory, Bar Harbor, ME USA

2.5 Reaction kits

Table 2.10: Reaction kits.

Name	Manufacturer
ADVANCE™HRP	Dako Deutschland GmbH, Hamburg, Germany
Agencourt® FormaPure® Kit	Beckman Coulter, Krefeld, Germany
DAB enhancing solution	VECTOR Laboratories, Burlingame, CA, USA
DNA Size Standard Kit- 400	Beckman Coulter, Krefeld, Germany
GenomeLab™GeXP Start Kit	Beckman Coulter, Krefeld, Germany
Liquid DAB+ Substrate Chromogen System	Dako Deutschland GmbH, Hamburg, Germany
KAPA Express Extract	PeqLab, Erlangen, Germany
NucleoSpin® FFPE RNA/DNA	Macherey-Nagel, Düren, Germany
peqGOLD Hot Start Mix S	PeqLab, Erlangen, Germany
QuickExtract™FFPE RNA Extraction Kit	Epicentre Technologies Corp., Chicago, IL, USA
RevertAid™First Strand cDNA Synthesis Kit	Thermo Scientific, Langenselbold, Germany
RNeasy FFPE Kit	Qiagen, Hilden, Germany
RNeasy Mini Kit	Qiagen, Hilden, Germany
RT^2 FFPE RNA Extraction kit	SABioscience, Frederick, MD, USA
Sensation Plus FFPE Amp	Affymetrix UK Ltd, High Wycombe, UK
VECTASTAIN ABC Kit	VECTOR Laboratories, Burlingame, CA, USA

2.6 Chemicals and reagents

Table 2.11: Chemicals and reagents.

Name	Manufacturer
2-Mercaptoethanol	Merck, Darmstadt, Germany
2-Propanol	Sigma-Aldrich, Munich, Germany
Agencourt®RNAClean®XP	Beckman Coulter, Krefeld, Germany
Aluminum sulfate	Merck, Darmstadt, Germany
Ammonium chloride	Merck, Darmstadt, Germany
Ammonium persulfate	Sigma-Aldrich, Munich, Germany
Antibody Diluent	Dako Deutschland GmbH, Hamburg, Germany
Auqa ad injectabilia	Delta Select, Pfullingen, Germany
Bovine serum albumin (BSA)	Roth, Karlsruhe, Germany
boric acid	Sigma–Aldrich, Munich, Germany
Bromophenol blue	Sigma–Aldrich, Munich, Germany
Citric acid	Sigma-Aldrich, Munich, Germany
Chloroform	Sigma-Aldrich, Munich, Germany
Dimethylsulfoxide	Roth, Karlsruhe, Germany
DNase I, RNase-free	Thermo Scientific, Langenselbold, Germany
Doxorubicin hydrochloride	medac GmbH, Hamburg
Ethanol	Sigma-Aldrich, Munich, Germany
GelRed®	Fermentas. St.Leonhardt, Germany
GenomeLab Separation Buffer	Beckman Coulter, Krefeld, Germany
Glucose	Sigma-Aldrich, Munich, Germany
Glucose oxidase type VII (Aspergillus niger)	Sigma-Aldrich, Munich, Germany

Continued on next page

Table 2.11 – *Continued from previous page*

Name	Manufacturer
Glycerol	Roth, Karlsruhe, Germany
Glycine	Merck, Darmstadt, Germany
Goat serum	Sigma-Aldrich, Munich, Germany
Hydrogen peroxide	Sigma-Aldrich, Munich, Germany
Maxima Hot Start Taq DNA polymerase	Thermo Scientific, Langenselbold, Germany
β–mercaptoethanol	Sigma-Aldrich, Munich, Germany
Methanol	Sigma-Aldrich, Munich, Germany
Mowiol	Thermo Scientific, Langenselbold, Germany
Nickel sulfate	Merck, Darmstadt, Germany
Nuclear fast red	Merck, Darmstadt, Germany
Paraformaldehyde	Sigma-Aldrich, Munich, Germany
peqGOLD Universal Agarose	PeqLab, Erlangen, Germany
Potassium chloride	Sigma-Aldrich, Munich, Germany
Potassium phosphate monobasic	Sigma-Aldrich, Munich, Germany
Propyl gallate	Sigma-Aldrich, Munich, Germany
Proteinase K Powder	Thermo Scientific, Langenselbold, Germany
Sodium citrate	Sigma-Aldrich, Munich, Germany
Sodium chloride	Sigma-Aldrich, Munich, Germany
Sodium dodecyl sulfate	Sigma-Aldrich, Munich, Germany
Sodium phosphate dibasic	Sigma-Aldrich, Munich, Germany
Sucrose	Sigma-Aldrich, Munich, Germany
Tissue – Tek O.C.T Compound	Miles Laboratories, Indiana, USA
Tris(hydroxymethyl)aminomethane	Merck, Darmstadt, Germany

Continued on next page

Table 2.11 – *Continued from previous page*

Name	Manufacturer
Tris-EDTA-Buffer (100x Concentrate)	Sigma-Aldrich, Munich, Germany
Triton-X-100	Sigma-Aldrich, Munich, Germany
Trizol	Invitrogen, Karlsruhe, Germany
Trypan blue solution 0.4%	Sigma-Aldrich, Munich, Germany
Xylol	Sigma-Aldrich, Munich, Germany

Table 2.12: Growth factors.

Name	Manufacturer
hEGF	MyBiosource, San Diego, CA USA
hFGFb	Invitrogen, Karlsruhe, Germany
hHGF	PreproTech, Hamburg, Germany
hIGF-1	PreproTech, Hamburg, Germany
hPDGF-BB	PreproTech, Hamburg, Germany
hSDF-1α	PreproTech, Hamburg, Germany
hVEGF	PreproTech, Hamburg, Germany

Table 2.13: Size markers and mass ladders.

Name	Manufacturer
100 bp DNA Ladder	Life Technologies, Darmstadt, Germany
Quantitas 10 kb Marker	Biozym Scientific, Hessisch Oldendorf Germany

2.7 Buffers and solutions

Ammonium chloride solution	3.3 M Ammonium chloride
Citrate buffer (10 mM)	9.9 ml 0.1 M Citric acid 45.1 ml 0.1 M Sodium citrate H_2O ad 500 ml
DAB-solution	67.5 ml Phosphate buffer 1.35 ml $NiSO_4$ 1.35 ml Glucose (10%) 150 µl NH_4Cl 1.5 ml DAB 225 µl Glucose oxidase
Loading buffer for agarose gel electrophoresis	0.1 M EDTA pH 6.8 50% Sucrose 1 spatula Bromphenol ad 100 ml H_2O
Lysis buffer for DNA isolation	1 M Tris-HCL, pH 8.5 500 mM EDTA, pH 8.0 20% SDS 5 M NaCl Add 100 µg proteinase K/ml before use
Mowiol	Mowiol 4-88 50% Glycerol 0.2 M Tris, pH 8.5
Nuclear fast red	75 mM $Al_2(SO_4)_3$ 2.8 mM Nuclear fast red dissolve hot, cool down and filtrate

Nickel sulfate	84 mM Nickel sulfate
NPG	60% (v/v) Glycerin in PBS 1.5% (w/v) N-propyl-gallate
Phosphate buffer	18 mM KH_2PO_4 82 mM $Na_2HPO_4 \times 2H_2O$ pH 7.4
PBS	137 mM NaCl 10.1 mM Na_2HPO_4 1.8 mM KH_2PO_4 2.7 mM KCL pH 7.4
TBE (10×)	890 mM Tris 890 mM Boric acid 20 mM EDTA

2.8 Consumables and equipment

Table 2.15: Consumables.

Name	Manufacturer
Aerosol-resistant Filter Tips	Mettler-Toledo, Gießen, Germany
Bulk Pipette Tips	Mettler-Toledo, Gießen, Germany
CE Buffer Microplate	Beckman Coulter, Krefeld, Germany
Cell Culture Flasks (T25, T75)	Greiner, Frickenhausen, Germany
Cell culture plates 6-, 48-well	Greiner, Frickenhausen, Germany
Cell scraper	Sarstedt, Newton NC, USA
Costar® 96-well round	Sigma-Aldrich, Munich, Germany

Continued on next page

Table 2.15 – *Continued from previous page*

Name	Manufacturer
round bottom microtiter plate	
Cover slips	Roth, Karlsruhe, Germany
Cryogenic vials (2 ml)	Thermo Scientific, Waltham MA, USA
Eppendorf Safe–Lock Tubes (1.5, 2 ml)	Eppendorf, Hamburg, Germany
Exam gloves	Medline, Kleve, Germany
Gauge needles	BD, Fraga, Spain
Greiner centrifuge tubes (50, 5 ml)	Greiner, Frickenhausen, Germany
Insulin syringe for U-40 Insulin	B. Braun, Melsungen, Germany
Parafilm M	American National Can, Greenwich CT, USA
PPPs-membrane 1.4 µm steel frames slides	Leica, Wetzlar, Germany
Sample microplates, 96 well	Beckman Coulter, Krefeld, Germany
Scalpel	B. Braun, Melsungen, Germany
Serological pipettes	Greiner, Frickenhausen, Germany
Sryinge	BD, Fraga, Spain
Syringe filter (0.45 µm)	Schleicher und Schuell, Dassel, Germany
Superfrost®Plus microscope slides	R.Langenbrick, Emmendingen, Germany
Terralin liquid	Schülke, Norderstedt, Germany

Table 2.16: Laboratory equipment.

Equipment	Name	Manufacturer
Agarose gel electrophoresis chamber	Horizon 11.14	GE Healthcare, Buckinghamshire, UK
Cell counting chamber	Neubauer-improved, depth 0.1 mm	Paul Marienfeld, Lauda Königshofen, Germany

Continued on next page

Table 2.16 – *Continued from previous page*

Equipment	Name	Manufacturer
Centrifuges	5417 R	Eppendorf, Hamburg, Germany
	5810 R	Eppendorf, Hamburg, Germany
	5451C	Eppendorf, Hamburg, Germany
	Allegra 21 R	Beckmann Coulter, Krefeld, Germany
	RC5B PLUS	Sorvall, Waltham, MA, USA
	Universal 16 A	Hettich, Tuttlingen, Germany
Fluorometer	Victor2^{TM} 1420 Multilabel Counter Wallac	PerkinElmer, Waltham, MA, USA
Freezing container	MR. FROSTY	Thermo Scientific, Waltham, MA, USA
Heating block	Thermomixer compact	Eppendorf, Hamburg, Germany
Hood	sterilGard, Class 2 Type A/B3	The Baker Company, Stanford, ME, USA
Incubator	Model 3336	Labotec, Göttingen, Germany
Magnetic mixer	IKA CombiMag RCT	Janke und Kunkel, Staufen, Germany
Magnetic particle concentrator	Dynal MPC-S	Dynal, Hamburg, Germany
Magnetic plate		IBA BioTAGnology, Göttingen, Germany
Micro scale		Scaltec, Heiligenstadt, Germany
Microscopes	Axiovert 25	Zeiss, Jena, Germany
	Axiovert 200	Zeiss, Jena, Germany
	Keyence BZ-9000	Neu-Isenburg, Germany
	Leica LMD6500	Leica, Wetzlar, Germany
Microwave		Sharp, Hamburg, Germany

Continued on next page

Table 2.16 – *Continued from previous page*

Equipment	Name	Manufacturer
PCR Cycler	T1	Biometra, Göttingen, Germany
pH meter	PHM 92 LAB	Radiometer, Kopenhagen, Denmark
Pipet aid	Accu-jet pro	Brand, Wertheim, Germany
Pipettes	Rainin	Mettler-Toledo, Gießen, Germany
Power supply	Consort	AGS, Heidelberg, Germany
Scale		Sartorius, Göttingen, Germany
Sequencer	CEQ^{TM}8000 Genetic Analysis System	Beckman Coulter, Krefeld, Germany
Shaker	Rotamax 120	Heidolph, Schwabach, Germany
Spectrophotometer	Nanodrop 2000c	Thermo Scientific, Waltham, MA, USA
Tissue homogenizer	ULTRA-TURRAX T8	IKA Labortechnik, Staufen, Germany
Tissue processor	TP1020	Leica, Bensheim, Germany
UV-Cleaner	UVC/T-AR	Biosan, Warren, MI, USA
UV-Transilluminator	TFX 35 M	Life Technologies, NY, USA
Vortex mixer	2 Genie	Scientific Industries, NY, USA
Water bath		Julabo MB, Seelbach, Germany

2.9 Software

BZ II Analyzer	Keyence Corporation
BZ II Viewer 1.4.2	Keyence Corporation
CEQ 8000 Genetic Analysis System 9.0.25 VIS	Beckman Coulter
Gitools 1.8.4	Biomedical Genomics Group, Barcelona
ImageJ 1.48v	National Institute of Health
Laser Microdissection Software 7.4	Leica Microsystems CMS GmbH
Leica Application Suite 4.2.0	Leica Microsystems CMS GmbH
Microsoft Office 2010	Microsoft Corporation
Photoshop CS2	Adobe Systems Incorporated
Prism5	GraphPad Software
VisiView 2.0.3	Visitron Systems GmbH

3 Experimental procedures

3.1 Cell culture techniques

3.1.1 Cell culture conditions

Cells were kept at 37 °C with 5% CO_2. All cell lines were cultured in Dulbecco's Modified Eagle's Medium (DMEM) containing 10% fetal calf serum (FCS) and 1% penicillin/streptomycin (P/S). Human umbilical vein endothelial cells (HUVECs) were cultured in endothelial growth medium (EGM). Prior to use all solutions except trypsin-ethylenediaminetetraacetic (EDTA) solution were preheated to 37 °C using a water bath.

Table 3.1: Amount of medium for culturing cells

Vessel	Volume [ml]
T75	15
T25	5
15 cm plate	30
10 cm plate	15
6-well-plate	2
48-well-plate	0.25

For harvesting of cells, medium was removed, cells were washed with phosphate buffered saline (PBS) and detached using trypsin-EDTA solution. Once cells were in suspension the trypsin reaction was stopped by adding medium containing FCS. To determine cell number a Neubauer chamber was used.

3.1.2 Cryopreservation and recovery

Cells were detached as described above, washed once with PBS at 100 × g for 5 min and resuspended in DMEM (10% FCS, 1% P/S) containing 10% dimethylsulfoxide

(DMSO). Of the cell suspension 1 ml was transferred to a cryogenic vial, which was placed in a freezing container. The container was kept at −80 °C for three days, then the cryogenic vial was transferred to the liquid nitrogen tank for prolonged storage. If cells were to be thawed, the cryogenic vial containing them was removed from liquid nitrogen and placed in a water bath set to 37 °C. The thawed cell suspension was transferred to the desired flask, containing the appropriate amount (Tab. 3.1) and type of medium. As soon as cells had settled down, the medium was changed to remove traces of DMSO and cell debris.

3.1.3 Stimulation experiments

Human umbilical cord cells were seeded at 2×10^5 in a 6-well plate in EGM. To investigate changes in the expression of transcription factors, HUVECs were stimulated with growth factors. Therefore HUVECs had to be starved first. Cells were washed with PBS and the media was exchanged for endothelial basal medium (EBM), which does not contain any growth factors, for a period of 16 h. After the starvation period the culture medium was changed to EBM containing a certain growth factor (VEGF-A, FGF-2, PDGF, HGF, SDF, IGF or EGF) at 20 ng/ml for 1 h. Cells serving as negative controls remained in EBM, positive controls were cultured in EGM. RNA was isolated using the RNeasy Mini Kit (see Chapter 3.3.1) for gene expression analysis. All experiments were conducted as triplicate.

3.2 Mammary carcinomas

Formalin fixed paraffin embedded (FFPE) mammary carcinoma samples were provided by the Institute of Pathology (University of Würzburg, Würzburg). The ductal and lobular mammary carcinomas were sampled in 2004 and 2006. The pathological stage according to the TNM system was determined and combined in stage grouping (Tab. 3.2) (Singletary et al., 2002). Mammary carcinomas were also graded on the stage of abnormality using the Nottingham grading system for breast cancer. This system grades breast tumors based on three features: tubule formation, nuclear grade and mitotic rate. The samples used in this study were graded G2 - 3 and stage IIa - IIIa. Patients had received no chemotherapy prior to tumor excision.

Table 3.2: Staging of mammary carcinomas according to TNM system

Category	Stage
Primary tumor (T)	1-3
Nearby lymph nodes (N)	0-3
Metastasis (M)	not assessed

Estrogen receptor (ER) and progesterone receptor (PR) status as well as presence of human epidermal growth factor receptor 2 (HER2) were determined at the Institute of Pathology using the immunoreactive score (IRS). This score lies between 0 and 12 and is calculated by multiplying the intensity of staining with the number of positive cells (Remmele and Stegner, 1987).

3.2.1 RNA isolation from mammary carcinomas

Before working with RNA, the working space and equipment were treated with 0.2% sodium dodecyl sulfate (SDS) to avoid RNase contamination. RNA isolation from FFPE samples was conducted in an UV-cleaner. RNA concentration was determined using the Nanodrop 2000c. RNA was stored at $-80\,^{\circ}\mathrm{C}$ immediately. To establish an optimal technique for the isolation of RNA from FFPE mammary carcinomas, several kits were tested. Using the QuickExtract™FFPE kit (Epicenter®), the KAPA Express Extract kit (peqlab), the RT2 FFPE RNA kit (SABiosciences), and the RNeasy FFPE kit (QIAGEN), RNA was isolated according to the manufacturers' instructions. FFPE samples of the respective thickness had been placed on superfrost plus glass slides and were scratched off with a scalpel.

3.2.1.1 NucleoSpin® FFPE RNA/DNA kit

Three sections of 50 µm thickness of each FFPE mammary carcinoma were placed in a 1.5 ml collection tube to which 400 µl paraffin dissolver were added. To melt the paraffin the samples were incubated in a heating block set to $60\,^{\circ}\mathrm{C}$ for 3 min and vortexed vigorously while still hot. After samples had cooled down to room temperature (RT), 100 µl of Buffer FL were added and the samples were vortexed vigorously. Centrifugation at $11,000 \times$ g for 1 min led to the formation of two phases. 10 µl of proteinase K were added to the lower aqueous phase and mixed by pipetting up and down. If more samples were processed a premix of Buffer FL and proteinase K was prepared.

Subsequently the samples were incubated at 60 °C until the tissue was lysed (no more than 3 h). After lysis the samples were vortexed for 5 s, 100 µl of Decrosslink Buffer D-Link were added to the tube, which was vortexed gently. To obtain phase formation the samples were centrifuged at 11,000 × g for 30 s. Next they were incubated at 90 °C for exactly 15 min, vortexed for 5 s and cooled down to RT. 200 µl of ethanol (96% - 100%) were added and mixed into the aqueous phase by vortexing twice for 5 s. This phase was then transferred onto a NucleoSpin® FFPE Column and centrifuged (2000 × g, 30 s). After the column had been placed in a new collection tube, 100 µl of Membrane Desalting Buffer were added and the tubes were centrifuged at 11,000 × g for 30 s. To digest DNA, a rDNase reaction mixture was prepared by adding 3 µl of reconstituted rDNase to 27 µl of Reaction Buffer for rDNase and mixed by flicking the tube. 25 µl of the mixture were applied directly onto the center of the silica membrane of the column and the samples were incubated at RT for 15 min. DNA digestion was followed by three washes. For the first wash 100 µl of Buffer FW1 were added to the column, incubated for 2 min at RT and centrifuged (11,000 × g for 30 s). The column was placed into a new collection tube and washed with 400 µl Buffer FW2 at 11,000 × g for 30 s. After the flow-through had been discarded, 200 µl of Buffer FW2 were added to the column, which was then centrifuged at 11,000 × g for 2 min. Finally the RNA was eluted into a 1.5 ml collection tube with 20 µl of RNase-free H_2O (11,000 × g for 30 s).

3.2.1.2 Agencourt® FormaPure® Kit

Sections of mammary carcinomas were weighed to determine the best conditions for RNA isolation. Samples that weighed up to 15 mg were treated as described below. For those heavier than 15 mg the suggested volumes of buffers was doubled. Volume of rDNase remained the same, independent of sample weight. If RNA was extracted from vessels dissected of FFPE tumor tissue, the volumes of all chemicals were cut by half. When using the kit for the first time proteinase K needs to be dissolved in PK buffer and 15 ml of 100% isopropanol have to be added to the Wash Buffer. Prior to starting the isolation process, Binding Buffer II is prepared by combining 20 µl of Bind 2 to with 300 µl of 100% isopropanol for each individual isolation. DNase solution was prepared by mixing 10 µl of 10 × buffer, 2 µl of DNase and 90 µl of RNase-free H_2O for each reaction. The samples were placed in a 1.5 ml tube, to which 200 µl of Lysis Buffer were added and incubated in a water bath set to 70 °C - 72 °C for

1 h. Following the incubation 20 µl of PK were added, mixed in by pipetting and the samples were incubated in a water bath at 55 °C for 1 h. Next the samples were cooled on ice for 2 min and the lysate was transferred to a new 1.5 ml tube. 150 µl Bind I Buffer and 320 µl of the prepared Bind II Buffer were added to each tube, mixed well by pipetting up and down five times and incubated in a 55 °C water bath for 5 min. For separation the samples were placed in a magnetic stand for 5 min until the solution appeared clear. The cleared solution was slowly aspirated from the tube and discarded without disturbing the magnetic beads. After the tubes were removed from the magnet, 750 µl of 70% ethanol were added and mixed by pipetting five times. The tubes were returned to the magnet to separate for 1 min and the cleared solution was again discarded. The tubes were removed from the magnet and 100 µl of prepared DNase solution were added, pipette mixed five times to resuspend the beads and then the tubes were incubated in a 37 °C water bath for 15 min to facilitate digestion of DNA. Next 550 µl of Wash Buffer were added, pipette mixed five times and the samples were incubated at RT for 5 min. Then the tubes were placed in the magnetic stand for 10 min and the cleared solution was discarded. The tubes were removed from the magnet and the samples were washed with 750 µl of 70% ethanol, placed on the magnet for 5 min and the cleared solution was discarded. After the tubes were removed from the magnet, 500 µl of 90% isopropanol were added and mixed by pipetting up and down five times. Next, the tubes were incubated in 70 °C water bath for 3 min, placed in the magnetic stand for 1 min and the cleared solution was discarded. This isopropanol wash was repeated. Then the samples were removed from the magnet, 750 µl of 70% ethanol were added and mixed by pipetting five times. The tubes were placed in the magnetic stand for 1 min and the cleared solution was discarded. The samples were air dried for about 10 min or until all visible traces of ethanol were evaporated. Finally the tubes were removed from the magnet and the beads were resuspended in 20 µl of nuclease-free H_2O by mixing five times. The samples were incubated at 70 °C for 30 s, placed in the magnetic stand for 1 min and the eluted nucleic acid was transferred to a new tube.

3.2.2 CD34 staining

Samples were cut and stained at the Institute of Pathology. Sections for steel-frame slides with polyphenylene sulfide (PPS)-membrane were cut at 5 µm, sections for su-

perfrost plus glass slides at 3 µm. Sections were deparaffinized in xylene for 25 min, washed in a series of alcohol solutions (100%, 90%, 80% and 70%) and placed in aqua dest. for 10 min. Next an enzymatic antigen retrieval was performed. Slides were covered with 100 µl proteinase K solution at 20 µg/ml in TE-buffer for 10 min at RT. To inactivate proteinase K the sections were washed three times for 5 min in PBS with agitation. In a humidified chamber the sections were incubated with the diluted CD34 antibody (1:1000 in antibody diluent) for 90 min. Afterward, the slides were washed three times for 5 min in PBS with agitation and subsequently incubated with ADVANCE^{TM}HRP Link from the ADVANCE^{TM}HRP kit in a humidified chamber for 30 min at RT. Next the sections were washed and incubated with ADVANCE^{TM}HRP Enzyme from the ADVANCE^{TM}HRP kit at RT for 30 min a humidified chamber. The slides were washed again and 100 µl 3,3'-Diaminobenzidine (DAB) solution were pipetted onto each section. Sections were then incubated at RT for 10 min. Since DAB is a suspected carcinogen it should be handled with care. All contaminated items were incubated in sodium hypochloride for deactivation of DAB. The sections were washed in PBS and nuclei were stained with hematoxylin for 3 min. The stained sections were washed in tap water for 10 min, dipped in 100% ethanol for rehydration and dried at 37 °C for 25 min. Sections on superfrost plus glass slides were mounted.

3.2.3 Laser microdissection

Laser microdissection (LMD) is a technique for the isolation of specific cells from a variety of samples such as tissue sections. For this method the tissue samples were cut at 5 µm and placed onto steel-frame slides with PPS-membrane. Tissue was stained with an antibody to CD34 to make endothelial cells (ECs) visible for dissection (see Section 3.2.2). Vessels were excised using the Leica LMD6500. First the specimen holder was removed from the microscope and the slide was placed on the specimen holder with the section facing downward. For each sample a new 0.2 ml collection tube was inserted into the collection device. The cap of the collection tube was filled with a drop of lysis buffer from the Agencourt® FormaPure® kit. Before the specimen holder was inserted, proper positioning of the reference point was checked and if necessary the reference point was repositioned. Then the specimen tray was inserted into the microscope. Next the laser was calibrated using the 40x cutting objective and the laser parameters were set as shown in Tab. 3.3.

Table 3.3: Laser parameters for dissecting vessels.

Parameters	Selected value
Power	57
Aperture	1
Speed	17

To dissect target areas, a line was drawn around stained vessels. The laser cuts along this line and the sample drops into the cap of the 0.2 ml collection tube by the force of gravity. After the dissection had been completed, the 0.2 ml collection tube was removed from the collection device and stored at −80 °C for RNA isolation. Around 1000 vessel were dissected from each sample and up to four sections of each specimen were available for dissection. For most samples ECs were collected on two consecutive days and were combined during RNA isolation.

3.2.4 Assessment of vessel quality

We examined different vessel parameters of mammary carcinomas. To investigate the percentage of CD34 positive area we used the Axiovert 200 microscope. Differential interference contrast microscopy pictures of each sample were taken utilizing the 40x objective and the blue filter. To evaluate further vessel parameters, slides with mammary carcinomas were scanned with the Keyence BZ-9000 (BIOREVO) utilizing the 40x objective. Pictures were evaluated using the software ImageJ.
Vessel circularity was calculated using

$$C = \frac{4\pi A}{P^2}, \tag{3.1}$$

where C is circularity, A is area and P is perimeter

3.3 RNA methods

Before working with RNA, the working space and equipment were treated with 0.2% SDS to avoid RNase contamination. RNA concentration was determined using the Nanodrop 2000c. RNA was stored at −80 °C immediately.

3.3.1 RNA Isolation from cells

For isolation of RNA from cells the RNeasy Mini Kit was used. About 2×10^5 cells were cultured in a 6-well plate. For cell lysis 10 µl of β-mercaptoethanol were added to each ml of lysis buffer RLT. 600 µl of lysis buffer were added to each well and cells were collected with a rubber police man. For homogenization the lysate was either placed in a QIAshredder spin column and centrifuged at full speed for 2 min or passed through a blunt 20-gauge needle (0.9 mm diameter) fitted to a 2 ml syringe five times. Subsequently 600 µl of 70% ethanol were added to the homogenized lysate. 700 µl of the sample were transferred to an RNeasy spin column placed in a 2 ml collection tube and centrifuged for 15 s at 8000 × g. Flow-through was discarded and the step was repeated until the entire sample had passed through the column. To wash the spin column membrane 700 µl of buffer RW1 were added and centrifuged as above. After disposal of the flow-through the membrane was washed twice with 500 µl of buffer RPE for 15 s at 8000 × g. For the second wash the centrifugation time was elongated to 2 min. To eliminate possible carryover from buffer RPE, the RNeasy spin column was placed in a new 2 ml collection tube and centrifuged at full speed for 1 min. Finally, the RNA was eluted into a 1.5 ml collection tube. Therefore, 40 µl of RNase-free water were added directly to the spin column membrane and centrifuged for 1 min at 8000 × g.

3.3.2 RNA isolation from tissue

To isolate RNA from tumor tissue, TRIzol® Reagent was used. Between 40 mg and 120 mg of tissue were placed in 500 µl TRIzol® Reagent and homogenized using an Ultra Turrax. Once the samples were homogenized, another 500 µl TRIzol® Reagent was added and the samples were incubated at RT for 5 min to permit complete dissociation of the nucleoprotein complex. Next, 200 µl of chloroform were added, the samples were shaken vigorously by hand for 15 s and incubated at RT for 3 min. For phase separation, the samples were centrifuged at 12,000 × g for 15 min at 4 °C. The aqueous phase, which contains the cellular RNA, was then transferred to a new collection tube. For precipitation, samples were incubated at RT with 500 µl of 100% isopropanol for 10 min and subsequently centrifuged at 12,000 × g for 10 min at 4 °C. Next, the supernatant was removed from the RNA pellet, which was then washed with 500 µl of 75% ethanol. The tube was inverted several times, centrifuged (7500 × g,

15 min, 4 °C) and the wash was discarded. The pellet was dried in heating block set to 37 °C for 5 min to 10 min with the lid of the collection tube remaining open, re-suspended in 50 µl RNase-free water and incubated in a heating block set to 56 °C for 15 min.

3.3.3 RNA Amplification

RNA was amplified using the Sensation Plus FFPE Amp kit. For each reaction 50 µg of total FFPE RNA was used, the volume was adjusted to 7 µl with nuclease-free water. On ice, 4 µl RT Primer Mix were added to the RNA and the mix was incubated in a thermalcycler at 80 °C for 10 min and at 4 °C for 2 min. During this incubation period the Amplification RT Master Mix was prepared in a separate tube on ice (Tab. 3.4), and added to the RNA-Primer Mix for a volume of 20 µl. This RT reaction was

Table 3.4: Amplification RT Master Mix

Component	Volume [µl]	Handling of kit components
RT Buffer Mix	4	Thaw at RT, briefly vortex and centrifuge. Keep at RT until use.
DTT	2	Thaw on ice, briefly vortex and centrifuge. Keep on ice.
dNTP Mix	1	Thaw on ice, briefly vortex and centrifuge. Keep on ice.
RT Enzyme Mix	1	Gently tap the tube, briefly centrifuge, then keep on ice at all times. Do not vortex.
Rnase Inhibitor	1	Gently tap the tube, briefly centrifuge, then keep on ice at all times. Do not vortex.
Total	9	

incubated at 42 °C for 60 min and at 25 °C for 2 min. During the incubation the RNA Purification beads have to be resuspended by shaking the bottle. For each reaction 36 µl of beads were aliquoted and kept at RT until used. The nuclease-free H_2O was preheated to 65 °C. For cDNA purification, 36 µl of RNA Purification beads were added to a well of a 96-well round bottom plate. The cDNA sample was transferred to the designated well and mixed with the beads by pipetting up and down 10 - 20 times. Next, 30 µl of 100% ethanol were mixed with the sample. The mixture was incubated

for 10 min at RT, and for 10 min on a magnetic stand to separate the beads from the solution. Afterward the cleared solution was slowly aspirated without disturbing the magnetic beads. For the following ethanol wash, the plate was placed on the magnet, 180 µl of 70% ethanol were added, incubated for 30 s at RT and slowly aspirated. This was repeated for a total of three washes. Next, the plate was air-dried on the magnetic stand for 5 min - 10 min, until all ethanol had evaporated. Then it was removed from the stand and 14 µl of nuclease-free water were added. To elute the sample from the magnetic beads it was shaken gently at RT for 3 min. To separate the beads from the solution the plate was again placed on the magnetic stand for 3 min and 12 µl of purified cDNA were carefully transferred to a new collection tube. For promotor synthesis the 12 µl of purified cDNA were heated to 80 °C for 10 min, cooled to 4 °C for 2 min and transferred on ice. The Tailing Master Mix (Tab. 3.5) was prepared on ice and added to the purified cDNA The Tailing Reaction was incubated at 37 °C

Table 3.5: Tailing Master Mix

Component	Volume [µl]	Handling of kit components
Tailing Buffer Mix	6	Thaw on ice, briefly vortex and centrifuge. Keep on ice
Tailing Enzyme Mix	2	Gently tap the tube, briefly centrifuge, then keep on ice at all times. Do not vortex.
Total	8	

for 2 min, at 80 °C for 10 min, cooled to 4 °C for 2 min and then transferred to ice. The Promotor Synthesis Master Mix was prepared in a separate tube on ice (Tab. 3.6) and added to the tailed cDNA. The Promotor Synthesis Reaction was incubated in a

Table 3.6: Promotor Synthesis Master Mix

Component	Volume [µl]	Handling of kit components
Promotor Synthesis Buffer Mix	4	Thaw on ice, briefly vortex and centrifuge. Keep on ice.
Promotor Synthesis Enyzme Mix	1	Gently tap the tube, briefly centrifuge, then keep on ice at all times. Do not vortex.
Total	5	

thermalcycler at 25 °C for 30 min. For preparation of the In Vitro Transcription (IVT) Master Mix the T7 Nucleotide Mix and the T7 Buffer Mix were thawed and kept at RT until use. The Master Mix was prepared in a separate tube at RT (Tab. 3.7).

Table 3.7: IVT Master Mix

Component	Volume [µl]	Handling Kit Components
T7 Nucleotide Mix	16	Thaw at RT, briefly vortex and centrifuge. Keep at RT until use.
T7 Buffer Mix	5	Thaw at RT, briefly vortex and centrifuge. Keep at RT until use.
T7 Enzyme	9	Gently tap the tube, briefly centrifuge, keep on ice until added to Master Mix.
Total	30	

The promotor-modified cDNA was transferred to RT and 30 µl of IVT Master Mix were added. The IVT reaction was incubated at 37 °C for 16 h - 18 h. For the purification of senseRNA, the RNA Purification beads and nuclease-free H_2O were prepared as described above. For senseRNA purification 36 µl of RNA Purification beads were added to a well of a 96-well round bottom plate. The senseRNA sample was transferred to the designated well and mixed with the beads by pipetting up and down 10 - 20 times. The mixture was incubated at RT for 10 min and for 10 min on a magnetic stand. This was followed by three ethanol washes as described above. After ethanol had completely evaporated, the plate was removed from the magnet and senseRNA was eluted using 23 µl of preheated nuclease-free H_2O. Therefore the plate was shaken gently at RT for 3 min. To separate the beads from the solution the plate was again placed on the magnetic stand for 3 min, and 20 µl of purified senseRNA were carefully transferred to a new collection tube. If senseRNA is very concentrated it might be difficult to aspirate from the beads. Then the plate needs to be removed from the magnet, and an additional 10 µl to 20 µl of nuclease-free H_2O may be added.

3.3.4 cDNA Synthesis

To make cDNA we used the RevertAid^{TM}First Strand cDNA Synthesis Kit. Between 0.5 µg and 5 µg isolated RNA was used for cDNA synthesis. The RNA volume was adjusted to 11 µl using RNase-free H_2O. To each reaction 1 µl of oligo (dT) 18 primer was

added. This mixture was incubated in a thermalcycler at 65 °C for 5 min. The tubes were removed from the cycler, placed on ice, and the prepared master mix (Tab. 3.8) was added. Then the tubes were shaken gently, and incubated at 42 °C for 1 h and at 70 °C for 5 min. cDNA was stored at −20 °C until used.

Table 3.8: Master mix for cDNA synthesis

Component	Volume [µl]
5× Reaction Buffer	4
RiboLock™RNase Inhibitor (20u/µl)	1
10 mM dNTP Mix	2
RevertAid™M-MuLV Reverse Transcriptase (200u/µl)	1

3.4 Gene expression analysis

The GenomeLab™GeXP Genetic Analysis System utilizes a multiplexed polymerase chain reaction (PCR) approach, known as eXpress Profiling™, to investigate the expression of gene sets. The GeXP multiplex feature allows to analyze multiple reference (housekeeping) genes and multiple genes of interest in a single reaction, using a two-step multiplex PCR. The first step (Fig. 3.1 A) is the reverse transcription reaction from total RNA, which uses gene-specific reverse primers that add a flanking universal reverse sequence to resulting cDNA. The second step (Fig. 3.1 B) is a multiplex PCR reaction with chimeric and universal primer sets. This reaction contains the tagged cDNA from step one. The chimeric primers, which are used to synthesize a double-stranded template, contain a gene-specific sequence with a universal tag at the 5'-end. The universal primer is covalently labeled with a fluorescent dye for detection during capillary electrophoresis. The result of this multiplex PCR is a pool of amplicons corresponding to the genes of interest. Each amplicon is designed to have a discrete length and is labeled with WellRED fluorescent dye for detection. For separation and evaluation of the amplified fragments the CEQ™8000 Genetic Analysis System is used.

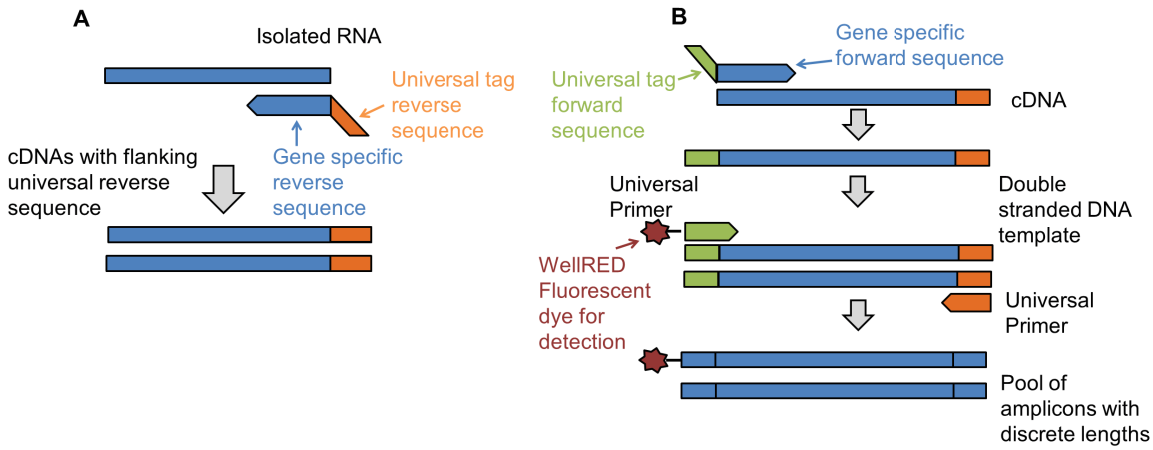

Figure 3.1: The GenomeLab^{TM}GeXP Genetic Analysis System. *A two-step multiplex PCR allows analyzing multiple genes in a single reaction. (A) During the reverse transcription reaction from total RNA, gene-specific reverse primers add a flanking universal reverse sequence to resulting cDNA. (B) Next is a multiplex PCR reaction with chimeric and universal primer sets. The result is a pool of labeled amplicons corresponding to the genes of interest.*

3.4.1 Custom design of primer multiplexes

Primer pairs for individual target-mRNAs were designed using Primer-Blast[1]. Possible primers had to be intron spanning, with a minimal combined intron size of 500 bp, produce a PCR product between 100 bp and 180 bp and have a minimal of four mispairings with unintended targets. Primers were permitted to amplify known transcript-variants. A universal sequence (reverse: GTACGACTCACTATAGGGA, forward: AGGTGACACTATAGAATA) for detection with the GenomeLab^{TM}GeXP System was added to each primer sequence. Primers that were to be combined in one plex had to produce amplicons that differed in size by 3 to 7 nucleotides. Primers were resuspended in TE-Buffer to a stock solution of 100 µM. Individual primer pairs were tested in a single-plex GeXP PCR using cellular cDNA to ensure a single amplicon of the correct size was generated. For this we used the peqGOLD Hot Start Mix S. The master mix for the PCR reaction was prepared according to Tab. 3.9 and 2 µl (approx. 100 ng) of cDNA were added.

[1] http://www.ncbi.nlm.nih.gov/tools/primer-blast/

Table 3.9: Master mix for primer testing

Component	Volume [µl]
PCR-Mix	12.5
H_2O	9.5
Forward primer [5 µM]	0.5
Reverse primer [5 µM]	0.5

After the reaction, 3 µl of the PCR-product were combined with 6 µl of loading buffer and loaded onto a 1% agarose gel. For the agarose gel, 1.2 g of peqGOLD Universal Agarose were dissolved in 120 ml TBE-buffer by heating in a microwave oven. The mixture was cooled to about 40 °C, and for DNA detection 2 µl of GelRed® were added. The gel was poured into a gel chamber and two combs were placed in the liquid gel. After the gel had hardened, the prepared samples were loaded and separated for 45 min at 130 V. Bands on the gel were visualized under UV light.

3.4.2 Optimization of primer plexes

The dynamics in a singlet PCR differ from those in multiplexed reactions. Subsequent optimization of the primer plexes incorporating multiplexed primer pairs was conducted with a mixture of cellular RNAs as well as individual cellular RNA and RNA isolated from FFPE tumors. No template controls were included to ensure absence of non-specific reaction products. A reverse multiplex primer mix was assembled by combining the reverse primers at 500 nM each and a forward multiplex primer mix by combining the forward primers at 200 nM each. In a working multiplex all primer pairs produce a signal of the expected fragment size. Gene signals that were extremely high or above the linear detection limit were attenuated by lowering the reverse primer concentration relative to the other reverse primers in the multiplex (Drew et al., 2011).

3.4.3 Quantitative gene expression profiling

To create expression profiles we used the GenomeLab™GeXP Start Kit. For the reverse transcription all reagents and RNA were thawed on ice. The Reverse Transcription reaction mix (Tab. 3.10) was prepared in a UV-Cleaner, and 7.5 µl of the mix were transferred to tubes of a 0.2 ml PCR strip.

Table 3.10: Reverse Transcription reaction mix. *RT: Reverse transcription, rv: reverse*

Components	Volume per reaction [µl]
DNase/RNase free H_2O	4
RT Buffer 5 ×	2
Reverse Transcriptase	0.5
Custom RT rv Primer Plex	1
Total	7.5

Next, 2.5 µl of the sample RNA were added to each tube. Total RNA input depended on sample type (Tab. 3.11). As negative control RNA was substituted by water.

Table 3.11: RNA input for GeXP System. *FFPE: Formalin fixed paraffin embedded*

Origin of RNA	RNA [ng]
FFPE tumors	37.5
Murine tumor tissue	25
Cells	12.5

The reaction components were mixed and the tightly covered strips were placed in a thermal cycler running the RT cycling program (Tab. 3.12).

Table 3.12: RT cycling program.

Temperature [°C]	Time [min]
48	1
37	5
42	60
95	5
4	hold

For the following PCR reaction all reagents were thawed on ice. The PCR reaction mix (Tab. 3.13) was prepared in a UV-Cleaner. For each reaction 5.35 µl of the PCR reaction mix were transferred to a new tube of a 0.2 ml PCR strip. The ThermoStart DNA-Polymerase and $MgCl_2$ (25 mM) are not included in the GenomeLab^{TM}GeXP Start Kit. Of each cDNA sample 4.65 µl were transferred to new tubes containing the

PCR reaction mix.

Table 3.13: PCR reaction mix. *fwd: forward; PCR: Polymerase chain reaction*

Components	Volume per reaction [µl]
PCR Buffer 5 ×	2
$MgCl_2$ (25 mM)	2
ThermoStart DNA-Polymerase	0.35
PCR fwd Primer Plex	1
Total	5.35

The reaction components and the cDNA were mixed and the tightly covered strips were placed in a thermal cycler running the PCR cycling program (Tab. 3.14). Steps two to four were repeated for an additional 34 cycles, resulting in a total of 35 cycles. The amount of sample loaded on the CEQ system depended on the quality

Table 3.14: PCR cycling program.

Step	Temperature [°C]	Time [min]
1	95	10
2	94	0.5
3	55	0.5
4	68	1
5	-	repeat steps 2-4 for an additional 34 cycles
6	4	hold

and quantity of the RNA template, instrument sensitivity and the reaction efficiency. Before loading, samples were prediluted at a range of 1:5 to 1:20 in GenomeLab sample loading solution. Some samples were not prediluted at all. The GenomeLab DNA Size Standard-400 was diluted 1:100 in sample loading solution. 30 µl of the diluted standard were pipetted into each well of a 96-well-plate. Between 0.5 µl and 2 µl of a prediluted sample was added to each well and mixed by pipetting up and down. Empty wells were filled with aqua dest. and each well was overlayed with one drop of mineral oil. The appropriate number of columns of a CE Buffer Microplate were filled with approximately 250 µl of GenomeLab Separation Buffer. To run the samples on the GenomeLab GeXP Genetic Analysis system the sample and buffer plate were loaded and the Frag-3 protocol was chosen. Depending on the sample type and primer

set, the injection time of the run varied between 15 s to 45 s. Separation time was set to 2 min. The size fragment analysis was conducted using the fragment analysis module of the GeXP system software to generate electorpherograms representing the electrophoresed and separated fragments. A size exclusion filter appropriate for the respective custom designed multiplex was applied to the detected signal peaks corresponding to the expected size fragments. Then the generated fragment data, as well as height and area of fragment peaks, were exported from the Express Analysis module to Excel 2010 for subsequent analysis. Peak height of genes of interest was normalized to the incorporated reference genes.

3.5 Immunhistochemistry

Immunohistochemical staining is accomplished with highly specific antibodies that recognize target proteins. For chromogenic detection, the enzyme horseradish peroxidase (HRP) is conjugated to the secondary antibody. HRP catalyzes the conversion of chromogenic substrates such as DAB, into a colored product at the location of the target protein.

3.5.1 CD34 Staining of murine tumor tissue

Samples were cut at the Institute of Anatomy and Cellular Biology (University of Würzburg, Würzburg). To remove paraffin, slides were placed in a rack and washed twice in xylene for 10 min. Then the rack was placed in a dilution series of ethanol (100%, 96%, 80% and 70%) for 5 min each. To reduce background staining endogenous peroxidase was blocked by incubating the slides in 3% H_2O_2 for 10 min. The slides were then washed twice in aqua dest. for 5 min with agitation. For the heat mediated antigen retrieval the samples were placed in a plastic cuvette filled with citrate buffer and heated in a microwave for 6 min. Therefore the microwave was set to full power and turned off once the buffer had been boiling for 10 s. After 50 s the microwave was again set to full power and the samples were boiled for another 10 s. This was repeated until the samples had been boiled seven times. The cuvette was then removed from the microwave and cooled at RT for 30 min. Next the citrate buffer was replaced by running aqua dest. For blocking, the slides were removed from the cuvette and incubated in a humidified chamber with 5% normal goat serum (NGS) in PBS for 2 h.

After the blocking solution had been removed, the primary antibody was pipetted onto the tissue and the slides were incubated in a humidified chamber at 4 °C overnight. The CD34 antibody was diluted 1:50 in 0.2% BSA with 1% NGS. Negative controls were incubated with 0.2% BSA with 1% NGS. The sections should now remain in the dark whenever possible.
The next day the slides were washed three times for 5 min in PBS with agitation and subsequently incubated with the biotinylated secondary goat-α-rat antibody diluted 1:2500 in PBS in a humidified chamber for 1 h at RT. During the incubation period the avidin-biotin complex (AB-complex) was prepared by diluting solutions A and B 1:125 in PBS, and stored in the dark until used. Incubation with the AB-complex leads to a significant increase in sensitivity. The avidin and the biotinylated enzyme form a complex, in which some of the binding sites on avidin are left unoccupied. These unoccupied binding sides can then bind to the secondary biotinylated antibody. Before incubation with the AB-complex the slides were washed again as described above. Then they were incubated with the AB complex for 30 min in a humidified chamber and washed twice with PBS for 5 min and twice with phosphate buffer for 5 min. Before the last wash, the slides were placed in a darkened cuvette and during this wash the HRP substrate DAB was prepared in a graduated flask wrapped in aluminum foil. Since DAB is a suspected carcinogen it should be handled with care. All contaminated items were incubated in sodium hypochloride for deactivation of DAB. During the DAB reaction slides were checked on regularly to avoid overstaining. After the reaction the slides were washed three times for 5 min with PBS with agitation. Sections were counterstained with nuclear fast red for 1.5 min and rinsed with aqua dest. to remove residual nuclear fast red. Finally the sections were rehydrated in a dilution series of ethanol (70%, 80% and 96%) for 1 min, respectively and twice in 100% ethanol for 3 min. Last they were placed twice in xylene for 5 min and mounted using DePeX.

3.5.2 Cre staining of murine tumor tissue

For staining of the enzyme cre recombinase the protocol from Section 3.5.1 was used with slight changes. The primary antibody was diluted 1:100 in 0.2% BSA with 1% NGS. The biotinylated secondary goat-α-mouse antibody was diluted 1:250 in PBS. Following the incubation with the secondary antibody, the sections were washed three times for 5 min in PBS with agitation. Afterward, the sections were incubated with

a mouse peroxidase-antiperoxidase complex (PAP-complex) for 30 min at RT in a humidified chamber. This complex consists of a mouse-antibody to peroxidase coupled with peroxidase at the ratio 2:3. The PAP-complex binds to the secondary antibody and amplifies the HRP signal. The slides were washed again as described above and incubated with the AB-complex.

3.6 Animal studies

3.6.1 Husbandry conditions

All experiments involving animals were reviewed and approved by the Regional Administration of Lower Franconia, Würzburg. All mice were kept and bred at the center for experimental molecular medicine (ZEMM) in Würzburg. For experiments different strains of C57BL/6 mice were used. Mice were kept at 22 ± 2 °C, a relative ambient humidity of 55 ± 10% and a diurnal 12 h light cycle. In a type II cage up to three male and up to four female mice were kept. In a type III cage up to eight male and up to ten female mice were kept. Mice were mated at 8 weeks either as pairs (monogamous) or trios (polygamous). Offspring was weaned 3 to 4 weeks after birth.

3.6.2 Mice strains

Mice showing tissue specific excision of SNAI1 were generated by using the Cre-loxP system (Fig. 3.2). This method involves the Cre recombinase, a protein of the P1 bacteriophage, which recognizes two loxP sites and catalyzes the recombination between them (Hamilton and Abremski, 1984). For this system, Cre and loxP mice strains are developed separately and then crossed to produce a Cre-loxP strain (reviewed in Nagy, 2000). The Cre expressing strain (b6.Cg-Tg(Cdh5-cre)7Mlia/J) carries the Cre transgene under the control of the EC-specific promoter Cdh5. The loxP flanked (floxed) strain B6;129S-Snai1^{tm2Grid}/J carries loxP sites flanking the *Snai1* target gene. In the resulting offspring *Snai1* is deleted in ECs. Before generating these knockdown mice, the B6;129S-Snai1^{tm2Grid}/J strain was backcrossed to the C57BL/6 background for seven generations. For animal studies we used mice with heterozygous knockdown of *Snai1* in ECs.

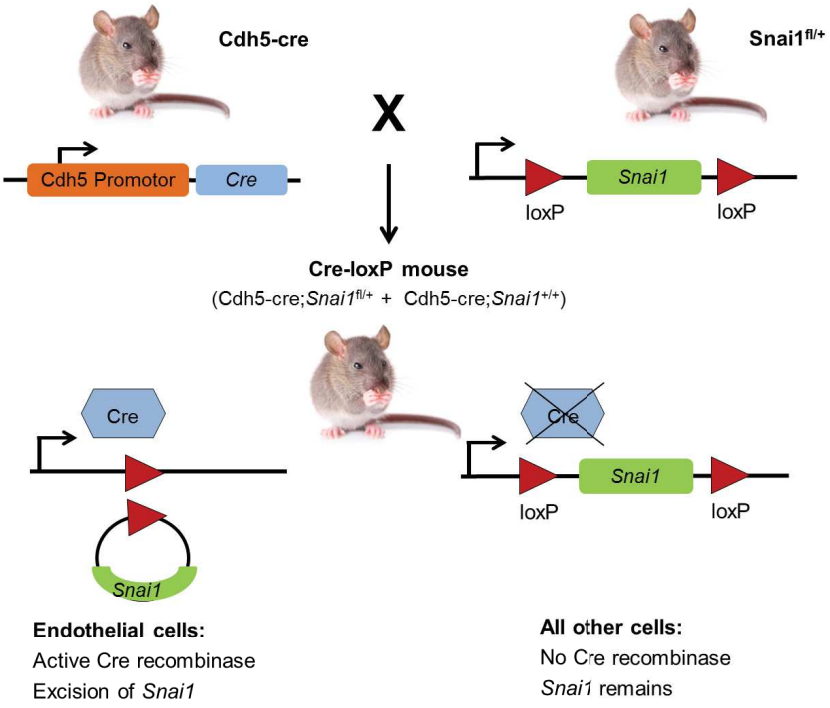

Figure 3.2: The cre-loxP system. *A mouse is generated in which the gene of interest (Snai1) is flanked by loxP sites (floxed). This mouse is then crossed with a Cre transgenic mouse, which expresses Cre recombinase under the control of a tissue-specific promoter (Cdh5). In the progeny, Cre is expressed only in endothelial cells, and Snai1 is excised specifically in these cells.*

3.6.3 Genotyping

All mice were marked by earpunching after weaning. Earpunches were stored at −20 °C for at least 24 h and then used for genotyping via PCR. Primers (see Tab. 2.3) were designed according to the genotyping protocol of the animal suppliers. For DNA isolation the tissue was placed in a 1.5 ml collection tube. 500 µl of lysis buffer containing 100 µg/ml proteinase K were added. For efficient lysis the tissue was incubated overnight at 56 °C and 300 rpm. The tubes were removed from the heater and centrifuged at 15,700 × g for 10 min. The supernatant was poured into a new 1.5 ml collection tube containing 500 µl isopropanol and DNA was precipitated by inverting the tube several times. The mixture was again centrifuged at 15,700 × g for 10 min and the supernatant was discarded. To dry precipitated DNA, the tube was opened and placed upside down onto a tissue paper until all liquid had evaporated. The dried

pellet was dissolved in 50 µl TE buffer and incubated at 56 °C and 300 rpm for 30 min. DNA was stored at −20 °C. For the PCR the reaction mix was prepared as shown in Tab. 3.9 and 2 µl (about 100 ng) of the isolated DNA were added. After the PCR reaction (Tab. 3.15) the PCR product was diluted 1:10 in aqua dest. and 5 µl were mixed with 3 µl loading buffer and loaded onto an 1% agarose gel (see Section 3.9).

Table 3.15: PCR program for genotyping.

Step	Temperature [°C]	Time [min]
1	94	3
2	94	0.5
3	62	0.5
4	72	0.5
5	-	repeat steps 2-4 for an additional 29 cycles
6	72	5
7	4	hold

3.6.4 Tumor models

Three different tumor models were implanted into B6.Cdh5-cre;B6.Snai1$^{fl/+}$ (Snai1$^{fl/+}$) and B6.Cdh5-cre;B6.Snai1$^{+/+}$ (Snai1$^{+/+}$) mice strains. In female mice either the murine breast cancer cell line E0771 was implanted into the mammary fat pat or the melanoma cell line B16-F10 was injected subcutaneously into the dorsal region close to the hind limb. Lewis lung carcinoma cells (LLC) were injected subcutaneously in the dorsal region close to the hind limb of male mice. Prior to implantation, mice were anesthetized using isoflurane and shaven at the site of tumor implantation. All animals in one experiment were of the same age. Mice that did not develop tumors were excluded from the respective study.

3.6.4.1 Tumor growth studies

For each tumor model a growth study was conducted. Tumor cells were cultured in DMEM with 10% FCS and 1% P/S as described above (see Section 3.1.1). Cells were harvested, washed twice with PBS, and stained with trypan blue to detect dead cells. Cell number was adjusted to 2×10^6 cells/ml. Two tumors were generated per mouse by injecting 10^6 cells in 50 µl PBS. Animals were monitored closely during the study

and tumor size was measured every other day using a caliper. Tumor volume was calculated using the equation

$$V = \frac{\pi}{6 \times l \times w^2}, \tag{3.2}$$

where V is volume, l is length and w is width. At the end of the study tumors were excised and weighed. For further experiments tumors were dissected into three parts. Two parts were immediately stored at −80 °C for RNA and protein extraction. The third part was fixed in 4% paraformaldehyde for immunohistochemical staining.

3.6.4.2 Biodistribution of doxorubicin

The method is based on the one developed by Laginha et al. (Laginha et al., 2005). To monitor biodistribution in tumors, mice were injected intravenously with 100 µg doxorubicin 2 h, prior to sacrifice. Tumor tissue was flash frozen and stored at −80 °C. For doxorubicin extraction tissue samples were homogenized by sonification in 9 parts water. Next 200 µl of the homogenate were transferred to a 2 ml collection tube and 50 µl 10% (v/v) Triton-X-100 and 750 µl acidified isopropanol (0.75 N HCl) were added. The mixture was vortexed briefly and doxorubicin was extracted overnight at −20 °C. The next day the samples were vortexed at RT and centrifuged at $20,000 \times$ g for 20 min at 4 °C. The amount of doxorubicin in tumor tissue was measured using the Victor$^{2\text{TM}}$1420 Multilabel Counter Wallac (λ_{ex}: 470 nm, λ_{em}: 590 nm). Measured values were corrected against a standard curve made by adding known amounts of doxorubicin to homogenized tissue of untreated mice.

3.6.4.3 Treatment study

For the treatment study LLC cells were implanted as described above (Section 3.6.4). Treatment of fully established tumors started on day 13 post implantation. Animals were treated with 5 mg/kg body weight (BW) doxorubicin at days 13, 15, 18, 20, 23 and 25 by intra peritoneal injection. Control animals received 100 µl 0.9% NaCl. Animals were monitored closely during the study and tumor size was measured every other day using a caliper. Tumor volume was calculated using Equation 3.2.

3.7 Statistics

For statistical analysis either GraphPad Prism 5 or Excel 2010 were used. For comparing two groups an unpaired t-test was applied. For correlation of vessel parameters with expression profiles the pearson correlation was used. For analysis and visualization of genomic data heat-maps the software Gitools 1.8.4 was used.

4 Results

4.1 Selection of mammary carcinoma samples

We included 18 mammary carcinomas of lobular and ductal origin in our study. All carcinoms had been staged according to the TNM system (Singletary et al., 2002) and graded on the stage of abnormality using the Nottingham grading system for breast cancer. This system grades breast tumors based on three features: tubule formation, nuclear grade and mitotic rate. The samples used in this study were graded G2 to G3. Estrogen receptor (ER), progesterone receptor (PR) and human epidermal growth factor receptor 2 (HER2) status of mammary carcinomas was classified according to the immunoreactive score (Remmele and Stegner, 1987). Patients from whom selected samples originated, had not received chemotherapy prior to tumor excision. All Samples were successfully stained for CD34, a marker of vascular endothelial cells and hematopoietic progenitors (reviewed in Nielsen and McNagny, 2008). Additionally, RNA yield had to be sufficient for downstream analysis. The selected mammary carcinomas and their characteristics are listed in Tab. 4.1. For further information on sample selection see Section 3.2.

Table 4.1: Selected mammary carcinomas and their characteristics. *Mammary carcinomas were staged according to the TNM system and hormone receptors were quantified according to IRS staging. ER: estrogen receptor; G: grade; IRS: immunoreactive score; L: invasion into lymphatic vessels; m: multiple foci of invasive carcinoma; N: regional lymph nodes, p: pathologic; PR: progesterone receptor; sn: sentinal node; T: primary tumor; X: not assessed*

Sample ID	Subtype	Stage					ER receptor status		PR receptor status		Her2 status
		Size [cm]	Tumor	Lymph node	Lymphatic invasion	Pathologic grading	pos. cells [%]	IRS score	pos. cells [%]	IRS score	
2937		2.8	pT2	pN0	L0	G2	> 80	8	> 90	9	neg. (0)
3189	Lobular	2.3	pT2	pN3a	L0	G2	> 80	12	20	4	neg. (0)
3190		1.3	pT1c	pN0	L0	G2	> 80	9	> 90	12	neg. (0)
3801		1.2	pT1c	pN0(sn)	-	G2	95	12	95	12	neg. (0)
4649	HER2	5.5	pT3	pN1c	-	G3	-	-	-	-	pos. (3+)
2849	enriched	4.3	pT2	pNX	L1	G3	-	-	-	-	pos. (3+)
1287		2.8	pT2	pN1a	L0	G3	-	-	-	-	neg. (0)
2774		2.5	pT2	pN0(sn)	L0	G3	-	-	-	-	neg. (0)
528	Basal-like	4.5	pT3,	pNX	L1	G2	10	2	-	-	neg. (1+)
4491		3.2	pT2	pN1(sn)	L1	G3	-	-	-	-	neg. (1+)
4783		2.7	pT2	pNX	L1	G2	-	-	-	-	neg. (1+)
624		3.5	pT2(m)	pN3a	-	G3	> 80	9	> 80	6	neg. (0)
738		1.4	pT1c	pN1(sn)	-	G2	> 80	12	70	9	neg. (0)
1888	Luminal A	2.9	pT2	pN1a p	pL1	G2	> 80	12	> 80	12	neg. (0)
3011		2.6	pT2	pN0	L0	G2	> 90	12	> 90	12	neg. (0)
3994		3.5	pT2	pN2	-	G2	> 80	12	> 80	12	neg. (0)
665	Luminal B	1.4	pT1	pT1 pN0(sn)	-	G2	> 80	9	> 80	12	pos. (2+)
5142		2.5	pT2(m)	pN2a	L1	G2	> 50	6	> 50	6	pos. (2+)

4.2 Development of techniques

A major part of this work was to establish various techniques such as immunostaining of tumor sections compatible with RNA extraction and processing, excision of endothelial cells (ECs) from stained mammary carcinoma samples by laser microdissection (LMD), RNA isolation from formalin fixed paraffin embedded (FFPE) tissue, and set up of primer multiplexes to generate expression profiles of angiogenic factors and endothelial transcription factors. For further details on these methods see Section 3.2.

4.2.1 Custom design of GeXP multiplex assays

In order to generate expression profiles of angiogenic factors of mammary carcinomas several custom GeXP multiplex assays were designed. This process involved several steps. First, each gene-specific primer pair was tested in a single-plex GeXP polymerase chain reaction (PCR) to ensure that only a single amplicon of the correct size was generated. For this we used a mix of RNA extracted from different celltypes, namely leukocytes, human umbilical cord endothelial cells (HUVEC), MCF-7 and MDA-MB-231. If the amplicon was not of the expected size, or no signal appeared at all, the primer pair was excluded from the multiplex. Next we analyzed the multiplex primer mixes. Each reverse multiplex primer mix was assembled by combining the reverse primers at 500 nM and each forward multiplex primer mix by combining the forward primers at 200 nM. Primers in one plex were designed to produce amplicons that differed in size by 3 nt to 7 nt, to allow for accurate signal detection. All sets contained primers for the detection of either β-2-microglobulin (B2M) or beta-actin (ACTB), which served as reference genes for normalization of signals. All primer sets were tested using cellular RNA as well as RNA isolated from FFPE samples. Several target genes yielded low signal peaks in the multiplexed GeXP assay. Consequently, gene-specific reverse primer concentrations were increased to improve detection of the respective mRNAs. Conversely, the reference genes approached the upper limits of linearity for accurate quantification. Thus gene-specific reverse primer concentrations were attenuated to reduce peak intensity. Table 4.2 shows three representative multiplexes for the detection of angiogenic factors. The final gene-specific reverse primer concentrations giving optimal detection of the gene panel set are listed with each designed multiplex. Additional multiplexes were established to detect the expression of transcription factors, markers of epithelial to mesenchymal transition and cell populations markers (see Supplement

Chapter 8).

Table 4.2: Primer sets for detection of angiogenic factors. *Final concentration of rv primer is included. Product size includes universal sequences needed for detection. rv: reverse*

	Gene name	Product [bp]	Concentration rv primer [nM]
Set 1	ACTB	123	7.8
	IL-8	132	62.5
	MCP-1	136	500
	ANGPT1	142	500
	IL-6	159	1000
	G-CSF	164	1000
	SDF1	173	500
	ANGPT2	177	500
	FGF-1	181	1000
	B2M	220	1000
Set 2	ACTB	123	7.8
	IP-10	132	62.5
	GROb	137	31.25
	GM-CSF	142	500
	TSP1	157	1000
	IL-12A	172	500
	B2M	220	1000
Set 3	ACTB	123	7.8
	VEGF-B	132	1000
	PDGF-A	137	500
	VEGF-A	141	62.5
	TGFB1	145	500
	HGF	149	1000
	PLGF	161	1000
	PDGF-B	167	1000
	FGF-2	173	1000
	VEGF-C	177	500
	EGF	181	1000
	B2M	220	1000

4.2.2 Identification of optimal RNA isolation techniques

Another important step for this work was the development of a method for RNA isolation from FFPE tissue, compatible with downstream processing. While fixation of tissue in formalin bears many diagnostic advantages it also leads to the degradation and chemical modification of RNA, making RNA isolation challenging. Thus we not only needed to find a method providing sufficient RNA yield and quality but also one compatible with the GeXP analysis system. Therefore we tested different amounts of sample input and the effects of staining of FFPE tissue on RNA yield, using commercially available kits from Epicenter® (QuickExtract™FFPE), MACHEREY-NAGEL (NucleoSpin®FFPE RNA/DNA), peqlab (KAPA Express Extract), SABiosciences (RT2 FFPE RNA) and QIAGEN (RNeasy FFPE). All products were specifically designed for the isolation of RNA from FFPE samples. To investigate whether sample thickness influenced RNA isolation, samples were cut in slices of 5 µm and 7.5 µm, respectively. As Fig. 4.1 A shows, there is hardly any difference in RNA yield concerning the thickness of slices for all tested kits. Yet there is a difference in the performance of the tested products. RNA yield was highest using the Epicenter® kit (11.6 µg/slide and 13 µg/slide), followed by SABiosciences (1.9 µg/slide and 2.5 µg/slide). The QIAGEN kit yielded only about half as much RNA (1.2 µg/slide and 1.1 µg/slide) and performance of the peqlab kit was poorest with only a quarter of the yield of SABiosciences (565 ng/slide and 438 ng/slide). To investigate whether RNA quality was adequate for downstream processing we used the GeXP System to amplify a short (123 bp) and a long (230 bp) fragment of ACTB. RNA isolated using the QIAGEN and the SABiosciences kit gave a strong signal for the amplified 123 bp ACTB compared to the other kits (Fig. 4.1 B top). Yet with regard to the 230 bp fragment, only the SABiosciences kit gave satisfying results (Fig. 4.1 B bottom).
Since some of the RNA used in this study would be isolated from stained samples we wanted to know how this procedure would affect RNA yield and quality. As shown in Fig. 4.1 C, staining reduced RNA yield by about 100 ng/slide for both the QIAGEN kit (from 327 ng/slide to 229 ng/slide) and the MACHEREY-NAGEL kit (from 152 ng/slide to 66 ng/slide). Despite the decline of RNA yield, the quality of RNA isolated from stained FFPE samples was still sufficient for downstream analysis. As the first six bands on the agarose gels in Fig. 4.1 D show, amplification of shorter fragments was easily achieved regardless of staining. Yet only RNA isolated from stained samples

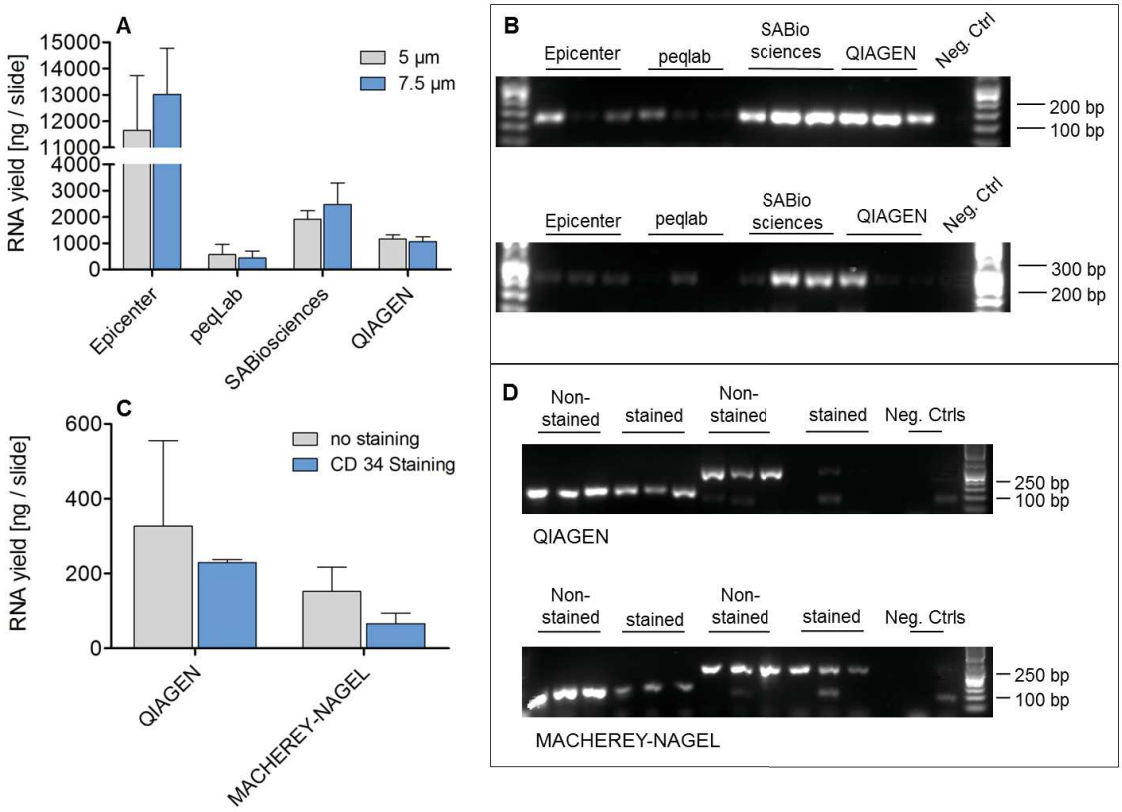

Figure 4.1: Yield and quality of different RNA isolation methods for FFPE samples. *(A) RNA yield differed between kits but was independent of thickness of sample slice. (B) Quality of isolated RNA was best using SABiosciences and QIAGEN kits. For amplification of longer RNA fragments performance of SABiosciences was superior. (C) RNA yield was reduced due to staining of samples. (D) Quality of RNA isolated from stained tissue was superior using the MACHEREY-NAGEL kit for amplification of the* 230 bp *fragment.* $n = 3$

with the MACHEREY-NAGEL kit gave strong bands for the 230 bp fragment (last three bands on lower gel). Based on these preliminary experiments we decided to use the NucleoSpin® FFPE RNA/DNA kit by MACHEREY-NAGEL for our study. While working with our actual samples we surprisingly noticed that for some mammary carcinomas RNA yield was too low for the assessment of tumor expression profiles. Thus we decided to include a RNA-amplification step into our workflow. Even though this amplification step improved RNA quantity, quality of RNA isolated with the NucleoSpin® FFPE RNA/DNA kit was not sufficient for proper analysis of gene expression. Finally, we chose to test the Agencourt® FormaPure® kit for the isolation of RNA. Beckman

Coulter recommended this kit for the analysis of RNA isolated from FFPE samples with their GeXP analysis system. As Tab. 4.3 demonstrates, use of the Agencourt®

Table 4.3: Comparison of RNA quantity and quality using the NucleoSpin® or the Agencourt®FormaPure® kit.

		NucleoSpin®			Agencourt®FormaPure®		
Sample ID	Subtype	RNA conc. [ng/µl]	RNA purity 260/280	260/230	RNA conc. [ng/µl]	RNA purity 260/280	260/230
2937		16.5	2.0	0.8	153.2	2.0	1.5
3189	Lobular	16.8	2.1	1.8	177.7	2.0	1.2
3190		9	2.2	1.8	17.4	2.1	1.1
3801		7.7	2.3	0.5	9.1	2.1	1.0
4649	Her2	49.2	2.1	1.4	67.5	2.0	1.6
2849	enriched	-	-	-	96.6	2.2	1.1
1287		8.7	2.5	0.5	231.8	1.9	1.5
2774		17.1	1.9	0.7	71.6	2.1	2.0
528	Basal-like	16.7	1.9	1.4	48.6	1.9	1.1
4491		33	1.6	0.5	200.9	2.0	2.0
4783		-	-	-	68.1	2.0	1.8
624		94.7	2.0	0.1	183.5	2.0	2.0
738		19.3	1.9	1.2	68.3	1.9	1.0
1888	Luminal A	62.7	2.1	0.9	74.9	1.8	1.5
3011		-	-	-	28	2.2	1.5
3994		37.2	2.0	1.2	63.9	2.0	1.4
665	Luminal B	11.7	1.8	0.9	116.9	2.0	1.6
5142		7.8	1.8	1.2	94.6	2.0	1.77

FormaPure® kit increased RNA concentration by factor two at the least, while the elution volume remained constant at 20 µl. RNA purity, according to 260/230 ratio, also increased for most samples (260/230 values are commonly in the range of 2.0 - 2.2), while the 260/280 ratio remained steady (a ratio of 2.0 is generally accepted as "pure" for RNA). Due to this improvement we were able to increase the RNA input into the GeXP system from 12.5 ng to 37.5 ng. Consequently signal intensity was improved and expression of previously undetectable genes could be analysed.

4.2.3 Microdissection of tumor vessels

Another technique we established was the dissection of tumor vessels from the FFPE mammary carcinomas by laser. For this method 5 µm thick sections of mammary carcinomas were placed on steel-frame slides with polyphenylene sulfide (PPS) membrane. These slides allow for the tissue to be dissected by laser, and collected in tubes (Fig. 4.2). After the tissue had been cut by the laser, the sample fell into the cap of a 0.2 ml collection tube containing a drop of lysis buffer.

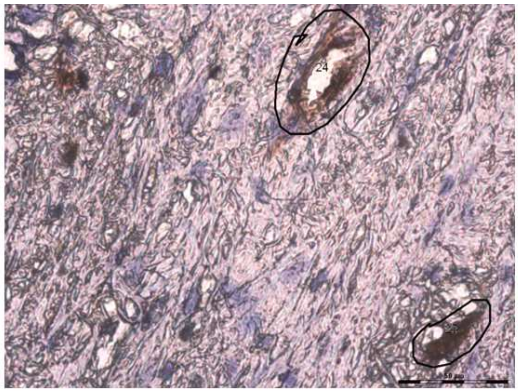

CD34 stained tissue before dissection

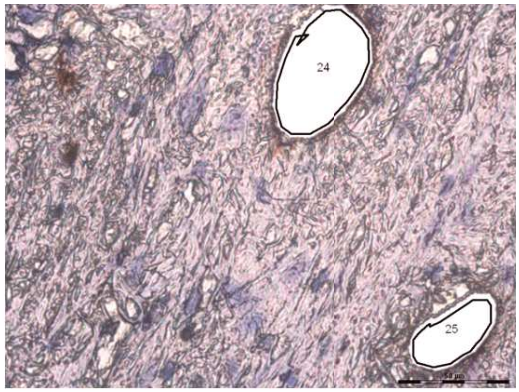

CD34 stained tissue after dissection

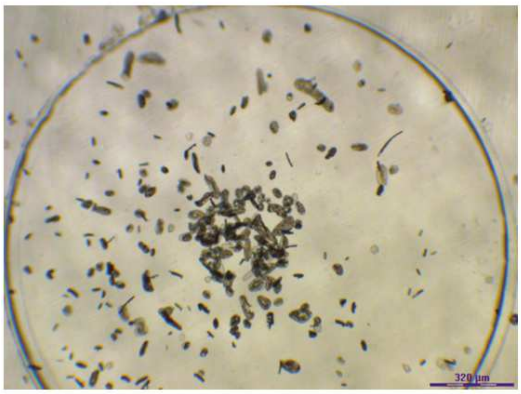

Dissected vessels in the cap of a collection tube

Figure 4.2: Laser microdissection of endothelial cells. *Tissue was cut to* 5 µm *thick slices and placed on steel-frame slides with PPS membrane. Endothelial cells were selected manually (top left) and dissected with a laser (top right). The dissected cells fell into the cap of collection tube (bottom) containing a drop of lysis buffer.*

In order to identify ECs, the samples were stained for CD34. We dissected about 1000 vessels or as many as we were able to identify from each of the ductal mammary carcinomas. These vessels were collected for later RNA isolation and expression profiling. Number and area of dissected fragments were documented automatically by the LMD6500. Only stained areas that had the characteristic morphology of vessels were excised. The quality of staining differed greatly between samples. Even though tumor vessels could be clearly identified in samples placed on superfrost slides, identification was difficult on PPS membrane. This, as well as a limitation of available tissue, led to a low yield for some samples (Tab. 4.4). Interestingly, for mammary carcinomas of the luminal A subtype dissection of around 1000 vessels was easily achieved. For individual samples (samples number 4649, 4491, 2774 and 665) of the other three subtypes (Her2-enriched, basal-like and luminal B) this was not possible. In the group of

basal-like tumors, dissection of 1000 vessel was not achieved for any of the samples. Interestingly, even while the number of dissected vessels and area were low, RNA yield was comparatively high (see samples 4649, 2774 and 665). RNA yield of dissected vessels ranged from 1 ng to 52 ng and RNA purity was poor.

Table 4.4: Number and area [mm^2] of dissected vessels and obtained RNA yield.

Sample ID	Subtype	Vessel number	Dissected area [mm^2]	RNA yield [ng]
4649	Her2 enriched	399	0.253	15
2849		981	0.794	14
2774	Basal-like	728	0.626	36
528		819	0.881	17
4491		545	0.296	1.0
624	Luminal A	1453	1.749	52
738		1100	0.789	30
1888		984	1.243	17
3011		939	0.936	30
3994		1087	0.909	14
665	Luminal B	675	0.649	36
5142		1152	0.857	4.0

Since the LMD6500 records the size of the dissected objects, we were able to take a look at the distribution of vessel size of mammary carcinomas subtypes.
As Tab. 4.5 shows, there was a great heterogeneity among vessel size of mammary carcinoma samples, regardless of subtype. Between 10.6% (luminal A) and 30.9% (Her2 enriched) of harbored vessels were smaller than 500 µm^2 (Fig. 4.3), and between 65,6% (Her2 enriched) and 44.4% (luminal A) measured between 500 and 1000 µm^2, thus accounting for most of the tumors' vessels. Objects larger than 1000 µm^2 only made up around 20% of total vessels in Her2 enriched, basal-like and luminal B carcinomas. On the contrary, about twice as many vessels (45.3%) larger than 1000 µm^2 were dissected from carcinomas of the luminal A subtype. In general tumors of the luminal A subtype showed a higher percentage of vessels with an area greater than 1000 µm^2 compared to the other three groups. Especially sample 1888 had a high percentage of larger vessels (82.5%).

Table 4.5: Classification of laser dissected fragments according to recorded area.

Sample ID	Subtype	% of dissected vessels [µm²] <500	500-1000	>1000
4649	Her2 enriched	40.3	48.5	11.1
2849		12.2	59.3	28.4
2774	Basal-like	16.9	36.5	46.6
528		14.5	63.9	21.6
4491		43.8	46.8	9.4
624	Luminal A	4.5	47.9	47.6
738		26.9	58.9	14.2
1888		1.2	16.3	82.5
3011		5.0	36.6	58.4
3994		14.1	62.1	23.8
665	Luminal B	15.0	55.0	30.1
5142		21.4	63.9	14.7

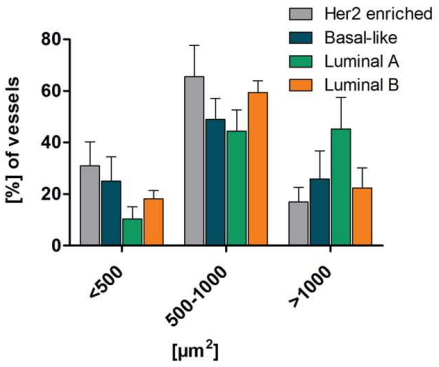

Figure 4.3: Classification of area of laser dissected fragments. *Area of dissected fragments did not differ between tumor subtypes.*

Next, we confirmed the identity of the excised microvessels. To distinguish between different cell populations we used custom multiplexes with primers for cell population marker genes. For a detailed description of the multiplexes of cell population markers see Supplement Chapter 8. Figure 4.4 shows electorpherograms corresponding to gene expression profiles generated of total RNA of a mammary carcinoma (top) and of dissected ECs (bottom) of that same tumor. Each blue fragment peak depicts a gene of interest. Amplicons are resolved based on length, measuring between 131 nt and 225 nt. B2M is included in two different sizes (131 nt and 223 nt) as a reference gene. The longer B2M amplicon is included to verify the amplification of longer RNA fragments in FFPE samples, as fixation in formalin degrades RNA.
Comparing the electorpherogram of the mammary carcinoma to that of the excised ECs, differences in gene expression are clearly visible. In the dissected tissue we detected CD34, smooth muscle actin (SMA), platetlet-derived growth factor-(PDGFR)B, CD11B and CD68. CD34 is a marker for ECs, SMA and PDGFRB are marker for pericytes, and CD11B as well as CD68 marker for leukocytes. In addition we detected estrogen receptor 1 (ESR1), collagen 6-α (COL6A) and N-cadherin (CDH2) in the RNA isolated from the FFPE mammary carcinoma but neither CD68 nor CD34. Both expression profiles exhibit two peaks corresponding to B2M at about 131 nt and 223 nt, showing that amplification of longer RNAs was successful.

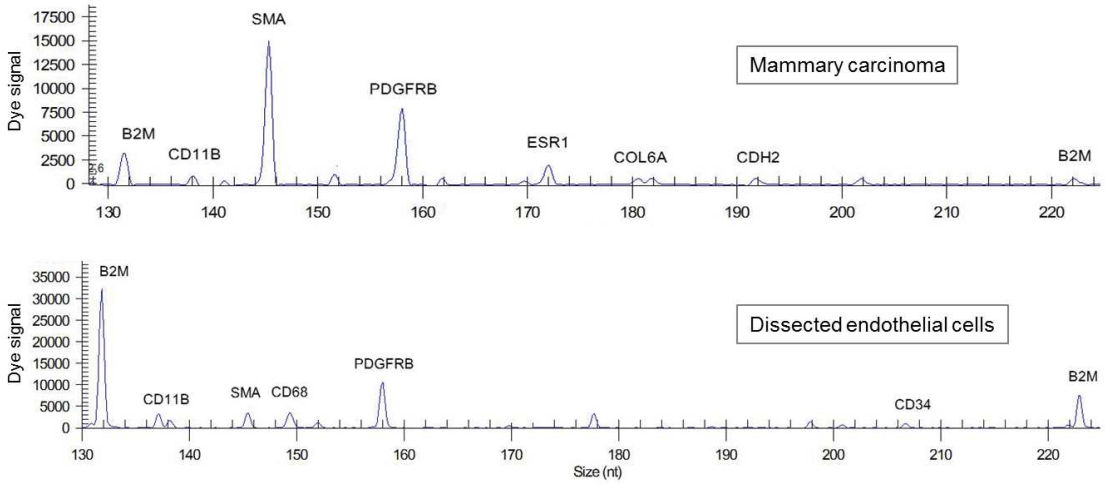

Figure 4.4: Electropherograms corresponding to expression profiles of a mammary carcinoma and excised endothelial cells. *Blue fragment peaks correspond to genes of interest. B2M served as a reference gene. The genes detected in the sample of dissected cells are markers for endothelial cells (CD34), pericytes (SMA and PDGFRB) and leukocytes (CD11B and CD68). In addition we detected ESR1, COL6A and CDH2 in the FFPE mammary carcinoma. B2M: β-2-microglobulin; CDH2: N-cadherin; COL6A: Collagen 6-α; ESR1: Estrogen receptor 1; nt: nucleotide; PDGFRB: Platelet-derived growth factor-β receptor; SMA: Smooth muscle actin.*

These results demonstrate that we were able to dissect an adequate number of ECs for subsequent RNA isolation, and that RNA quality was sufficient for expression profiling. In addition, it shows the ability to differentiate between cell types using our custom multiplexes.

Altogether, we developed a workflow for FFPE sample staining, RNA isolation from stained and non-stained FFPE samples and for downstream analysis. We applied these methods to prove the dissection of ECs from mammary carcinomas.

4.3 Vascular parameters of mammary carcinomas

We investigated whether differences in the vessel morphology of HER2 enriched, basal-like, luminal A and luminal B ductal mammary carcinomas as well as lobular mammary carcinomas existed. Therefore we assessed vascular parameters such as vessel area (%CD34 positive area), average vessel size, microvessel density (MVD) and circularity of microvessels in CD34 stained tissue sections.

The percentage of area that stained positive for CD34 varied greatly among individual samples (Fig. 4.5 A). It lay between 0.26% (sample 3801) and 2% (sample 1287). If the data was combined for the five subtypes, it was more alike (Fig. 4.5 B). In the basal-like and the luminal A and luminal B tumors, vessels made up around 1.2% of total tissue. In lobular and Her2 enriched carcinomas vessel area was lower, 0.86% and 0.76%, respectively. The average vessel size was also very heterogeneous among

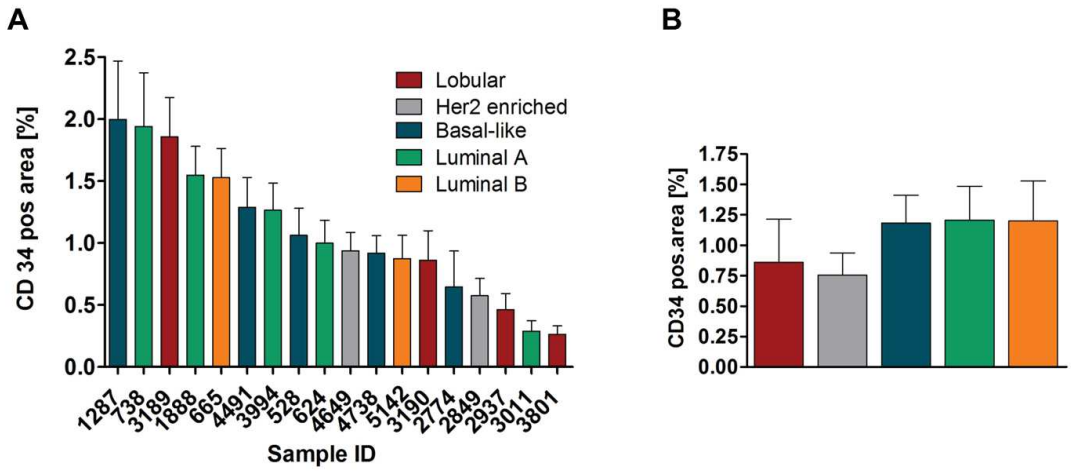

Figure 4.5: Percentage of CD34 positive area in mammary carcinomas. *(A) CD34 positive area of mammary carcinomas varied highly between individual samples (B) but less between subtypes.*

individual samples (Fig. 4.6 A). The measured vessel size ranged from 45 μm^2 (sample 528) to 173 μm^2 (sample 3011). Tumor vessels were larger in luminal A (213 μm^2), luminal B (247 μm^2) and the basal-like (208 μm^2) tumors, whereas average vessel size was 122 μm^2 in lobular and 96 μm^2 in Her2 enriched carcinomas (Fig. 4.6 B).

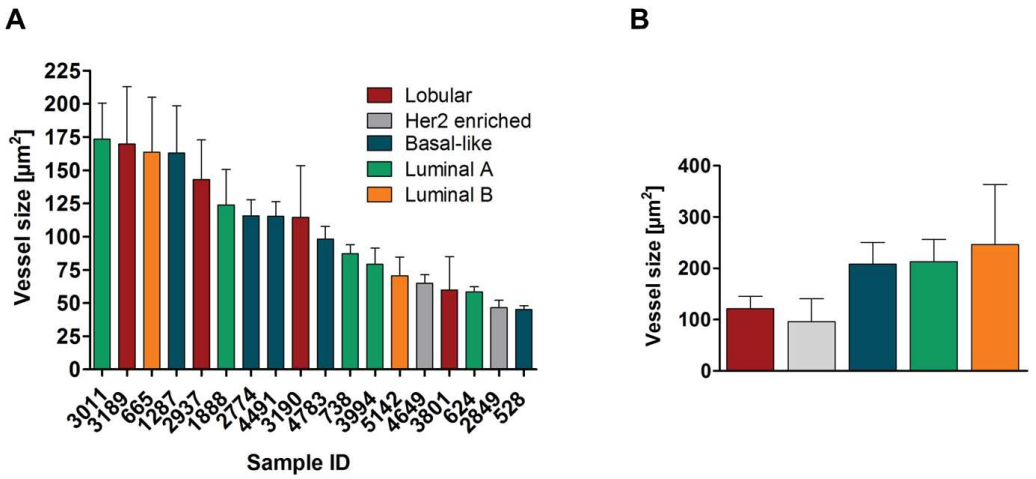

Figure 4.6: Size of vessels in mammary carcinomas. *(A) Vessel size in mammary carcinomas varied strongly between individual samples (B) but less between subtypes.*

MVD was also inhomogeneous across samples of a specific subtype (Fig. 4.7 A). While sample 1888 had a density of 10.8 vessels/mm^2 on average, sample 4491 showed 36.8 vessels/mm^2. The highest MVD was found for Her2 enriched (22.2 vessels/mm^2) and luminal B carcinomas (22.4 vessels/mm^2), followed by luminal A and basal-like tumors with 20.7 and 20.4 vessels/mm^2, respectively. With a density of 16.7 vessels/mm^2, lobular carcinomas showed the lowest MVD of all groups (Fig. 4.7 B).

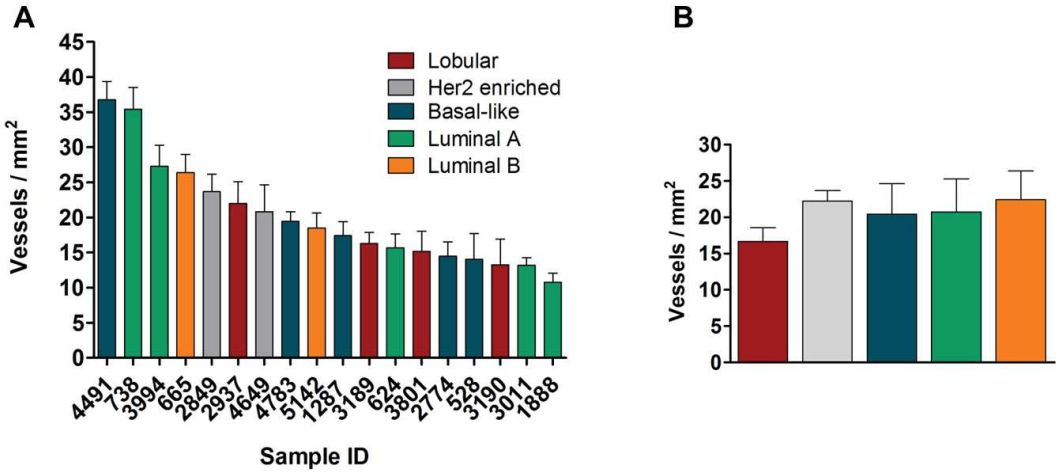

Figure 4.7: Microvessel density in mammary carcinomas. *(A) Microvessel density in mammary carcinomas varied highly between individual samples (B) but less between subgroups.*

The vessel circularity index depicts the roundness of vessels. Values range from 0 to 1, where 1 indicates a perfect circle. The mean values for individual samples lay between 0.58 (sample 2849) and 0.70 (sample 4649), both belonging to the Her2 enriched subtype (Fig. 4.8 A). Looking at the different subtypes, vessel circularity varied only slightly and lay between 0.64 in the Her2 enriched subtype and 0.66 in the other four subtypes (Fig. 4.8 B).

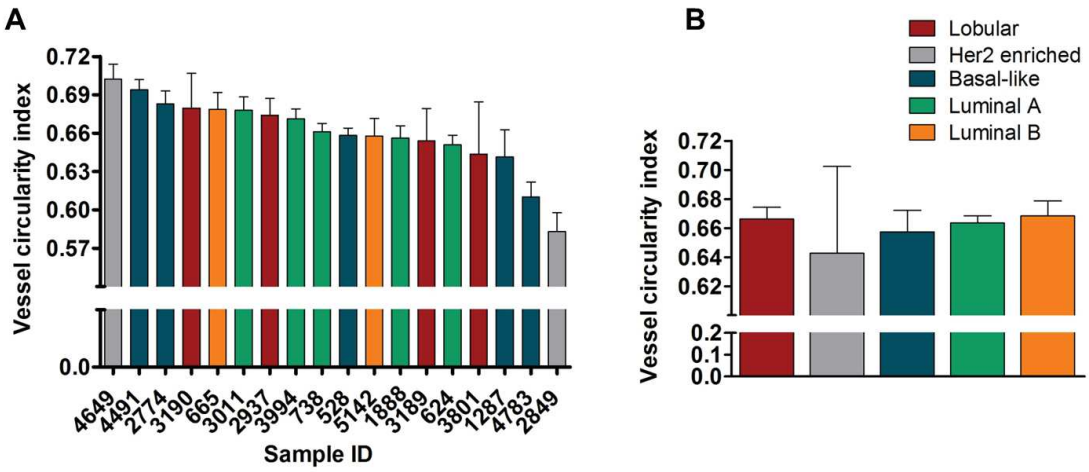

Figure 4.8: Circularity index of vessels in mammary carcinomas. *(A) Circularity of vessels in mammary carcinomas samples varied only slightly between individual samples (B) and hardly at all between subgroups.*

Altogether, strong differences of CD34 positive area, average vessel size, MVD and circularity were observed between individual tumors. However, these strong variations did not correlate with tumor subtypes, indicating that individual differences in molecular characteristics but not affiliation with a molecular subclass, determine vessel characteristics in breast tumors. Also, no general difference between lobular carcinomas, which originate from the milk-producing lobules, and the four subtypes of ductal carcinomas, which originate from the milk-carrying ducts, were found. Yet vessel area and size in Her2 enriched carcinomas seemed to be rather similar to those of lobular carcinomas than to those of the other three ductal subtypes. Respective to all parameters, three subtypes (luminal A and B and basal-like) tended to show a similar vessel morphology. Of all parameters vessel size was most dissimilar and circularity was most similar.

4.4 Correlation of histological parameters with angiogenic factors

Next, we investigated the expression of tumor and tumor microenvironment derived angiogenic factors in the mammary carcinomas. For this purpose we used the three custom-made primer multiplexes shown in Tab. 4.2, which contained pro- and anti-angiogenic factors. Overall, expression profiles showed a heterogeneous pattern regarding the four tumor subtypes investigated (HER2 enriched, basal-like, luminal A and B). In HER2 enriched tumors, inhibitors of angiogenesis such as the chemokines IP-10 and GROb, colony stimulating factor 2 (GM-CSF), thrombospondin 1 (TSP-1) and interleukin-12A (IL-12A) were expressed in lower levels relative to the other subtypes. This is surprising, as we discovered slightly smaller vessels and a smaller percentage of CD34 positive area in these tumors, compared to the other subtypes (see Fig. 4.6 B and 4.5 B). Yet HER2 enriched tumors also showed a lower expression of some proangiogenic factors such as the MCP-1, ANGPT-1 and -2, VEGF-A and -B and FGF-1 (for complete data see Tab. 8.5 to 8.7 in Supplement 8).

Finally we combined the expression data of tumor and tumor microenvironment derived angiogenic factors with the data from the histological analysis of the tumor vasculature (microvessel density, area, size and circularity), to discover any interdependence of tumor-, stroma-, and immune cell derived factors and resulting vessel types. In mammary carcinomas of the subtype luminal A two growth factors were correlated with vessel area and one with vessel size. Expression of PDGF-B ($p = 0.036$; Fig. 4.9 B) as well as that of VEGF-A ($p = 0.031$; Fig. 4.9 D) was inversely correlated with the vessel area. As Fig. 4.9 A and C show, this was not observed for the entire set of mammary carcinomas (PDGF-B: $p = 0.602$; VEGF-A: $p = 0.208$). Both VEGF-A and PDGF-B are inducers of angiogenesis. In addition the expression of the anti-angiogenic cytokine IL-12A was positively correlated with the size of tumor vessels (Fig. 4.9 F). Again this was not observed for the entire sample set (Fig. 4.9 E; $p = 0.137$).

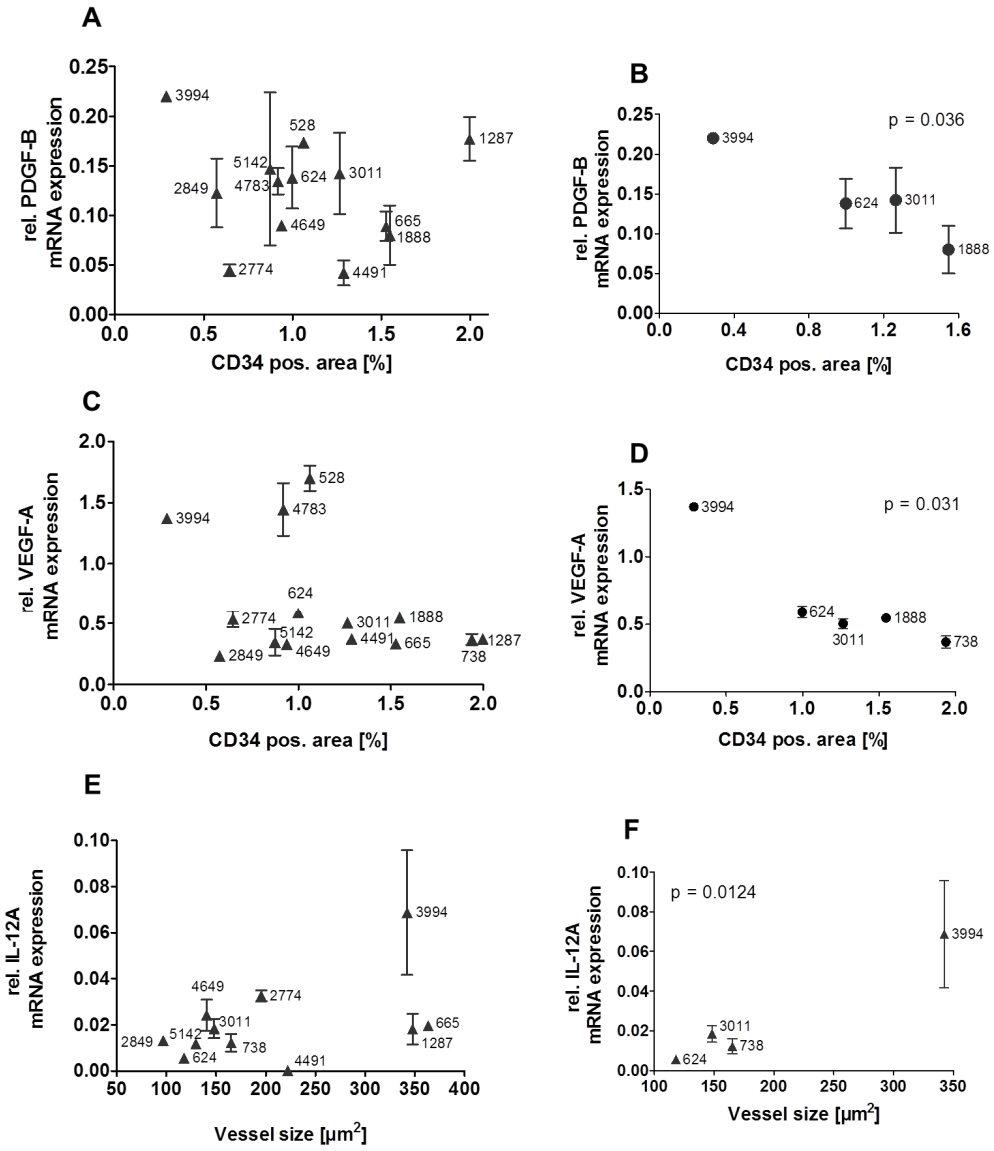

Figure 4.9: Correlation of histological parameters with expression of angiogenic factors. *In samples of the luminal A subtype, CD34 positive area was inversely correlated with the expression of PDGF-B (B) and VEGF-A (D). (A and C) No such relation existed for all samples. (F) In the luminal A subtype, vessel size was also correlated with the expression of IL-12A. (E) Again no such relation existed for all samples. Numbers indicate sample ID. Error bars: ± SEM.*

Neither MVD nor circularity were correlated with the expression of any angiogenic factors in any sample subgroup.

4.5 Stimulation of HUVEC with growth factors

The response of ECs to angiogenic signals is regulated by transcription factors, which control different processes during vascularization. We investigated how treatment with epidermal growth factor (EGF), fibroblast growth factor (FGF)-2, hepatocyte growth factor (HGF), insulin-like growth factor (IGF), PDGF-B, stromal-cell derived growth factor (SDF) or VEGF-A influenced the expression of various transcription factors in ECs. For this purpose HUVECs were starved for 16 h and subsequently incubated with 20 ng/ml of a certain growth factor. Interestingly, treatment with EGF, FGF-2,

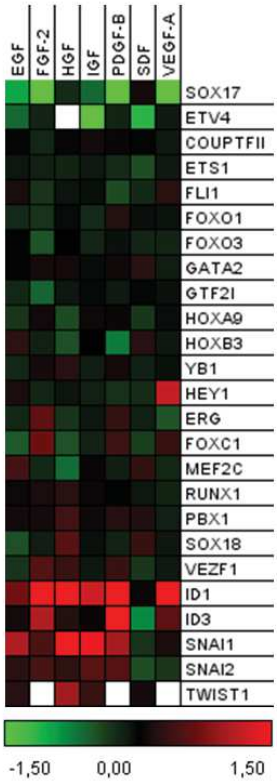

Figure 4.10: Heatmap of gene expression of transcription factors. *Green indicates repressed mRNA levels, red elevated levels and white no data. Intensities are normalized for each gene. Stimulation of HUVEC with growth factors leads to the up-regulation of the transcription factors ID1 and ID3 as well as SNAI1 and SNAI2 and TWIST1.*

HGF, IGF and PDGF caused up-regulation of genes coding for the transcription factors SNAI1, SNAI2 and TWIST1 (Fig. 4.10). These transcription factors are involved in

epithelial to mesenchymal transition. *SNAI1* mRNA levels were the most elevated after stimulation with EGF, HGF, IGF and PDGF. A weaker effect was observed due to stimulation with FGF-2 and VEGF-A. Expression of *SNAI2* was less pronounced and not observed after treatment with SDF and VEGF-A. Detectable levels of *TWIST1* mRNA were measured after the stimulation of HUVEC with EGF, IGF, HGF and SDF.

Interestingly, we also found elevated levels of Inhibitor of DNA binding (ID) 1 and 3. *ID1* mRNA expression was up-regulated by all growth factors. mRNA levels of *ID3* were less elevated and a down-regulation was observed after stimulation with SDF. ID1 and ID3 are regulators of the basic helix-loop-helix (bHLH) family. They form heterodimers with bHLH transcription factors, such as TWIST1, and inhibit DNA binding. These findings encouraged us to further investigate the role of Snai1 in tumor vessels in animal studies.

4.6 Animal studies

4.6.1 Generation of mice

We investigated the influence of the knockdown of the transcription factor SNAI1 in tumor ECs. Mice showing tissue specific excision of *Snai1* were generated by using the Cre-loxP system. For the experiments we used mice with heterozygous knockdown of *Snai1* in ECs. To obtain the transgenic mouse line for our studies, the B6;129S-*Snai1*^{tm2Grid}/J strain was first backcrossed to the C57BL/6 background for seven generations. Next these mice were crossed with the B6.Cdh5-cre strain as shown in Fig. 3.2 to create the mouse strain B6.Cdh5-cre;B6.Snai1$^{fl/+}$ (Snai1$^{fl/+}$). This strain exhibits heterozygous knockdown of the transcription factor SNAI1 specifically in ECs. The B6.Cdh5-cre;B6.Snai1$^{+/+}$ (Snai1$^{+/+}$) control mice were wild-type (wt) littermates for *Snai1* and still expressed the transcription factor in all cells. To differentiate between mice, offspring was always genotyped.

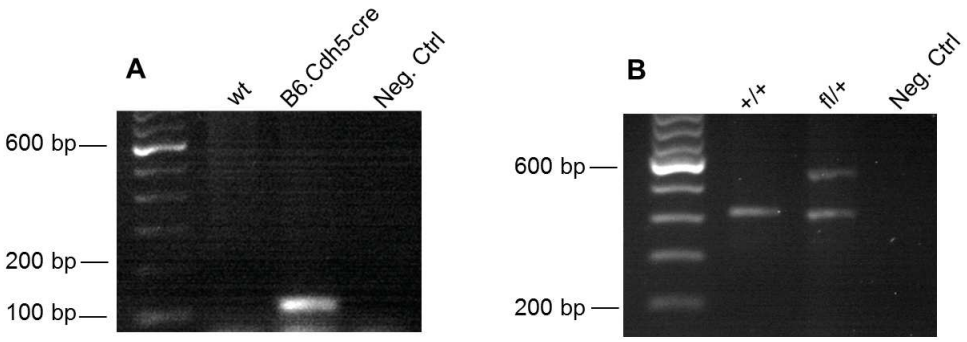

Figure 4.11: PCR genotyping results. *PCR was performed on DNA obtained from ear punches. (A) PCR results to differentiate wt from Cre mice. A band at* 100 bp *corresponds to the Cre transgene. (B) PCR results to differentiate Snai1*$^{+/+}$ *from Snai1*$^{fl/+}$ *mice. A band at* 394 bp *corresponds to the wt allele, one at* 480 bp *to the floxed allele. Water was used as negative control. PCR: Polymerase chain reaction; wt: wild-type; fl: floxed.*

While the B6.Cdh5-cre strain showed the Cre transgene at about 100 bp (Fig. 4.11 A), wt animals did not carry it. Wild-type mice (+/+) carried *Snai1* alleles at 394 bp, while alleles in floxed (fl/fl) mice are slightly larger (480 bp). Hence heterozygotes (+/fl) show alleles at 394 bp and 480 bp respectively (Fig. 4.11 B).

After generating the Snai1$^{fl/+}$ and Snai1$^{+/+}$ mice for the following experiments, the expression of Cre recombinase in ECs was verified. As Fig. 4.12 shows Cre recombinase was detected in tumor vessels but not in the surrounding tissue.

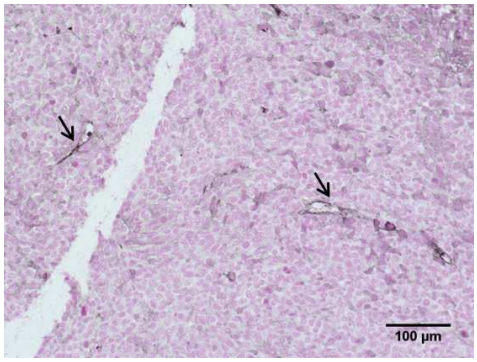

Figure 4.12: Staining of LLC tumor tissue for Cre recombinase. *The active enzyme was detected in tumor vessels but not in the surrounding tissue. Arrows indicate blood vessels. LLC: lewis lung carcinoma.*

4.6.2 Tumor growth studies

To investigate whether knockdown of *Snai1* in ECs had an effect on tumor growth and tumor microvessels, we conducted studies using three different tumor models. In female mice either the murine breast cancer cell line E0771 was implanted into the mammary fat pat, or the melanoma cell line B16-F10 was injected subcutaneously into the dorsal region close to the hind limb. In a third study, lewis lung carcinoma cells (LLC) were injected subcutaneously in the dorsal region close to the hind limb of male mice. Tumor growth was monitored every other day.
E0771 tumors seemed to grow faster in floxed mice, yet this observation was not statistically significant due to a low take rate in both groups (Fig. 4.13 A), and no significant difference in tumor weight after excision on day 28 was observed (Fig. 4.13 D). Growth of B16-F10 melanomas was increased significantly in knockdown animals compared to the control group (Fig. 4.13 B). After excision on day 17, tumor weight was also increased ($p = 0.0432$; Fig. 4.13 E). In the LLC tumor model no difference in tumor volume or weight after excision on day 28 between study groups was observed (Fig. 4.13 C and F).

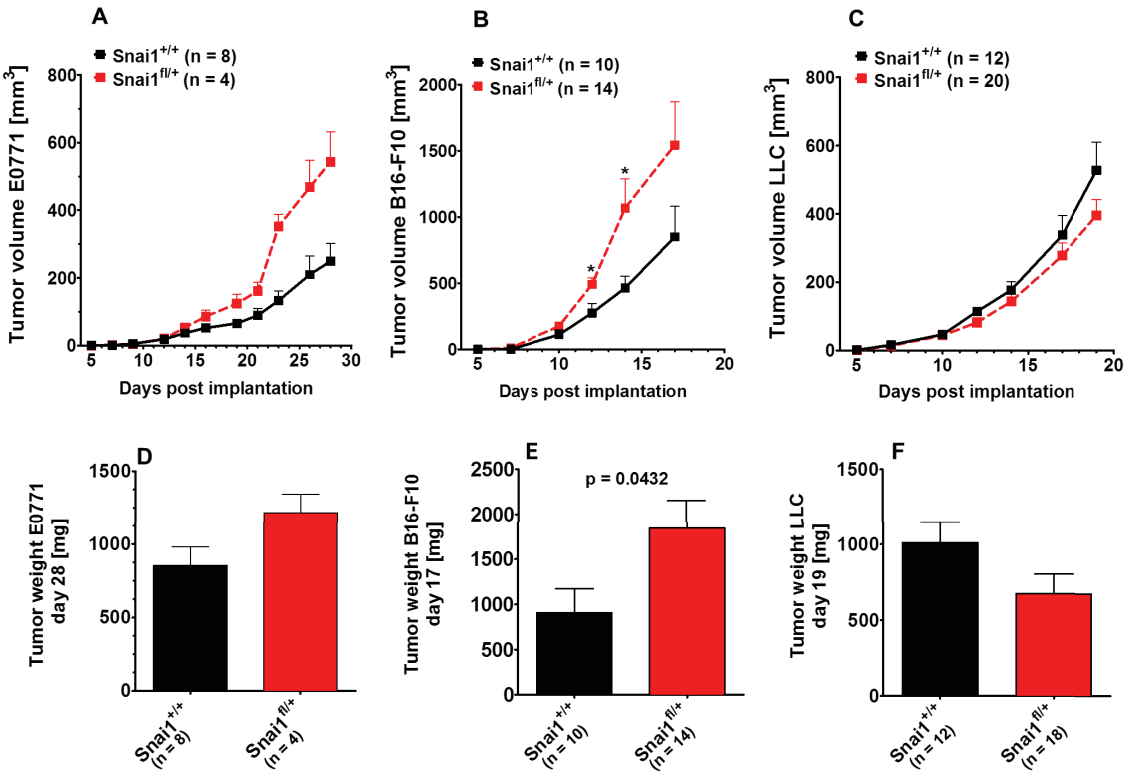

Figure 4.13: Growth of E0771, B16-F10 and LLC tumors. *E0771 or B16-F10 were implanted in Snai1$^{fl/+}$ and Snai1$^{+/+}$ female mice. LLC were implanted into male mice. (A and D) In the E0771 tumor model, heterozygous knockdown of Snai1 in ECs showed no effect on tumor growth. (B and E) In the B16-F10 tumor model, heterozygous knockdown of Snai1 in ECs increased tumor growth and weight significantly. (C and F) In the LLC tumor model heterozygous knockdown of Snai1 in ECs caused no difference in tumor growth. LLC: lewis lung carcinoma. Error bars: ± SEM; ∗ indicates $p \leq 0.05$.*

To examine whether tumors' vasculature was affected by *Snai*1 knockdown, excised B16-F10 melanomas and LLCs were fixed in formalin and stained for CD34. In the B16-F10 melanomas, study groups differed neither in vessel area (Fig. 4.14 A) nor in MVD (Fig. 4.14 B). Another distinction of the B16-F10 tumors was the observation of areas of necrosis.

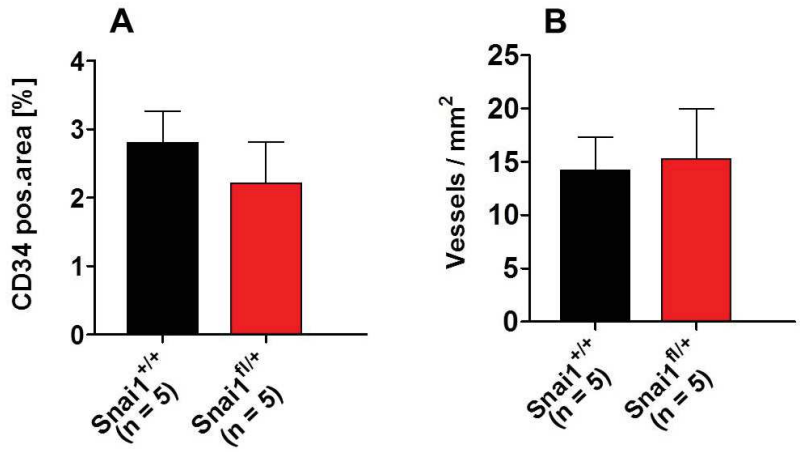

Figure 4.14: Microvessels in B16-F10 melanomas. *Quantification of vessels via immunostaining for the endothelial marker CD34 revealed no difference in (A) vessel area and (B) microvessel density due to heterozygous knockdown of Snai1. Error bars: ± SEM.*

To monitor biodistribution in tumors, mice were injected intravenously with doxorubicin 2 h prior to sacrifice. Doxorubicin is an anthracycline, which either leads to formation of double-stranded breaks of DNA or intercalates directly with DNA. Fluorescent quantification of extracted doxorubicin showed that deposition of doxorubicin had doubled in knockdown animals, compared to controls ($p = 0.0175$; Fig. 4.15 A). Knockdown animals showed an increase of MVD ($p = 0.0381$; Fig. 4.15 B) and of vessel area ($p = 0.0147$; Fig. 4.15 C). CD34 staining revealed a better vascularization in tumor tissue of floxed animals (Fig. 4.15 D and E). These experiments show that knockdown of *Snai1* in ECs in the LLC tumors significantly improved the tumors' vasculature and consequently biodistribution of the chemotherapeutic doxorubicin.

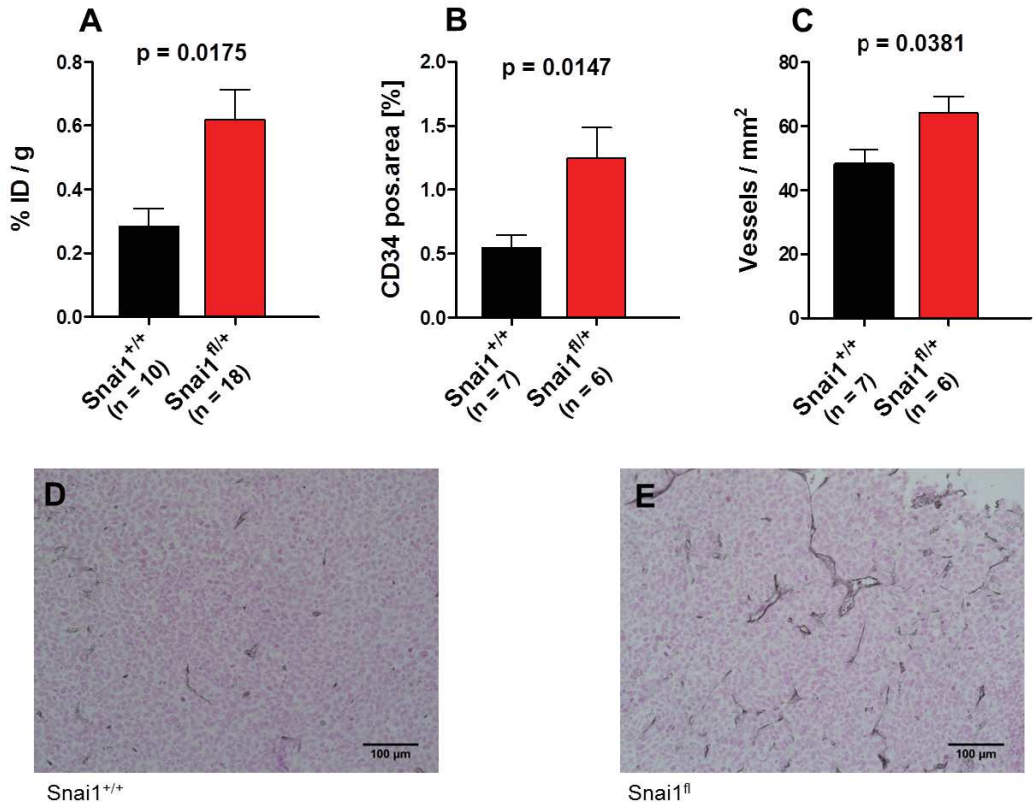

Figure 4.15: Biodistribution of doxorubicin and microvessels in LLC tumors. *(A) Knockdown mice showed an increased deposition of doxorubicin. (B and C) Quantification of vessels revealed an increase of (B) vessel area and (C) microvessel density in tumors grown in knockdown mice. (D and E) Immunostaining for the endothelial marker CD34. ID: injected dose; LLC: lewis lung carcinoma. Error bars: ± SEM.*

We also examined the expression of markers of hypoxia in tumors. In hypoxic regions of tumors several hypoxia-inducible genes are upregulated through hypoxia-inducible factor (HIF)-1. Among others, these target genes include angiogenic factors, glycolytic enzymes and glucose or lactate transporters. Carbonic anhydrase IX (CAIX) is an enzyme that assists rapid inter-conversion of carbon dioxide and water into carbonic acid, protons and bicarbonate ions. HIF-1 is the essential transcription factor of the *Ca9* gene, driving its transcription in response to intratumoral hypoxia (Wykoff et al., 2000). Glucose transporter-1 (GLUT-1) is another marker of hypoxia. Tumors frequently show overexpression of the hypoxia responsive GLUT-1 as they increase their glucose uptake (Airley et al., 2001). Furthermore, hypoxia stimulates VEGF-A protein expression. In E0771 tumors, selective knockdown of *Snai1* in ECs led to a decrease

of the mRNA levels of *Ca9*, *Glut-1* and *Vegfa*. This hints that tumors in knockdown animals were less hypoxic than controls. Changes of mRNA levels in B16-F10 melanomas and LLCs were minor and the knockdown seemed to have little effect on hypoxia (Fig. 4.16).

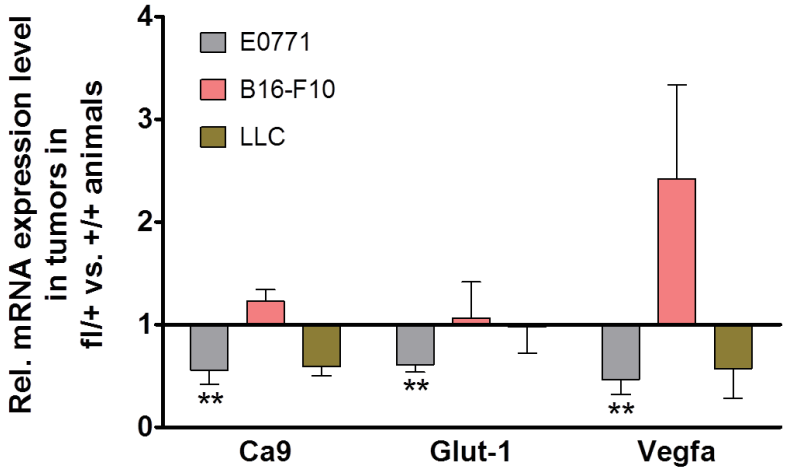

Figure 4.16: Expression of biomarkers of hypoxia in tumor tissue. *Excised tumors were frozen and RNA was extracted using TRIzol® reagent. Expression profiles of tumors were generated using the GenomeLab™GeXP Genetic Analysis System. mRNA expression was measured in triplicate in four tumors, respectively. Error bars: ± SEM; ∗∗ indicates $p \leq 0.01$.*

4.6.3 Treatment of LLC with Doxorubicin

To investigate the influence of *Snai1* knockdown in ECs on the effectiveness of drug therapy, established LLCs were treated with doxorubicin. Doxorubicin is an extensively used chemotherapeutic, that shows antitumor activity against a wide range of cancers. Yet dosage is limited as this anticancer drug is also cardiotoxic. A number of mechanisms have been proposed for the cytotoxicity of doxorubicin. A likely mechanism of action is the stabilization of topoisomerase II-DNA complexes or the formation of doxorubicin-DNA adducts (reviewed in Cutts et al., 2005).
Animals were divided into four groups. One group of wt and one of fl/+ animals was treated with 5 mg/kg body weight (BW) doxorubicin. The other two groups (one wt and one fl/+) served as controls and therefore received 100 µl 0.9% NaCl. Animals received treatment at days 13, 15, 18, 20, 23 and 25 by intra peritoneal injection. On day 27, tumor weight was significantly reduced in floxed mice treated with doxorubicin

compared to all other groups (Fig. 4.17 A). Treatment with doxorubicin alone did not decrease tumor weight in wt mice. As depicted by the dotted lines in Fig. 4.17 B, doxorubicin impeded tumor growth significantly, after treatment with the second dose. The EC-specific knockdown of *Snai1* alone did not reduce tumor growth (red line) but the additional treatment of fl/+ mice with doxorubicin (dotted red line), showed an increased effect in slowing tumor growth down.

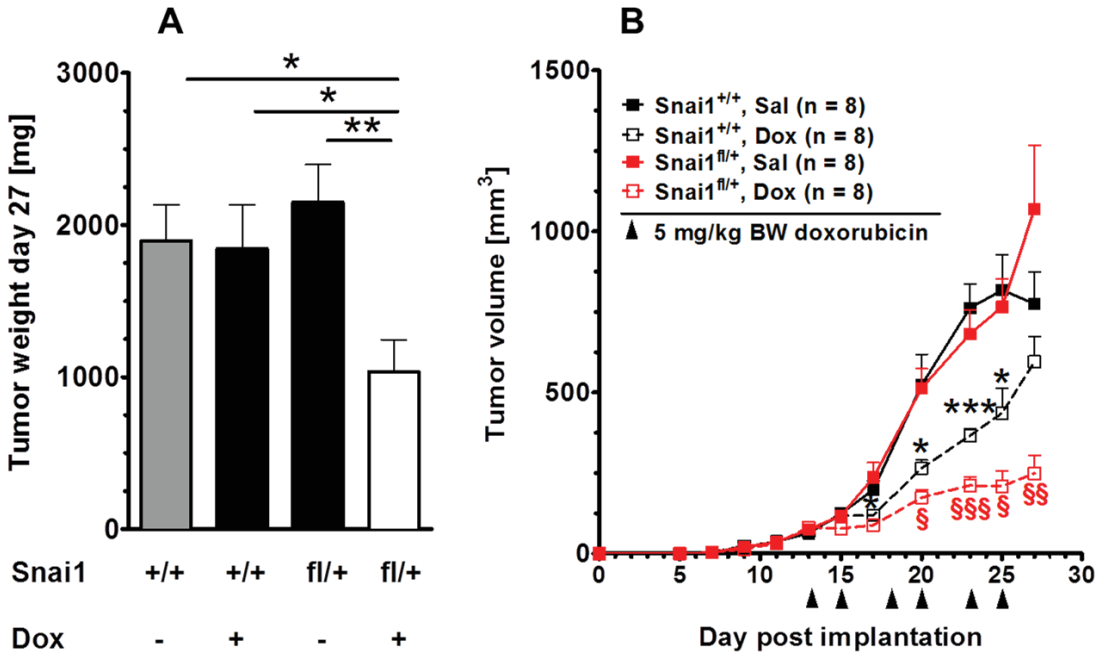

Figure 4.17: Treatment of LLC with doxorubicin. *LLC implanted in male mice were treated with* 5 mg/kg *BW doxorubicin at days 13, 15, 18, 20, 23 and 25 by intra peritoneal injection. Control animals received* 100 µl *0.9% NaCl instead. (A) In fl/+ mice treated with doxorubicin, tumor weight was significantly reduced compared to other groups. (B) Doxorubicin treatment slowed tumor growth significantly in +/+ and fl/+ mice. Arrows indicate days of treatment. § indicates significant difference between groups receiving doxorubicin. Error bars: ± SEM; ∗ indicates $p \leq 0.05$; ∗∗∗ indicates $p \leq 0.001$; § indicates $p \leq 0.05$; §§ indicates $p \leq 0.01$; §§§ indicates $p \leq 0.001$; BW: body weight; Dox: doxorubicin; fl: floxed; Sal: 0.9% NaCl; LLC: lewis lung carcinoma*

5 Discussion

5.1 Tumor microenvironment and tumor vasculature

Over the past years, the importance of the interaction between tumor cells and their microenvironment has been recognized. Apart from malignant cells, the tumor microenvironment (TME) consists of infiltrating immune cells, the tumor's vasculature and lymphatics, fibroblasts, and the extracellular matrix. The tumor and the surrounding stromal cells communicate by secreting various cytokines, chemokines, growth factors, and inflammatory and matrix remodeling enzymes. Thus the TME is able to contribute to tumor proliferation and survival (reviewed in Hanahan and Coussens, 2012). This is also true for breast cancer, where the TME plays a pivotal role in stimulating tumor progression. During tumor growth, the proliferating cancer cells interact with their microenvironment, causing it to continually change (reviewed in Bissell and Radisky, 2001). The expression of angiogenic factors varies between tumors (McClelland et al., 2007). Since pro-and anti-angiogenic factors are involved in tumor angiogenesis, these variations might lead to differences in the stimulation of endothelial cells (ECs). This in turn would cause diverse vessel phenotypes in tumors.

Previous studies have investigated differences between tumor-associated and normal vasculature (Bhati et al., 2008; Hill et al., 2011; Parker et al., 2004), or have concentrated on identifying tumor endothelial markers (Seaman et al., 2007; St Croix et al., 2000) but did not correlate this data with vessel phenotypes. Using human breast cancer samples with different microvessel density (MVD), Pepin et al. investigated the existence of intratumoral vascular subtypes. They found two subtypes of vasculature with distinct expression profiles, which could not be solely linked to MVD and were independent of estrogen receptor (ER) and human epidermal growth factor receptor-2 (HER2) status. The authors hypothesized that these subtypes reflect different stages of vessel maturity (Pepin et al., 2012).

We searched for differences among the vessel morphology of HER2-enriched, basal-

like, luminal A, luminal B and lobular mammary carcinomas by assessing vascular parameters such as vessel area (%CD34 positive area), average vessel size, MVD and circularity of microvessels. While we found that these parameters varied greatly for individual tumor samples we did not find significant differences between the subgroups. Studying patient samples, others as well did not find differences in the MVD of breast cancer subtypes (Chuangsuwanich et al., 2014; Kraby et al., 2015). In our study, vessel area, average vessel size and MVD tended to be lower in lobular carcinomas compared to ductal carcinomas (basal-like, luminal A and luminal B). In Her2-enriched tumors, vessel area and average vessel size were rather similar to the values measured in lobular carcinomas. Circularity of tumor vessel has been shown to increase following irradiation or therapy, indicating vascular normalization (Chlenski et al., 2010; Kakodkar et al., 2012; Klug et al., 2013). We found vessel circularity to be similar across the mammary carcinoma subtypes.

Apart from taking a closer look at the tumors' vasculature, we searched for correlations between vascular parameters and the expression of angiogenic factors. In mammary carcinomas of the subtype luminal A, expression of platelet-derived growth factor (PDGF)-B as well as of vascular endothelial growth factor (VEGF)-A was inversely correlated with vessel area. This correlation was not detected for the entire sample set of mammary carcinomas. Our observation indicates that in samples of the luminal A subtype, *VEGF-A* expression declines with a larger CD34 positive area. The luminal A subtype is positive for ER and progesterone receptor (PR) but negative for HER2. Ductal mammary carcinomas express high levels of VEGF (Toi et al., 1996) and VEGF expression is correlated with ER negativity, PR negativity and HER2 over-expression (Linderholm et al., 2009). Estrogens can directly regulate VEGF expression since the *VEGF* gene contains two estrogen response elements (Hyder et al., 2000). Because VEGF expression in tumors increases due to hypoxia (Bos et al., 2001), our results indicate a correlation between vessel area of tumors and hypoxia. Hypoxia should be less prominent as CD34 positive area increases. Additional staining of samples for markers of hypoxia such as carbonic anhydrase IX (CAIX) would reveal further insights. Differences in *VEGF-A* expression levels linked to breast cancer subtype have been discovered before. A large study, investigating VEGF expression in 1,788 breast cancer patients, found it to be inversely correlated with the expression of ER and PR. VEGF was less commonly detected in luminal A tumors versus luminal B, HER2-enriched, and basal-like subtypes (Liu et al., 2011). Another group studying primary breast

carcinomas, found a correlation between MVD and VEGF across all cancer subtypes but not among them (Chuangsuwanich et al., 2014).

For the subtype luminal A, we also found an inverse correlation of PDGF-B with vessel area. PDGF-B is a member of the PDGF family, which consist of PDGF-A, PDGF-B, PDGF-C and PDGF-D. PDGF-B either homodimerizes or, alternatively, heterodimerizes with PDGF-A. These proteins then bind and activate the PDGF-β receptor (reviewed in Li and Eriksson, 2003). PDGF-B is synthesized by many different cells types including fibroblasts, vascular smooth muscle cells, endothelial cells, macrophages and also mammary epithelial cells (reviewed in Heldin and Westermark, 1999). The detection of PDGF-B in human mammary carcinoma cells, and the finding that its receptor is expressed in the surrounding tumor stroma, suggest that PDGF-B may influence epithelial cell proliferation via a paracrine mechanism (Coltrera et al., 1995). PDGF-B, which is expressed by the sprouting endothelium, plays a crucial role in the recruitment of pericytes via PDGF-B/PDGFR-β signaling to sites of angiogenesis (Lindahl et al., 1997; Gerhardt et al., 2003). Thus by releasing PDGF-B, tumors might enhance angiogenesis. Our data shows that PDGF-B expression is negatively correlated with vessel area in luminal A carcinomas. This hints that recruitment of pericytes and consequently sprouting angiogenesis have slowed down. Coltrera et al. found that neither ER nor PR status correlated with PDGF-B production in breast tumors but Weigel et al. discovered an interaction between ER and the PDGF/Abl signal transduction pathway (Coltrera et al., 1995; Weigel et al., 2012). After a short period of estrogen deprivation PDGF/Abl signaling was up-regulated in vitro. This observation was confirmed in ER positive primary breast cancer patients treated with aromatase inhibitors (Weigel et al., 2012). Interestingly, we did not observe inverse correlations for VEGF-A and PDGF-B with MVD.

In addition, we found that the expression of interleukin (IL)-12A, a subunit of the anti-angiogenic cytokine IL-12, was positively correlated with vessel size in tumors of the subtype luminal A. Tumors of this subgroup express higher levels of IL-12A while exhibiting larger vessels. The cytokine IL-12 is composed of a 35-kD (IL-12A) and a 40-kD subunit (IL-12B) and is produced by phagocytes, dendritic cells and B cells. IL-12 is necessary for the induction of interferon (IFN)-γ production by T cells and natural killer cells, as well as for the differentiation of type 1 T helper (Th1) and Th2 cells (Hsieh et al., 1993; reviewed in Gately et al., 1998). Using the mouse corneal neovascularization model, Voest et al. discovered that IL-12 exhibits potent

anti-angiogenic effects, which are mediated by IFN-γ (Voest et al., 1995). IP-10 was found to be another mediator of IL-12, inhibiting tube formation of ECs in vitro (Angiolillo et al., 1996). In addition IL-12 has antitumorigenic effects. The ability of IL-12 to inhibit tumor growth is most likely mediated via a Th1-type immune response but other mechanisms are involved in tumor regression (Brunda et al., 1993, Nastala et al., 1994; reviewed in Lasek et al., 2014). Several groups have investigated IL-12 serum levels in breast cancer patients with conflicting results. Derin et al. did not find any difference in IL-12 levels between patient and control group, nor a correlation between IL-12 serum levels and either ER- or PR-status (Derin et al., 2007). In addition an earlier study discovered no positive correlation between breast cancer progression and IL-12 (Kovacs, 2001). Interestingly, others have detected decreased IL-12 serum levels in breast cancer patients, which were linked to defects in the IL-12 production of patients' monocytes (Merendino et al., 1999). In contrast, Chavey et al. discovered higher serum levels in patient tissue in comparison to healthy breast tissue. They also found IL-12 to be more abundant in PR-negative as well as in ER-negative tumors (Chavey et al., 2007). Another study investigating a large number of breast carcinomas, also revealed an inverse correlation between PR-status and IL-12 (Toi et al., 1999).
A limitation of this work is the small number of formalin fixed paraffin embedded (FFPE) mammary carcinomas that were available for our study. Sample size in the HER2-enriched, as well as in the luminal B group was very low (n = 2). In the other groups it was only slightly higher (lobular carcinomas: n = 4; basal-like: n = 5; luminal A: n = 5). Therefore, a correlation of HER2-enriched and luminal B carcinomas with the expression of angiogenic factors was not possible. Initially a greater number of samples had been selected. Some had to be excluded due to poor staining, low RNA yield or insufficient amount of FFPE tumor material. The mammary carcinomas samples used in this study had been stored at room temperature for about five years.

5.2 Methodical developments

Biopsied tissues are either stored as fresh frozen (FF) or as FFPE samples. FFPE samples are routinely used for diagnosis, since they are suitable for immunohistochemical staining and morphological analysis, stable at room temperature and easy to store. Consequently, FFPE samples are widely available and are likely to be linked to clinical history and prognosis. During the preservative process formalin may lead to chemical modification of RNA and nucleic acids, including crosslinking with proteins and other biomolecules (Ahlfen et al., 2007; Masuda et al., 1999). Additionally, subsequent storage may promote RNA degradation (Penland et al., 2007). Therefore FF samples are preferred over FFPE samples for molecular analysis. Yet archival breast cancer samples have been used in studies for gene-expression profiling (Ibusuki et al., 2013; Jarzab et al., 2008).
For this study we used FFPE samples, as this method of tissue conservation renders it possible to asses vessel morphology. When working with FFPE samples it is crucial to identify the best techniques for RNA isolation, RNA amplification and down stream analysis. To identify such an approach we tested different products for the isolation of RNA from FFPE samples. Based on the resulting RNA quantity and quality we chose the Agencourt® FormaPure®kit for our study. Nevertheless, RNA yield was still low for some samples. This is likely due to prolonged storage of samples at room temperature, which led to RNA degradation. Next, we established the GenomeLab™GeXP Genetic Analysis System as a method for downstream analysis of isolated RNA. This novel technique has recently been validated in various studies, some of them assessing gene expression profiles in tumor tissue (Drew et al., 2011; Rai et al., 2009). The GeXP system, which utilizes a multiplexed polymerase chain reaction (PCR) approach to investigate the expression of gene sets, allows the analysis of multiple genes of interest in a single reaction. Unfortunately, nucleic acids isolated from FFPE samples are highly fragmented due to crosslinking of tissue components. Thus it is necessary to select PCR primers that produce short amplicons, preferably below 200 bp (Godfrey et al., 2000; Lehmann and Kreipe, 2001). In addition to keeping amplicons short, primers that were combined in one plex had to produce amplicons differing in size by 3 nt to 7 nt. To ensure the amplification of larger PCR amplicons, we included a primer pair to detect a 225 bp amplicon of β-2-microglobulin (B2M). This fragment was successfully detected in all samples included in the study, proving that isolated RNA was not too

degraded for analysis. Normalizing expression data to a shorter beta-actin (ACTB) fragment of 123 bp generated broadly similar results. Because of the above factors, establishing multiplexes was laborious. In an empirical process each multiplex had to be optimized individually. Adding or removing primers had to be done carefully, since one primer pair may impact another. In addition, some genes were of higher abundance than others, making it necessary to balance the detection signal by increasing or decreasing the concentration of reverse primers. This was especially challenging, since gene expression varied greatly between mammary carcinomas. We successfully established primer plexes for the detection of cell population markers, transcription factors and angiogenic factors. While most studies working with GeXP use FF samples, Sirirattanakul et al. successfully used RNA isolated from FFPE breast cancer samples (Sirirattanakul et al., 2015).

Endothelial cells only make up a small proportion of the tumor microenvironment. To investigate gene expression solely in tumor vessels, we had to selectively remove them from the tumor tissue. Laser microdissection (LMD) is a method applied to obtain pure cell populations from FFPE or FF tissues. Other studies used LMD to dissect ECs from immunostained FFPE (Kaneko et al., 2009) or FF (Bhati et al., 2008; Hill et al., 2011) breast cancer samples for the analysis of gene expression. Especially the excision of smaller vessels was challenging. While cutting, we had to ensure that the laser would neither destroy the target, nor excise surrounding tumor tissue. We confirmed the identity of the excised microvessels using primer multiplexes with cell population markers. The exemplary electropherogram (Fig. 4.4) of dissected tumor vessels shows the expression of CD34 as well as smooth muscle actin (SMA) and PDGFRB, confirming the enrichment of ECs and pericytes. Additionally, we detected CD11B and CD68. CD11B encodes the integrin α_M chain. Integrins are heterodimeric integral cell adhesion proteins, composed of an alpha and a beta chain. The α_M chain combines with the β_2 chain (CD18) to form a leukocyte-specific integrin referred to as macrophage receptor 1 (reviewed in Harris et al., 2000). The firm adhesion of neutrophils and monocytes to the endothelium and the following transendothelial migration are mediated by the interaction between CD11B/CD18 and adhesion molecules on ECs (reviewed in Langer and Chavakis, 2009). CD68 is an extensively glycosylated transmembrane protein expressed by monocytes and tissue macrophages (Parwaresch et al., 1986; Rabinowitz and Gordon, 1991). Thus, as shown before by Bhati et al., LMD of microvessels included not only ECs but also other vessel components such as pericytes, macrophages

and leukocytes (Bhati et al., 2008).

5.3 Role of SNAI1 in tumor angiogenesis

To learn more about the down-stream effects of angiogenic factors on EC we treated human umbilical cord endothelial cells (HUVEC) with epidermal growth factor (EGF), fibroblast growth factor (FGF)-2, hepatocyte growth factor (HGF), insulin-like growth factor (IGF), PDGF, stromal-cell derived growth factor (SDF) or VEGF-A. *SNAI1* expression in HUVECs was up-regulated after treatment with EGF, FGF-2, HGF, IGF, PDGF and to a lesser extent due to VEGF-A stimulation. Up-regulation of *SNAI2* mRNA levels was less pronounced and not observed after stimulation with SDF or VEGF-A. Growth factors that act through receptor tyrosine kinases (RTKs), such as the signaling molecules we used for stimulation, are able to induce epithelial to mesenchymal transition (EMT), and thus expression of members of the Snail family in epithelial cells (Onoue et al., 2006, Yang et al., 2006; reviewed in Barrallo-Gimeno and Nieto, 2005 and in Lamouille et al., 2014). Our observation in ECs after the stimulation with various growth factors suggests the involvement of these angiogenic factors in endothelial to mesenchymal transition (EndMT). Despite the importance of EndMT for embryonic development and pathological conditions, such as cardiac (Zeisberg et al., 2007b) and renal fibrosis (Zeisberg et al., 2007c), little about this process is known. In a model of cardiac fibrosis, SNAI1 was shown to induce a mesenchymal phenotype in ECs and suppression of SNAI1 reduced cardiac fibrosis (Lee et al., 2013). The role of EndMT in cancer is still investigated. Using the B16-F10 melanoma model and the Rip-Tag2 spontaneous pancreatic carcinoma model, a study demonstrated EndMT in angiogenic tumor vessels to be a source of carcinoma-associated fibroblasts (CAFs). Around 40% of CAFs coexpressed CD31 and fibroblast secreted protein (FSP)-1, and 11% coexpressed CD31 and α-SMA (Zeisberg et al., 2007a). A recent study investigated whether SNAI2 was able to induce EndMT in tip cells. The authors found that SNAI1 and 2 were necessary for sprouting. As *Snai2* was expressed in the vessels of different cancers it might rather be a marker for ongoing angiogenesis than EndMT (Welch-Reardon et al., 2014). In the tumor's microenvironment, ECs are exposed to continuous activating signals. Subsequently these endothelial cells might remain in a mesenchymal state and vessel maturation is inhibited. Studies show that transforming growth factor (TGF)β, which is abundantly expressed in tumors, plays a key role in EndMT (Cooley

et al., 2014; Zeisberg et al., 2007b). In EMT, *Snai1* expression is induced by TGFβ (Peinado et al., 2003). TGFβ2 can induce EndMT via SNAI1 in mouse embryonic stem cell-derived endothelial cells (MESECs). Upregulation of *Snai1* led to differentiation of MESECs into mural cells, while knockdown of *Snai1* abolished the TGF-β induced differentiation (Kokudo et al., 2008). Therefore, SNAI1 might be a potential target for treatment of cardiac fibrosis (Lee et al., 2013) as well as for the normalization of the tumor's vasculature. Using the Cre-loxP system, we were able to establish a transgenic mouse line with heterozygous knockdown of *Snai1* specifically in ECs. In this mouse line we examined the role of SNAI1 in ECs in three tumor models (B16-F10, E0771 and lewis lung carcinoma). Growth of the murine breast cancer cell line E0771 was slightly increased in floxed (fl) animals and we observed a significant decrease in the expression of markers of hypoxia *(Ca9*, *Glut-1* and *Vegfa*) in tumor tissue. Since hypoxia was decreased, knockdown of *Snai1* likely improved blood flow in these tumors, which subsequently promoted tumor growth. B16-F10 melanomas also grew bigger in fl/+ animals compared to controls, yet staining for CD34 showed no changes in vasculature. This tumor model exhibited large areas of necrosis independent of the genotype of mice. Concomitant with the observed necrosis no change in hypoxia was detected. Thus the knockdown seemed to have no implication on the tumor vasculature but significantly enhanced tumor growth. In the lewis lung carcinomas (LLC) in contrast, neither tumor growth nor hypoxia were influenced by *Snai1* knockdown. Since MVD and vessel area were increased and biodistribution of doxorubicin was improved in fl/+ animals, one would have expected a concomitant decrease in hypoxia. As expected, LLC growth was significantly impaired by doxorubicin treatment. This effect was even stronger in fl/+ animals, indicating the benefits of chemotherapy in combination with vascular remodeling.

In some of the conducted experiments tumor take rate was low, reducing the number of animals in the study groups. Another challenge was the availability of mice of the right genotype, age, and gender. We studied the heterozygous knockdown of *Snai1* in ECs, instead of fl/fl mice. Recently, Wu et al. demonstrated that EC-specific deletion of *Snai1* induces embryonic lethality at E11.5 or E12.5 (Wu et al., 2014).

Altogether, our experiments show that knockdown of *Snai1* has an influence on tumor vasculature. Yet the exact effects depend on the respective tumor model. Heterozygous knockdown of *Snai1* was sufficient to improve microvessel density in LLCs and to reduce hypoxia in E0771 tumors. In LLCs, the delivery of doxorubicin to the tumor

was improved and tumors remained smaller after doxorubicin treatment.

6 Summary

In contrast to normal vessels, tumor vasculature is structurally and functionally abnormal. Tumor vessels are highly disorganized, tortuous and dilated, with uneven diameter and excessive branching. Consequently, tumor blood flow is chaotic, which leads to hypoxic and acidic regions in tumors. These conditions lower the therapeutic effectiveness and select for cancer cells that are more malignant and metastatic. The therapeutic outcome could be improved by increasing the functionality and density of the tumor vasculature. Tumor angiogenesis also shows parallels to epithelial to mesenchymal transition (EMT), a process enabling metastasis. Metastasis is a multi-step process, during which tumor cells have to invade the surrounding host tissue to reach the circulation and to be transported to distant sites.

We hypothesize that the variability in the phenotype of the tumor vasculature is controlled by the differential expression of key transcription factors. Inhibiting these transcription factors might be a promising way for angiogenic intervention and vascular re-engineering. Therefore, we investigated the interdependence of tumor-, stroma- and immune cell-derived angiogenic factors, transcription factors and resulting vessel phenotypes. Additionally, we evaluated whether transcription factors that regulate EMT are promising targets for vascular remodeling.

We used formalin fixed paraffin embedded samples from breast cancer patients, classified according to estrogen-, progesterone- and human epidermal growth factor receptor (HER) 2 status. Establishing various techniques (CD34 staining, laser microdissection, RNA isolation and expression profiling) we systematically analyzed tumor and stroma-derived growths factors. In addition, vascular parameters such as microvessel size, area, circularity and density were assessed. Finally the established expression profiles were correlated with the observed vessel phenotype. As the SNAI1 transcriptional repressor is a key regulator of EMT, we examined the effect of vascular knockdown of *Snai1* in murine cancer models (E0771, B16-F10 and lewis lung carcinoma).

Among individual mammary carcinomas, but not among subtypes, strong differences

of vascular parameters were observed. Also, little difference between lobular carcinomas and ductal carcinomas was found. Vessel phenotype of Her2 enriched carcinomas was similar to that of lobular carcinomas. Vessel morphology of luminal A and B and basal-like tumors resembled each other. Expression of angiogenic factors was variable across subtypes. We discovered an inverse correlation of PDGF-B and VEGF-A with vessel area in luminal A tumors. In these tumors expression of IL12A, an inhibitor of angiogenesis, was also correlated with vessel size. Treatment of endothelial cells with growth factors revealed an increased expression of transcription factors involved in the regulation of EMT. Knockdown of *Snai1* in endothelial cells of mice increased tumor growth and decreased hypoxia in the E0771 and the B16-F10 models. In the lewis lung carcinomas, tumor vascularity and biodistribution of doxorubicin were improved. Here, doxorubicin treatment in combination with the endothelial cell-specific knockdown did slow tumor growth. This shows that SNAI1 is important for a tumor's vascularization, with the significance of its role depending on the tumor model.
The methods established in this work open the way for the analysis of the expression of key transcription factors in vessels of formalin fixed paraffin embedded tumors. This research enables us to find novel targets for vascular intervention and to eventually design novel targeted drugs to inhibit these targets.

7 Zusammenfassung

In Tumoren, im Vergleich zu gesundem Gewebe, sind Aufbau und Funktionsweise von Blutgefäßen abnormal. Tumorgefäße sind unorgansiert, stark gewunden und geweitet, und weisen einen ungleichmäßigen Durchmesser sowie häufige Verzweigungen auf. Die chaotische Durchblutung führt zu hypoxischen und sauren Regionen. Diese abnormale Gefäßstruktur verringert sowohl die Einbringung, als auch die Wirksamkeit von Medikamenten und fördert zudem Invasivität und Metastasierung. Die Tumorbehandlung könnte durch eine "Normalisierung" der Gefäße sowie durch die Verbesserung der Dichte der Tumorblutgefäße erleichtert werden, da Medikamente so leichter das Tumorzentrum erreichen. In Tumoren weist der Prozess der Angiogenese Parallelen zur epithelial-mesenchymalen Transition (EMT) auf. Die EMT spielt eine zentrale Rolle bei der Metastasierung. Hierbei handelt es sich um einen mehrstufigen Prozess, bei dem Tumorzellen in das umgebende Wirtsgewebe eindringen um den Blutkreislauf zu erreichen und so zu weiter entfernten Organen zu gelangen.
Laut unserer Hypothese werden die unterschiedlichen Phenotypen der Tumorblutgefäße durch die Expression verschiedener Schlüssel-Transkriptionsfaktoren kontrolliert. Die Hemmung dieser Transkriptionsfaktoren wäre folglich eine vielversprechende Möglichkeit in die Gefäßsturktur einzugreifen und sie zu restrukturieren. Deshalb wurde die Wechselwirkungen zwischen angiogenen Faktoren, die von Tumorzellen, Stromazellen und Zellen des Immunsystems abgesondert werden und Transkriptionsfaktoren sowie den resultierenden Gefäßphenotypen untersucht. Zudem wurde evaluiert, ob Transkriptionsfaktoren, die bei der EMT von Bedeutung sind, ein therapeutisches Ziel zur Umorganisation der Gefäßstruktur darstellen könnten.
Für diese Studie wurden humane, in Formalin fixierte und in Paraffin eingebette, Proben von Brustkrebspatienten verwendet. Diese Proben wurden anhand des Rezeptorstatus von Östrogen-, Progesteron- und humanem epidermalen Wachstumsfaktor-Rezeptor (HER) 2 in tumorbiologische Untergruppen eingeordnet. Die Etablierung verschiedener Techniken (CD34 Gewebefärbung, Laser-Mikrodissektion, RNA-Isolierung

und Erstellung von Expressionsprofilen) ermöglichte es, systematisch Wachstumsfaktoren, die von den Tumoren und ihrem umgebenden Stroma sezerniert werden, zu analysieren. Zusätzlich untersuchten wir vaskuläre Parameter wie Gefäßgröße, -fläche, -dichte und -zirkularität. Schließlich wurden die erstellten Expressionsprofile mit den Gefäßeigenschaften korreliert. In verschiedenen murinen Krebsmodellen (E0771, B16-F10 und Lewis-Lungenkarzinom) untersuchten wir die Auswirkung der Herrunterregulierung des Transkriptionsfaktors SNAI1 in Blutgefäßen. SNAI1 spielt eine Schlüsselrolle bei der Regulierung der EMT.
Es zeigte sich, dass die einzelnen Brustkrebsproben sich bezüglich der untersuchten Gefäßparameter stark voneinander unterschieden. Zwischen den Subtypen hingegen waren keine Unterschiede zu sehen. Lobuläre und duktale Karzinome unterschieden sich kaum voneinander. Der Gefäßphenotyp der HER2-positiven Proben ähnelte dem der lobulären. Des Weiteren ähnelten sich Karzinome vom Luminal A- und B-Typ so wie vom Basal-Zell-Typ in ihrer Gefäßmorphologie. Das Expressionsmuster der Wachstumsfaktoren variierte von Tumor zu Tumor und innerhalb der Subytpen. Es stellte sich heraus, dass die Expression von PDGF-B und VEGF-A im Subtyp Luminal A invers mit der Gefäßfläche korreliert ist. Außerdem war in dieser Gruppe die Expression des Angiogenese-Hemmers IL-12A direkt mit der Gefäßgröße korreliert. Die Behandlung von Endothelzellen mit Wachstumsfaktoren zeigte eine erhöhte Expression von Transkriptionsfaktoren, die an der Regulierung der EMT beteiligt sind. Die Herrunterregulierung von *Snai1* in Endothelzellen im Tierversuch führte zu einer Zunahme des Tumorwachstums sowie zu einem Rückgang der Hypoxie in den Tumormodellen E0771 und B16-F10. In den Lewis-Lungenkarzinomen kam es zu einer Verbesserung der Blutgefäßmorphologie und der Verteilung von Doxorubicin im Tumorgewebe. Die Therapie mit Doxorubicin in Kombination mit der endothellzell-spezifischen Herrunterregulierung von *Snai1* zeigte zudem eine stärkere Hemmung des Tumorwachstums. Die Methoden, die in dieser Arbeit etabliert wurden, ermöglichen die Analyse der Expression von Schlüssel-Transkriptionsfaktoren in den Gefäßen von Formalin fixierten und in Paraffin eingebetten Proben. Dies macht es wiederum möglich neue Angriffspunkte für die Gefäßmodulation zu finden und schlußendlich neue, darauf gerichtete Medikamente zu entwickeln.

8 Supplement

8.1 Primer sets

We designed different multiplexes for use with the GeXP system. The sets shown in Tab 8.1 to Tab. 8.3 were used to generate expression profiles of RNA isolated from cultured cells or formalin fixed paraffin embedded tumor samples. The multiplex shown in Tab. 8.4 was used on RNA isolated from tumors grown in transgenic mice. For further details on methods see Section 3.4, and for primer sequences see Tab. 2.1 in Chapter 2.

Table 8.1: Primer sets for detection of cell population markers. *Final concentration of reverse primer is included. Product size includes universal sequences needed for detection. rv: reverse*

	Gene name	Product [bp]	Concentration rv primer [nM]
Set 1	CDH5	137	500
	KRT17	144	500
	GATA3	149	500
	IGJ	156	500
	COL18A1	163	500
	CD45	169	500
	KRT5	176	500
	VWF	187	500
	CD11A	192	500
	KRT8	197	31.25
	KRT18	205	125.00
	B2M	220	125.00
Set 2	CD11b	137	500
	SMA	144	500
	CD68	150	500
	PDGFRB	158	500
	CD3D	164	500
	CDH1	168	500
	ESR1	172	500
	COL6A1	181	500
	CDH2	191	500
	CD34	205	500
	B2M	220	125.00

Table 8.2: Primer sets for detection of transcription factors. *Final concentration of reverse primer is included. Product size includes universal sequences needed for detection. rv: reverse*

	Gene name	Product [bp]	Concentration rv primer [nM]
Set 1	ID3	137	500
	FOXO3	161	500
	FOXO1	173	500
	HEY1	178	500
	SNAI2	183	500
	COUPTFII	197	31.25
	B2M	221	62.5
Set 2	FLI1	151	500
	ETS1	157	125
	FOXC1	164	500
	HOXB3	169	500
	ETV4	176	500
	RUNX1	182	500
	GTF2I	186	125
	ETV1	190	500
	MEF2C	196	500
	SNAI1	200	500
	B2M	221	31.25
Set 3	ERG	138	500
	VEZF1	147	500
	HOXA9	155	500
	PBX1	168	500
	ID1	173	500
	YB1	178	125
	TWIST1	197	500
	HEY2	194	500
	FOXF1	200	500
	B2M	221	62.5

Table 8.3: Primer sets for detection of markers of EMT. *Final concentration of reverse primer is included. Product size includes universal sequences needed for detection. rv: reverse*

Gene name	Product [bp]	Concentration rv primer [nM]
CDH5	137	62.5
SMA	144	1000
ZO1	148	250
CTNNA1	164	500
CDH1	168	1000
VIM	180	125
CDH2	191	500
FN1	194	500
B2M	220	62.5

Table 8.4: Primer sets for detection of markers of hypoxia in mice. *Final concentration of reverse primer is included. Product size includes universal sequences needed for detection. rv: reverse*

Gene name	Product [bp]	Concentration rv primer [nM]
Ca9	166	1000
Glut-1	186	62.5
Vegfa	226	1000
Rsp29	255	7.8125

8.2 Expression data

The following tables depict the results of the expression profiling of tumor and tumor microenvironment derived angiogenic factors in mammary carcinomas. Table 8.5 shows data generated with primer set 1 for angiogenic factors, Tab. 8.6 shows data generated with primer set 2 and Tab. 8.7 shows data generated with primer set-3. All data was normalized to reference gene B2M. Mean as well as standard deviation were calculated.

Table 8.5: Expression data of angiogenic factors in mammary carcinomas (primer set 1) *SD: standard deviation*

Sample ID	Gene	Replicate 1	Replicate 2	Replicate 3	Mean	SD
	IL-8	0.3484	0.2694	0.2901	0.3026	0.0410
	MCP-1	0.5649	0.5696	0.6015	0.5787	0.0199
	ANGPT1	0.0391	0.0593	0.0649	0.0544	0.0136
2937	G-CSF	0.0115	0.0103	0.0134	0.0117	0.0015
	SDF-1	1.3676	1.4468	1.4031	1.4058	0.0397
	ANGPT2	0.1124	0.1021	0.0990	0.1045	0.0070
	FGF-1	0.0226	0.0257	0.0340	0.0275	0.0059
	IL-8	10.3747	7.9600	12.5302	10.2883	2.2863
	MCP-1	3.8251	3.5658	3.7929	3.7279	0.1414
	ANGPT1	0.2705	0.4800	-	0.3753	0.1481
3801	G-CSF	0.1787	0.2227	0.2788	0.2267	0.0502
	SDF-1	12.3406	12.0920	13.2248	12.5525	0.5954
	ANGPT2	0.6522	0.7706	-	0.7114	0.0837
	IL-8	1.7618	2.0096	1.5255	1.7656	0.2421
	MCP-1	3.1718	2.1422	2.4559	2.5900	0.5277
	ANGPT1	0.2547	0.1606	0.0949	0.1701	0.0803
3189	SDF-1	0.9145	0.6450	0.8042	0.7879	0.1355
	ANGPT2	0.1439	0.0898	0.0567	0.0968	0.0440
	FGF-1	0.0826	-	0.0321	0.0574	0.0357
	IL-8	0.4915	0.4023	0.4705	0.4548	0.0466
4649	MCP-1	0.8115	0.5045	0.7040	0.6733	0.1558

Continued on next page

Table 8.5 – *Continued from previous page*

Sample ID	Gene	Replicate 1	Replicate 2	Replicate 3	Mean	SD
	ANGPT1	0.0582	0.0612	0.0726	0.0640	0.0076
4649	IL-6	0.0355	0.0292	0.0281	0.0309	0.0040
	SDF-1	0.6200	0.6538	0.6219	0.6319	0.0190
	ANGPT2	0.0356	0.0401	0.0388	0.0382	0.0023
	FGF-1	-	0.0134	0.0172	0.0153	0.0027
	IL-8	0.0647	0.0687	0.0651	0.0662	0.0022
	MCP-1	0.1813	0.1979	0.2316	0.2036	0.0257
	ANGPT1	0.0201	-	0.0246	0.0223	0.0032
2849	IL-6	0.0039	0.0042	-	0.0040	0.0002
	G-CSF	-	-	0.0057	0.0057	-
	SDF-1	0.5469	0.5547	0.5624	0.5547	0.0078
	ANGPT2	0.0130	0.0139	0.0156	0.0142	0.0013
	FGF-1	0.0149	0.0290	0.0136	0.0192	0.0086
	IL-8	0.1851	0.2814	0.2521	0.2395	0.0493
	MCP-1	0.9066	1.1657	1.0278	1.0334	0.1296
	ANGPT1	0.0405	0.0561	0.0284	0.0417	0.0139
1287	IL-6	0.0370	0.0793	0.0515	0.0559	0.0215
	G-CSF	0.0072	-	-	0.0072	-
	SDF-1	0.9384	1.1290	1.0276	1.0316	0.0954
	ANGPT2	0.0763	0.0779	0.0817	0.0786	0.0028
	FGF-1	0.0226	0.0298	0.0320	0.0281	0.0049
	IL-8	0.3715	0.3125	0.2447	0.3096	0.0634
	MCP-1	0.7325	0.7272	0.7017	0.7205	0.0165
	ANGPT1	0.0392	-	0.0235	0.0313	0.0111
4491	IL-6	0.0166	-	-	0.0166	-
	SDF-1	0.3810	0.3878	0.3601	0.3763	0.0144
	ANGPT2	0.0268	0.0342	0.0329	0.0313	0.0040
	FGF-1	0.0145	-	0.0077	0.0111	0.0048
	IL-8	1.9650	2.3064	1.9947	2.0887	0.1891
	MCP-1	3.0940	2.6879	3.0897	2.9572	0.2332
	ANGPT1	0.0500	-	0.0547	0.0524	0.0033
4783	IL-6	0.0512	0.0528	0.0378	0.0473	0.0082
	SDF-1	0.5811	0.5941	0.6025	0.5926	0.0108
	ANGPT2	0.0341	0.0363	0.0316	0.0340	0.0024
	FGF-1	-	0.0255	0.0532	0.0394	0.0196
	IL-8	0.4504	0.3141	0.4113	0.3919	0.0702
	MCP-1	0.9496	0.9565	0.8238	0.9100	0.0747
	ANGPT1	0.0353	0.0345	0.0250	0.0316	0.0057
2774	IL-6	0.0406	0.0185	0.0179	0.0257	0.0129
	G-CSF	0.0082	-	-	0.0082	-
	SDF-1	0.1646	0.1080	0.1717	0.1481	0.0349
	ANGPT2	0.0303	0.0334	0.0200	0.0279	0.0070
	FGF-1	0.0302	-	-	0.0302	-

Continued on next page

Table 8.5 – *Continued from previous page*

Sample ID	Gene	Replicate 1	Replicate 2	Replicate 3	Mean	SD
	IL-8	1.0570	0.7924	0.9665	0.9386	0.1344
	MCP-1	2.4406	2.7359	3.6037	2.9267	0.6046
	ANGPT1	0.1718	0.1563	-	0.1640	0.0110
528	IL-6	0.0552	-	0.0476	0.0514	0.0054
	SDF-1	1.5298	1.0507	1.5602	1.3802	0.2858
	ANGPT2	0.1627	0.1660	0.0924	0.1404	0.0415
	FGF-1	-	0.0752	-	0.0752	-
	IL-8	0.3995	0.5089	0.3613	0.4232	0.0766
	MCP-1	0.7427	0.8027	0.6567	0.7340	0.0734
	ANGPT1	0.0744	0.0922	0.0584	0.0750	0.0169
1888	IL-6	-	0.0144	0.0158	0.0151	0.0009
	G-CSF	-	0.0194	-	0.0194	-
	SDF-1	1.0832	1.2099	0.9965	1.0965	0.1073
	ANGPT2	0.0384	0.0472	0.0802	0.0553	0.0221
	FGF-1	0.0401	0.0350	0.0399	0.0383	0.0029
	IL-8	0.2071	0.2570	0.2074	0.2238	0.0287
	MCP-1	0.7557	0.8243	0.6934	0.7578	0.0655
	ANGPT1	0.0508	0.0427	0.0562	0.0499	0.0068
738	IL-6	0.0114	0.0091	0.0234	0.0146	0.0077
	G-CSF	0.0076	-	0.0104	0.0090	0.0020
	SDF-1	0.9523	0.9327	0.9271	0.9374	0.0132
	ANGPT2	0.0489	0.0458	0.0524	0.0490	0.0033
	FGF-1	0.0218	0.0289	-	0.0253	0.0051
	IL-8	0.2764	0.3462	0.2647	0.2958	0.0441
	MCP-1	0.4305	0.6131	0.4773	0.5070	0.0949
	ANGPT1	0.0254	0.0380	0.0267	0.0300	0.0069
624	IL-6	0.0308	0.0185	0.0173	0.0222	0.0075
	SDF-1	0.4569	0.5885	0.4988	0.5147	0.0672
	ANGPT2	0.0491	0.0547	0.0430	0.0489	0.0058
	FGF-1	0.0211	0.0244	0.0194	0.0216	0.0025
	IL-8	-	0.3595	0.3849	0.3722	0.0179
	MCP-1	-	1.4528	1.2669	1.3599	0.1314
	ANGPT1	-	0.2116	0.4202	0.3159	0.1474
3994	IL-6	-	0.1517	0.1749	0.1633	0.0164
	G-CSF	-	0.2995	0.1092	0.2043	0.1346
	SDF-1	-	0.8463	0.4855	0.6659	0.2551
	ANGPT2	-	0.1935	0.5105	0.3520	0.2241
	FGF-1	-	0.2106	0.2596	0.2351	0.0346
	IL-8	0.2383	0.1945	0.1709	0.2013	0.0342
	MCP-1	0.8356	0.6340	0.5829	0.6841	0.1336
	ANGPT1	0.3470	0.1825	0.2509	0.2602	0.0826
3011	IL-6	-	0.0807	0.1283	0.1045	0.0337
	SDF-1	0.8289	1.2403	0.8319	0.9670	0.2367
	ANGPT2	0.3150	0.1101	0.2281	0.2178	0.1028

Continued on next page

Table 8.5 – *Continued from previous page*

Sample ID	Gene	Replicate 1	Replicate 2	Replicate 3	Mean	SD
3011	FGF-1	-	0.0900	0.0719	0.0809	0.0128
	IL-8	0.1971	0.2285	0.2155	0.2137	0.0158
	MCP-1	0.8610	1.0824	1.2921	1.0785	0.2156
	ANGPT1	0.1330	0.1528	0.1598	0.1485	0.0139
665	IL-6	0.0566	0.0537	0.0487	0.0530	0.0040
	G-CSF	-	0.0164	0.0083	0.0123	0.0057
	SDF-1	1.7713	1.8995	2.0530	1.9079	0.1410
	ANGPT2	0.1125	0.1189	0.1059	0.1124	0.0065
	FGF-1	0.0395	0.0605	0.0516	0.0505	0.0105
	IL-8	0.3417	0.3861	0.2986	0.3421	0.0438
	MCP-1	0.3173	0.3187	0.3558	0.3306	0.0218
	ANGPT1	0.0360	0.0412	0.0391	0.0388	0.0026
5142	IL-6	0.0237	0.0163	0.0206	0.0202	0.0037
	G-CSF	0.0055	0.0068	0.0065	0.0063	0.0007
	SDF-1	0.6576	0.7666	0.6789	0.7010	0.0578
	ANGPT2	0.0376	0.0474	0.0417	0.0422	0.0049
	FGF-1	0.0286	0.0360	0.0264	0.0304	0.0050

Table 8.6: Expression data of angiogenic factors in mammary carcinomas (primer set 2). *SD: standard deviation*

Sample ID	Gene	Replicate 1	Replicate 2	Replicate 3	Mean	SD
	IP-10	0.2105	0.1642	0.1449	0.1732	0.0337
	GROb	2.3848	2.4985	2.3199	2.4010	0.0904
2937	GM-CSF	-	0.0271	0.0143	0.0207	0.0090
	TSP-1	0.0918	0.0898	0.0879	0.0898	0.0020
	IL-12A	-	-	0.0056	0.0056	-
	IP-10	0.9458	0.7678	-	0.8568	0.1258
3801	GROb	7.9589	8.2182	7.2415	7.8062	0.5059
	GM-CSF	0.1644	0.0806	-	0.1225	0.0592
	TSP-1	0.4590	0.5536	0.3492	0.4539	0.1023
	IL-12A	0.0960		0.0562	0.0761	0.0282
	IP-10	1.0810	-	-	1.0810	-
3189	GROb	-	7.8052	8.8566	8.3309	0.7434
	GM-CSF	-	-	0.1119	0.1119	-
	TSP-1	0.3939	0.3527	0.5489	0.4318	0.1034
	GROb	-	2.9628	3.3242	3.1435	0.2556
3190	GM-CSF	-	0.0671	0.1947	0.1309	0.0902
	TSP-1	-	0.1359	0.0519	0.0939	0.0594
4649	IP-10	0.0159	0.0090	0.0132	0.0127	0.0034
	GROb	1.4989	1.4901	1.8021	1.5970	0.1777

Continued on next page

Table 8.6 – *Continued from previous page*

Sample ID	Gene	Replicate 1	Replicate 2	Replicate 3	Mean	SD
4649	GM-CSF	0.0072	0.0068	0.0076	0.0072	0.0004
	TSP-1	0.1200	0.1053	0.1173	0.1142	0.0078
	IL-12A	0.0236	0.0126	0.0362	0.0241	0.0118
	IP-10	0.1427	0.1891	0.3248	0.2189	0.0946
	GROb	0.8438	0.9665	0.8986	0.9030	0.0615
2849	GM-CSF	-	0.0092	0.0101	0.0096	0.0006
	TSP-1	0.0183	0.0115	0.0268	0.0189	0.0076
	IL-12A	-	-	0.0131	0.0131	-
	IP-10	-	0.0386	0.2511	0.1449	0.1503
	GROb	2.2288	2.6004	2.6555	2.4949	0.2321
1287	GM-CSF	0.0093	0.0098	0.0114	0.0102	0.0011
	TSP-1	0.0241	0.0333	0.0457	0.0344	0.0109
	IL-12A	0.0248	0.0116	-	0.0182	0.0094
	IP-10	0.0352	0.0604	0.0456	0.0471	0.0127
	GROb	1.4116	1.1094	1.0093	1.1768	0.2094
4491	GM-CSF	-	0.0093	0.0178	0.0136	0.0060
	TSP-1	0.0155	0.0139	0.0120	0.0138	0.0018
	IL-12A	-	-	0.0031	0.0031	-
	IP-10	0.0365	0.0387	0.0482	0.0411	0.0062
4783	GROb	4.5581	3.3187	4.2261	4.0343	0.6416
	GM-CSF	-	-	0.0201	0.0201	-
	TSP-1	0.3597	0.3274	0.2721	0.3197	0.0443
	IP-10	0.0169	0.1530	0.0142	0.0614	0.0794
	GROb	1.5998	1.3375	1.3656	1.4343	0.1440
2774	GM-CSF	0.0260	0.0251	0.0358	0.0290	0.0060
	TSP-1	0.0214	0.0094	0.0108	0.0139	0.0065
	IL-12A	0.0341	0.0357	0.0280	0.0326	0.0040
	IP-10	0.0431	-	0.1378	0.0905	0.0669
528	GROb	9.0851	7.9657	7.6033	8.2180	0.7725
	GM-CSF	-	-	0.0707	0.0707	-
	TSP-1	-	0.0501	0.1198	0.0850	0.0493
	IP-10	0.0219	-	0.1136	0.0678	0.0648
1888	GROb	2.8814	2.4244	3.1728	2.8262	0.3772
	GM-CSF	0.0332	0.0255	-	0.0293	0.0054
	TSP-1	0.1897	0.1833	0.1760	0.1830	0.0069
	IP-10	0.0754	0.0332	0.0079	0.0388	0.0341
	GROb	4.0539	4.9717	4.4269	4.4842	0.4616
738	GM-CSF	0.0026	-	0.0102	0.0064	0.0053
	TSP-1	0.1449	0.2121	0.1252	0.1607	0.0456
	IL-12A	0.0077	0.0198	0.0092	0.0122	0.0066
624	IP-10	-	-	0.1039	0.1039	-

Continued on next page

Table 8.6 – *Continued from previous page*

Sample ID	Gene	Replicate 1	Replicate 2	Replicate 3	Mean	SD
	GROb	4.0539	4.9717	4.4269	4.4842	0.4616
624	GM-CSF	0.0067	-	0.0088	0.0078	0.0015
	TSP-1	0.0274	-	0.0369	0.0321	0.0067
	IL-12A	0.0063	-	0.0049	0.0056	0.0010
	IP-10	0.1105	0.1636	0.1855	0.1532	0.0386
3994	GROb	5.0987	3.9692	0.0000	3.0226	2.6779
	GM-CSF	-	0.1123	0.1472	0.1298	0.0247
	IL-12A	0.0996	0.0149	0.0915	0.0686	0.0467
	IP-10	0.0709	0.2076	0.1489	0.1424	0.0686
	GROb	3.9305	4.0603	0.0000	2.6636	2.3077
3011	GM-CSF	0.0264	0.0268	0.0000	0.0177	0.0154
	TSP-1	0.0197	0.0387	0.0588	0.0391	0.0196
	IL-12A	0.0226	0.0142	0.0000	0.0123	0.0114
	IP-10	-	-	0.0423	0.0423	-
	GROb	3.3309	2.6534	2.9088	2.9644	0.3422
665	GM-CSF	0.0433	0.0149	0.0300	0.0294	0.0142
	TSP-1	0.1200	0.1406	0.1015	0.1207	0.0195
	IL-12A	-	-	0.0197	0.0197	-
	IP-10	-	0.0138	0.0740	0.0439	0.0425
	GROb	1.9965	2.4215	2.1664	2.1948	0.2139
5142	GM-CSF	0.0090	-	0.0109	0.0099	0.0014
	TSP-1	0.1588	0.1574	0.1461	0.1541	0.0070
	IL-12A	-	-	0.0118	0.0118	-

Table 8.7: Expression data of angiogenic factors in mammary carcinomas (primer set 3). *SD: standard deviation*

Sample ID	Gene	Replicate 1	Replicate 2	Replicate 3	Mean	SD
	VEGF-B	0.1454	0.1467	0.0980	0.1300	0.0277
	PDGF-A	0.0327	0.0532	0.0218	0.0359	0.0159
	VEGF-A	0.6254	0.6336	0.4273	0.5621	0.1168
2937	HGF	-	-	0.0071	0.0071	-
	PLGF	0.0275	0.0343	0.0096	0.0238	0.0128
	PDGF-B	0.1551	0.1770	0.0728	0.1350	0.0549
	FGF-2	0.0685	0.0785	0.0863	0.0778	0.0089
	VEGF-C	0.0227	-	0.0125	0.0176	0.0072
	EGF	0.0173	-	0.0112	0.0142	0.0043
	VEGF-B	1.4496	1.4609	0.9347	1.2817	0.3006
	PDGF-A	-	0.2732	0.1860	0.2296	0.0617
3801	VEGF-A	5.1240	4.2867	2.5722	3.9943	1.3008
	PDGF-B	-	-	0.2226	0.2226	-
	FGF-2	-	0.4559	0.4570	0.4565	0.0008

Continued on next page

Table 8.7 – *Continued from previous page*

Sample ID	Gene	Replicate 1	Replicate 2	Replicate 3	Mean	SD
3801	VEGF-C	-	-	3.5344	3.5344	-
3189	VEGF-B	0.2286	-	0.4323	0.3304	0.1440
	PDGF-A	0.1798	-	-	0.1798	-
	VEGF-A	1.1529	-	1.9309	1.5419	0.5501
	PDGF-B	0.1000	-	-	0.1000	-
3190	VEGF-B	0.8331	0.8498	1.0338	0.9056	0.1114
	PDGF-A	-	0.2655	0.3963	0.3309	0.0925
	VEGF-A	0.5148	0.5054	0.6466	0.5556	0.0789
	PLGF	-	-	0.3227	0.3227	-
	PDGF-B	-	0.2309	0.3498	0.2904	0.0841
	FGF-2	0.4125	0.3620	-	0.3872	0.0357
4649	VEGF-B	-	0.0180	-	0.0180	-
	PDGF-A	0.0169	-	-	0.0169	-
	VEGF-A	0.3527	0.3341	0.3022	0.3297	0.0256
	HGF	-	-	-	-	-
	PLGF	0.0254	0.0187	0.0265	0.0235	0.0042
	PDGF-B	0.0900	0.0989	0.0763	0.0884	0.0114
	FGF-2	0.0280	-	0.0318	0.0299	0.0027
2849	VEGF-B	0.0160	0.0146	-	0.0153	0.0010
	PDGF-A	-	0.0069	0.0124	0.0096	0.0039
	VEGF-A	0.3087	0.2140	0.1753	0.2327	0.0686
	HGF	0.0141	0.0092	-	0.0117	0.0035
	PLGF	0.0333	0.0258	-	0.0296	0.0053
	PDGF-B	0.1728	0.1427	0.0548	0.1235	0.0613
	FGF-2	0.1246	0.1161	0.0871	0.1093	0.0197
	VEGF-C	0.0174	0.0125	-	0.0149	0.0035
1287	VEGF-B	0.1016	0.1454	0.0941	0.1137	0.0277
	PDGF-A	0.0303	0.0586	0.0503	0.0464	0.0146
	VEGF-A	0.3943	0.4356	0.2866	0.3722	0.0769
	HGF	0.0188	-	-	0.0188	-
	PLGF	0.0581	0.0916	0.0530	0.0676	0.0209
	PDGF-B	0.1992	0.1549	0.0000	0.1180	0.1046
	FGF-2	0.0924	0.0891	0.0877	0.0898	0.0024
4991	VEGF-B	0.0392	0.0404	0.0324	0.0373	0.0043
	PDGF-A	0.0438	0.0297	0.0329	0.0354	0.0074
	VEGF-A	0.4604	0.3408	0.3207	0.3740	0.0755
	HGF	-	-	0.0126	0.0126	-
	PLGF	0.0151	0.0162	0.0145	0.0153	0.0008
	PDGF-B	0.0363	0.0663	0.0235	0.0420	0.0219
	FGF-2	0.0388	0.0371	0.0271	0.0343	0.0063
	VEGF-C	-	0.0093	-	0.0093	-
	EGF	-	0.0104	0.0112	0.0108	0.0005

Continued on next page

Table 8.7 – *Continued from previous page*

Sample ID	Gene	Replicate 1	Replicate 2	Replicate 3	Mean	SD
	VEGF-B	-	-	0.0599	0.0599	-
	PDGF-A	-	0.0662	-	0.0662	-
4783	VEGF-A	1.6048	1.0172	1.7106	1.4442	0.3736
	TGFB1	-	0.0583	0.0520	0.0552	0.0045
	PDGF-B	0.1127	0.1323	0.1584	0.1345	0.0229
	VEGF-C	0.2052	-	-	0.2052	-
	VEGF-A	0.4063	0.6217	0.5840	0.5373	0.1150
	PDGF-B	0.0538	0.0459	0.0344	0.0447	0.0098
2774	FGF-2	0.1091	0.1728	0.1135	0.1318	0.0356
	VEGF-C	0.0137	-	-	0.0137	-
	EGF	0.0073	-	-	0.0073	-
	VEGF-B	-	0.1891	0.2128	0.2009	0.0167
	PDGF-A	-	-	-	-	-
528	VEGF-A	-	1.5967	1.8024	1.6995	0.1454
	PDGF-B	-	-	0.1734	0.1734	-
	FGF-2	-	0.1774	0.2272	0.2023	0.0352
	VEGF-B	0.1329	0.1200	-	0.1265	0.0091
	PDGF-A	-	0.0779	-	0.0779	-
	VEGF-A	0.5755	0.5214	-	0.5485	0.0382
1888	TGF-b	0.0485	-	-	0.0485	-
	HGF	-	-	-	-	-
	PLGF	-	-	-	-	-
	PDGF-B	0.0502	0.1118	-	0.0810	0.0435
	FGF-2	0.1014	0.1249	-	0.1131	0.0166
	VEGF-B	0.0452	0.0571	0.0674	0.0566	0.0111
	PDGF-A	0.0186	0.0142	0.0138	0.0155	0.0027
	VEGF-A	0.5288	0.6636	0.5803	0.5909	0.0680
	HGF	-	0.0155	-	0.0155	-
624	PLGF	0.0222	0.0146	0.0323	0.0230	0.0089
	PDGF-B	0.0760	0.1655	0.1730	0.1381	0.0540
	FGF-2	0.0270	0.0261	0.0334	0.0288	0.0040
	VEGF-C	-	0.0093	-	0.0093	-
	EGF	-	0.0104	0.0101	0.0102	0.0002
	VEGF-B	-	-	0.1078	0.1078	-
738	VEGF-A	0.4132	0.4140	0.2791	0.3688	0.0777
	PLGF	-	-	-	-	-
	FGF-2	-	-	0.1186	0.1186	-
	VEGF-B	-	0.8096	0.7988	0.8042	0.0077
	PDGF-A	-	0.2401	-	0.2401	-
3994	VEGF-A	-	1.3429	1.3991	1.3710	0.0397
	PDGF-B	-	0.2202	-	0.2202	-
	FGF-2	-	0.1227	-	0.1227	-
	EGF	-	0.1301	-	0.1301	-

Continued on next page

Table 8.7 – *Continued from previous page*

Sample ID	Gene	Replicate 1	Replicate 2	Replicate 3	Mean	SD
	VEGF-B	0.4247	0.4711	0.4762	0.4573	0.0284
	PDGF-A	-	0.0325	0.0535	0.0430	0.0148
	VEGF-A	0.5783	0.4722	0.4648	0.5051	0.0635
3011	HGF	0.0842	0.0641	0.0523	0.0669	0.0161
	PLGF	0.0619	0.0667	0.0539	0.0608	0.0065
	PDGF-B	0.2222	0.1178	0.0868	0.1423	0.0709
	FGF-2	0.3655	0.3956	0.2954	0.3522	0.0514
	EGF	0.0358	0.0614	0.0395	0.0456	0.0139
	VEGF-B	0.09846	0.11569	0.14622	0.1201	0.0242
	PDGF-A	0.03362	0.04066	0.08183	0.0520	0.0260
	VEGF-A	0.33027	0.37166	0.30097	0.3343	0.0355
	TGF-b	0.03429	0.02628	0.08155	0.0474	0.0299
665	HGF	-	0.01944	-	0.0194	-
	PLGF	0.03349	0.02284	-	0.0282	0.0075
	PDGF-B	0.09693	0.10969	0.06221	0.0896	0.0246
	FGF-2	0.27501	0.23012	0.38098	0.2954	0.0775
	VEGF-C	-	0.01984	-	0.0198	-
	EGF	-	0.01976	-	0.0198	-
	VEGF-B	-	0.0286	0.0314	0.0300	0.0020
	PDGF-A	-	0.0697	0.0270	0.0483	0.0302
	VEGF-A	0.1817	0.3087	0.5525	0.3476	0.1885
	TGF-b	-	0.0357	0.0115	0.0236	0.0171
5142	HGF	-	-	0.0077	0.0077	-
	PLGF	-	-	0.0331	0.0331	-
	PDGF-B	-	0.0699	0.2242	0.1470	0.1092
	FGF-2	0.0737	0.0727	0.0797	0.0753	0.0038
	VEGF-C	-	-	0.0114	0.0114	-

Bibliography

Abramsson, A., Lindblom, P., and Betsholtz, C. (2003). Endothelial and nonendothelial sources of pdgf-b regulate pericyte recruitment and influence vascular pattern formation in tumors. *The Journal of clinical investigation*, 112(8):1142–1151.

Achen, M. G., Jeltsch, M., Kukk, E., Mäkinen, T., Vitali, A., Wilks, A. F., Alitalo, K., and Stacker, S. A. (1998). Vascular endothelial growth factor d (vegf-d) is a ligand for the tyrosine kinases vegf receptor 2 (flk1) and vegf receptor 3 (flt4). *Proceedings of the National Academy of Sciences of the United States of America*, 95(2):548–553.

Adams, R. H. and Alitalo, K. (2007). Molecular regulation of angiogenesis and lymphangiogenesis. *Nature Reviews Molecular Cell Biology*, 8(6):464–478.

Ahlfen, S. v., Missel, A., Bendrat, K., and Schlumpberger, M. (2007). Determinants of rna quality from ffpe samples. *PloS one*, 2(12):e1261.

Airley, R., Loncaster, J., Davidson, S., Bromley, M., Roberts, S., Patterson, A., Hunter, R., Stratford, I., and West, C. (2001). Glucose transporter glut-1 expression correlates with tumor hypoxia and predicts metastasis-free survival in advanced carcinoma of the cervix. *Clinical cancer research : an official journal of the American Association for Cancer Research*, 7(4):928–934.

American Cancer Society (2013). Breast cancer facts & figures 2013-2014. *Atlanta: American Cancer Society, Inc.*

Angiolillo, A. L., Sgadari C., and Tosato G. (1996). A role for the interferon-inducible protein 10 in inhibition of angiogenesis by interleukin-12. *Annals of the New York Academy of Sciences*, 759(1 Interleukin 1):158–167.

Armulik, A. (2005). Endothelial/pericyte interactions. *Circulation Research*, 97(6):512–523.

Armulik, A., Genové, G., and Betsholtz, C. (2011). Pericytes: developmental, physiological, and pathological perspectives, problems, and promises. *Developmental cell*, 21(2):193–215.

Asahara, T., Murohara, T., Sullivan, A., Silver, M., van der Zee, R, Li, T., Witzenbichler, B., Schatteman, G., and Isner, J. M. (1997). Isolation of putative progenitor endothelial cells for angiogenesis. *Science (New York, N.Y.)*, 275(5302):964–967.

Baluk, P., Hashizume, H., and McDonald, D. M. (2005). Cellular abnormalities of blood vessels as targets in cancer. *Current Opinion in Genetics & Development*, 15(1):102–111.

Barrallo-Gimeno, A. and Nieto, M. A. (2005). The snail genes as inducers of cell movement and survival: implications in development and cancer. *Development (Cambridge, England)*, 132(14):3151–3161.

Batlle, E., Sancho, E., Francí, C., Domínguez, D., Monfar, M., Baulida, J., and García De Herreros, A (2000). The transcription factor snail is a repressor of e-cadherin gene expression in epithelial tumour cells. *Nature cell biology*, 2(2):84–89.

Behrens, J., von Kries, J P, Kühl, M., Bruhn, L., Wedlich, D., Grosschedl, R., and Birchmeier, W. (1996). Functional interaction of beta-catenin with the transcription factor lef-1. *Nature*, 382(6592):638–642.

Benjamin, L. E., Golijanin, D., Itin, A., Pode, D., and Keshet, E. (1999). Selective ablation of immature blood vessels in established human tumors follows vascular endothelial growth factor withdrawal. *The Journal of clinical investigation*, 103(2):159–165.

Bergers, G. and Hanahan, D. (2008). Modes of resistance to anti-angiogenic therapy. *Nature Reviews Cancer*, 8(8):592–603.

Bhati, R., Patterson, C., Livasy, C. A., Fan, C., Ketelsen, D., Hu, Z., Reynolds, E., Tanner, C., Moore, D. T., Gabrielli, F., Perou, C. M., and Klauber-DeMore, N. (2008). Molecular characterization of human breast tumor vascular cells. *The American Journal of Pathology*, 172(5):1381–1390.

Bissell, M. J. and Radisky, D. (2001). Putting tumours in context. *Nature reviews. Cancer*, 1(1):46–54.

Blanco, M. J., Moreno-Bueno, G., Sarrio, D., Locascio, A., Cano, A., Palacios, J., and Nieto, M. A. (2002). Correlation of snail expression with histological grade and lymph node status in breast carcinomas. *Oncogene*, 21(20):3241–3246.

Bos, R., Zhong, H., Hanrahan, C. F., Mommers, E. C. M., Semenza, G. L., Pinedo, H. M., Abeloff, M. D., Simons, J. W., van Diest, P. J., and van der Wall, E. (2001). Levels of hypoxia-inducible factor-1 during breast carcinogenesis. *JNCI Journal of the National Cancer Institute*, 93(4):309–314.

Boscolo, E., Mulliken, J. B., and Bischoff, J. (2013). Pericytes from infantile hemangioma display proangiogenic properties and dysregulated angiopoietin-1. *Arteriosclerosis, thrombosis, and vascular biology*, 33(3):501–509.

Brabletz, T., Jung, A., Reu, S., Porzner, M., Hlubek, F., Kunz-Schughart, L. A., Knuechel, R., and Kirchner, T. (2001). Variable beta-catenin expression in colorectal cancers indicates tumor progression driven by the tumor environment. *Proceedings of the National Academy of Sciences of the United States of America*, 98(18):10356–10361.

Brown, J. M. and Giaccia, A. J. (1998). The unique physiology of solid tumors: opportunities (and problems) for cancer therapy. *Cancer research*, 58(7):1408–1416.

Brown, L. F., Berse, B., Jackman, R. W., Tognazzi, K., Guidi, A. J., Dvorak, H. F., Senger, D. R., Connolly, J. L., and Schnitt, S. J. (1995). Expression of vascular permeability factor (vascular endothelial growth factor) and its receptors in breast cancer. *Human pathology*, 26(1):86–91.

Brunda, M. J., Luistro, L., Warrier, R. R., Wright, R. B., Hubbard, B. R., Murphy, M., Wolf, S. F., and Gately, M. K. (1993). Antitumor and antimetastatic activity of interleukin 12 against murine tumors. *The Journal of experimental medicine*, 178(4):1223–1230.

Caduff, J. H., Fischer, L. C., and Burri, P. H. (1986). Scanning electron microscope study of the developing microvasculature in the postnatal rat lung. *The Anatomical record*, 216(2):154–164.

Cano, A., Pérez-Moreno, M. A., Rodrigo, I., Locascio, A., Blanco, M. J., del Barrio, M G, Portillo, F., and Nieto, M. A. (2000). The transcription factor snail controls

epithelial-mesenchymal transitions by repressing e-cadherin expression. *Nature cell biology*, 2(2):76–83.

Carey, L. A., Perou, C. M., Livasy, C. A., Dressler, L. G., Cowan, D., Conway, K., Karaca, G., Troester, M. A., Tse, C. K., Edmiston, S., Deming, S. L., Geradts, J., Cheang, Maggie C U, Nielsen, T. O., Moorman, P. G., Earp, H. S., and Millikan, R. C. (2006). Race, breast cancer subtypes, and survival in the carolina breast cancer study. *JAMA*, 295(21):2492–2502.

Carter, P., Presta, L., Gorman, C. M., Ridgway, J. B., Henner, D., Wong, W. L., Rowland, A. M., Kotts, C., Carver, M. E., and Shepard, H. M. (1992). Humanization of an anti-p185her2 antibody for human cancer therapy. *Proceedings of the National Academy of Sciences of the United States of America*, 89(10):4285–4289.

Chang, Y. S., Di Tomaso, E., McDonald, D. M., Jones, R., Jain, R. K., and Munn, L. L. (2000). Mosaic blood vessels in tumors: frequency of cancer cells in contact with flowing blood. *Proceedings of the National Academy of Sciences of the United States of America*, 97(26):14608–14613.

Chavey, C., Bibeau, F., Gourgou-Bourgade, S., Burlinchon, S., Boissière, F., Laune, D., Roques, S., and Lazennec, G. (2007). Oestrogen receptor negative breast cancers exhibit high cytokine content. *Breast cancer research : BCR*, 9(1):R15.

Cheang, M. C., Chia, S. K., Voduc, D., Gao, D., Leung, S., Snider, J., Watson, M., Davies, S., Bernard Philip S., Parker, J. S., Perou, C. M., and Ellis, M. J. (2009). Ki67 index, her2 status, and prognosis of patients with luminal b breast cancer. *Journal of the National Cancer Institute*, 101(10):736–750.

Chlenski, A., Guerrero, L. J., Peddinti, R., Spitz, J. A., Leonhardt, P. T., Yang, Q., Tian, Y., Salwen, H. R., and Cohn, S. L. (2010). Anti-angiogenic sparc peptides inhibit progression of neuroblastoma tumors. *Molecular cancer*, 9:138.

Chuangsuwanich, T., Pongpruttipan, T., O-charoenrat, P., Komoltri, C., Watcharahirun, S., and Sa-nguanraksa, D. (2014). Clinicopathologic features of breast carcinomas classified by biomarkers and correlation with microvessel density and vegf expression: A study from thailand. *Asian Pacific Journal of Cancer Prevention*, 15(3):1187–1192.

Chumsri, S., Howes, T., Bao, T., Sabnis, G., and Brodie, A. (2011). Aromatase, aromatase inhibitors, and breast cancer. *The Journal of steroid biochemistry and molecular biology*, 125(1-2):13–22.

Coltrera, M. D., Wang, J., Porter, P. L., and Gown, A. M. (1995). Expression of platelet-derived growth factor b-chain and the platelet-derived growth factor receptor beta subunit in human breast tissue and breast carcinoma. *Cancer research*, 55(12):2703–2708.

Cooley, B. C., Nevado, J., Mellad, J., Yang, D., St Hilaire, C., Negro, A., Fang, F., Chen, G., San, H., Walts, A. D., Schwartzbeck, R. L., Taylor, B., Lanzer, J. D., Wragg, A., Elagha, A., Beltran, L. E., Berry, C., Feil, R., Virmani, R., Ladich, E., Kovacic, J. C., and Boehm, M. (2014). Tgf-beta signaling mediates endothelial-to-mesenchymal transition (endmt) during vein graft remodeling. *Science translational medicine*, 6(227):227ra34.

Cutts, S. M., Nudelman, A., Rephaeli, A., and Phillips, D. R. (2005). The power and potential of doxorubicin-dna adducts. *IUBMB life*, 57(2):73–81.

Davis, S., Aldrich, T. H., Jones, P. F., Acheson, A., Compton, D. L., Jain, V., Ryan, T. E., Bruno, J., Radziejewski, C., Maisonpierre, P. C., and Yancopoulos, G. D. (1996). Isolation of angiopoietin-1, a ligand for the tie2 receptor, by secretion-trap expression cloning. *Cell*, 87(7):1161–1169.

Derin, D., Soydinc, H. O., Guney, N., Tas, F., Camlica, H., Duranyildiz, D., Yasasever, V., and Topuz, E. (2007). Serum il-8 and il-12 levels in breast cancer. *Medical oncology (Northwood, London, England)*, 24(2):163–168.

Dewhirst, M. W., Tso, C. Y., Oliver, R., Gustafson, C. S., Secomb, T. W., and Gross, J. F. (1989). Morphologic and hemodynamic comparison of tumor and healing normal tissue microvasculature. *International Journal of Radiation Oncology*Biology*Physics*, 17(1):91–99.

Döme, B., Paku, S., Somlai, B., and Tímár, J. (2002). Vascularization of cutaneous melanoma involves vessel co-option and has clinical significance. *The Journal of Pathology*, 197(3):355–362.

Drew, J. E., Mayer, C.-D., Farquharson, A. J., Young, P., and Barrera, L. N. (2011). Custom design of a gexp multiplexed assay used to assess expression profiles of inflammatory gene targets in normal colon, polyp, and tumor tissue. *The Journal of molecular diagnostics : JMD*, 13(2):233–242.

Dumont, D. J., Gradwohl, G., Fong, G. H., Puri, M. C., Gertsenstein, M., Auerbach, A., and Breitman, M. L. (1994). Dominant-negative and targeted null mutations in the endothelial receptor tyrosine kinase, tek, reveal a critical role in vasculogenesis of the embryo. *Genes & Development*, 8(16):1897–1909.

Dumont, D. J., Yamaguchi, T. P., Conlon, R. A., Rossant, J., and Breitman, M. L. (1992). tek, a novel tyrosine kinase gene located on mouse chromosome 4, is expressed in endothelial cells and their presumptive precursors. *Oncogene*, 7(8):1471–1480.

Eberhard, A., Kahlert, S., Goede, V., Hemmerlein, B., Plate, K. H., and Augustin, H. G. (2000). Heterogeneity of angiogenesis and blood vessel maturation in human tumors: implications for antiangiogenic tumor therapies. *Cancer research*, 60(5):1388–1393.

Egeblad, M., Littlepage, L. E., and Werb, Z. (2005). The fibroblastic coconspirator in cancer progression. *Cold Spring Harbor symposia on quantitative biology*, 70:383–388.

Eilken, H. M. and Adams, R. H. (2010). Dynamics of endothelial cell behavior in sprouting angiogenesis. *Current Opinion in Cell Biology*, 22(5):617–625.

Fakhrejahani, E. and Toi, M. (2014). Antiangiogenesis therapy for breast cancer: an update and perspectives from clinical trials. *Japanese journal of clinical oncology*, 44(3):197–207.

Ferguson, J. E., Kelley, R. W., and Patterson, C. (2005). Mechanisms of endothelial differentiation in embryonic vasculogenesis. *Arteriosclerosis, thrombosis, and vascular biology*, 25(11):2246–2254.

Ferlay, J., Soerjomataram, I., Ervik, M., Dikshit, R., Eser, S., Mathers, C., Rebelo, M., Parkin, D., Forman, D., and Bray, F. (2013). Globocan 2012 v1.0: Cancer incidence and mortality worldwide: Iarc cancerbase no. 11 [internet]. *Lyon, France: International Agency for Research on Cancer*.

Ferrara, N. (2004). Vascular endothelial growth factor: basic science and clinical progress. *Endocrine reviews*, 25(4):581–611.

Ferrara, N. (2009). Vegf-a: a critical regulator of blood vessel growth. *European cytokine network*, 20(4):158–163.

Ferrara, N. and Henzel, W. J. (1989). Pituitary follicular cells secrete a novel heparin-binding growth factor specific for vascular endothelial cells. *Biochemical and biophysical research communications*, 161(2):851–858.

Folkman, J. (1971). Tumor angiogenesis: therapeutic implications. *The New England journal of medicine*, 285(21):1182–1186.

Forsythe, J. A., Jiang, B. H., Iyer, N. V., Agani, F., Leung, S. W., Koos, R. D., and Semenza, G. L. (1996). Activation of vascular endothelial growth factor gene transcription by hypoxia-inducible factor 1. *Molecular and cellular biology*, 16(9):4604–4613.

Frixen, U. H., Behrens, J., Sachs, M., Eberle, G., Voss, B., Warda, A., Löchner, D., and Birchmeier, W. (1991). E-cadherin-mediated cell-cell adhesion prevents invasiveness of human carcinoma cells. *The Journal of cell biology*, 113(1):173–185.

Gately, M. K., Renzetti, L. M., Magram, J., Stern, A. S., Adorini, L., Gubler, U., and Presky, D. H. (1998). The interleukin-12/interleukin-12-receptor system: role in normal and pathologic immune responses. *Annual review of immunology*, 16:495–521.

Gerber, H.-P., Malik, A. K., Solar, G. P., Sherman, D., Liang, X. H., Meng, G., Hong, K., Marsters, J. C., and Ferrara, N. (2002). Vegf regulates haematopoietic stem cell survival by an internal autocrine loop mechanism. *Nature*, 417(6892):954–958.

Gerhardt, H., Golding, M., Fruttiger, M., Ruhrberg, C., Lundkvist, A., Abramsson, A., Jeltsch, M., Mitchell, C., Alitalo, K., Shima, D., and Betsholtz, C. (2003). Vegf guides angiogenic sprouting utilizing endothelial tip cell filopodia. *The Journal of cell biology*, 161(6):1163–1177.

Gilles, C., Polette, M., Mestdagt, M., Nawrocki-Raby, B., Ruggeri, P., Birembaut, P., and Foidart, J.-M. (2003). Transactivation of vimentin by beta-catenin in human breast cancer cells. *Cancer research*, 63(10):2658–2664.

Gimbrone, M. A., Cotran, R. S., Leapman, S. B., and Folkman, J. (1974). Tumor growth and neovascularization: an experimental model using the rabbit cornea. *Journal of the National Cancer Institute*, 52(2):413–427.

Godfrey, T. E., Kim, S.-H., Chavira, M., Ruff, D. W., Warren, R. S., Gray, J. W., and Jensen, R. H. (2000). Quantitative mrna expression analysis from formalin-fixed, paraffin-embedded tissues using 5′ nuclease quantitative reverse transcription-polymerase chain reaction. *The Journal of Molecular Diagnostics*, 2(2):84–91.

Good, D. J., Polverini, P. J., Rastinejad, F., Le Beau, M M, Lemons, R. S., Frazier, W. A., and Bouck, N. P. (1990). A tumor suppressor-dependent inhibitor of angiogenesis is immunologically and functionally indistinguishable from a fragment of thrombospondin. *Proceedings of the National Academy of Sciences of the United States of America*, 87(17):6624–6628.

Goss, P. E. and Strasser-Weippl, K. (2004). Prevention strategies with aromatase inhibitors. *Clinical cancer research : an official journal of the American Association for Cancer Research*, 10(1 Pt 2):372S–9S.

Gottardi, C. J. and Gumbiner, B. M. (2001). Adhesion signaling: how beta-catenin interacts with its partners. *Current biology : CB*, 11(19):R792–4.

Goumans, M.-J., Valdimarsdottir, G., Itoh, S., Rosendahl, A., Sideras, P., and Dijke, P. (2002). Balancing the activation state of the endothelium via two distinct tgf-beta type i receptors. *The EMBO Journal*, 21(7):1743–1753.

Grant, C. A. and Twigg, P. C. (2013). Pseudostatic and dynamic nanomechanics of the tunica adventitia in elastic arteries using atomic force microscopy. *ACS nano*, 7(1):456–464.

Greenberg, J. I., Shields, D. J., Barillas, S. G., Acevedo, L. M., Murphy, E., Huang, J., Scheppke, L., Stockmann, C., Johnson, R. S., Angle, N., and Cheresh, D. A. (2008). A role for vegf as a negative regulator of pericyte function and vessel maturation. *Nature*, 456(7223):809–813.

Gumbiner, B., Stevenson, B., and Grimaldi, A. (1988). The role of the cell adhesion molecule uvomorulin in the formation and maintenance of the epithelial junctional complex. *The Journal of cell biology*, 107(4):1575–1587.

Gumbiner, B. M. (2005). Regulation of cadherin-mediated adhesion in morphogenesis. *Nature reviews. Molecular cell biology*, 6(8):622–634.

Hajra, K. M., Chen, D. Y.-S., and Fearon, E. R. (2002). The slug zinc-finger protein represses e-cadherin in breast cancer. *Cancer research*, 62(6):1613–1618.

Hamilton, D. L. and Abremski, K. (1984). Site-specific recombination by the bacteriophage p1 lox-cre system. cre-mediated synapsis of two lox sites. *Journal of molecular biology*, 178(2):481–486.

Hanahan, D. and Coussens, L. M. (2012). Accessories to the crime: functions of cells recruited to the tumor microenvironment. *Cancer cell*, 21(3):309–322.

Hanahan, D. and Folkman, J. (1996). Patterns and emerging mechanisms of the angiogenic switch during tumorigenesis. *Cell*, 86(3):353–364.

Harris, E. S., McIntyre, T. M., Prescott, S. M., and Zimmerman, G. A. (2000). The leukocyte integrins. *The Journal of biological chemistry*, 275(31):23409–23412.

Hashizume, H., Baluk, P., Morikawa, S., McLean, J. W., Thurston, G., Roberge, S., Jain, R. K., and McDonald, D. M. (2000). Openings between defective endothelial cells explain tumor vessel leakiness. *The American Journal of Pathology*, 156(4):1363–1380.

Hattori, K., Heissig, B., Wu, Y., Dias, S., Tejada, R., Ferris, B., Hicklin, D. J., Zhu, Z., Bohlen, P., Witte, L., Hendrikx, J., Hackett, N. R., Crystal, R. G., Moore, Malcolm A S, Werb, Z., Lyden, D., and Rafii, S. (2002). Placental growth factor reconstitutes hematopoiesis by recruiting vegfr1(+) stem cells from bone-marrow microenvironment. *Nature medicine*, 8(8):841–849.

Hazan, R. B., Qiao, R., Keren, R., Badano, I., and Suyama, K. (2004). Cadherin switch in tumor progression. *Annals of the New York Academy of Sciences*, 1014:155–163.

Heldin, C. H. and Westermark, B. (1999). Mechanism of action and in vivo role of platelet-derived growth factor. *Physiological reviews*, 79(4):1283–1316.

Hellström, M., Phng, L.-K., Hofmann, J. J., Wallgard, E., Coultas, L., Lindblom, P., Alva, J., Nilsson, A.-K., Karlsson, L., Gaiano, N., Yoon, K., Rossant, J.,

Iruela-Arispe, M. L., Kalén, M., Gerhardt, H., and Betsholtz, C. (2007). Dll4 signalling through notch1 regulates formation of tip cells during angiogenesis. *Nature*, 445(7129):776–780.

Hendrix, M. J., Seftor, E. A., Hess, A. R., and Seftor, Richard E. B. (2003). Angiogenesis: Vasculogenic mimicry and tumour-cell plasticity: lessons from melanoma. *Nature reviews. Cancer*, 3(6):411–421.

Hendrix, M. J., Seftor, E. A., Seftor, R. E., and Trevor, K. T. (1997). Experimental co-expression of vimentin and keratin intermediate filaments in human breast cancer cells results in phenotypic interconversion and increased invasive behavior. *The American Journal of Pathology*, 150(2):483–495.

Hicklin, D. J. and Ellis, L. M. (2005). Role of the vascular endothelial growth factor pathway in tumor growth and angiogenesis. *Journal of clinical oncology : official journal of the American Society of Clinical Oncology*, 23(5):1011–1027.

Hill, J. J., Tremblay, T.-L., Pen, A., Li, J., Robotham, A. C., Lenferink, Anne E. G., Wang, E., O'Connor-McCourt, M., and Kelly, J. F. (2011). Identification of vascular breast tumor markers by laser capture microdissection and label-free lc−ms. *Journal of Proteome Research*, 10(5):2479–2493.

Holash, J., Maisonpierre, P. C., Compton, D., Boland, P., Alexander, C. R., Zagzag, D., Yancopoulos, G. D., and Wiegand, S. J. (1999). Vessel cooption, regression, and growth in tumors mediated by angiopoietins and vegf. *Science (New York, N.Y.)*, 284(5422):1994–1998.

Howell, A., Pippen, J., Elledge, R. M., Mauriac, L., Vergote, I., Jones, S. E., Come, S. E., Osborne, C. K., and Robertson, John F R (2005). Fulvestrant versus anastrozole for the treatment of advanced breast carcinoma: a prospectively planned combined survival analysis of two multicenter trials. *Cancer*, 104(2):236–239.

Hsieh, C. S., Macatonia, S. E., Tripp, C. S., Wolf, S. F., O'Garra, A., and Murphy, K. M. (1993). Development of th1 cd4+ t cells through il-12 produced by listeria-induced macrophages. *Science (New York, N.Y.)*, 260(5107):547–549.

Hurwitz, H., Fehrenbacher, L., Novotny, W., Cartwright, T., Hainsworth, J., Heim, W., Berlin, J., Baron, A., Griffing, S., Holmgren, E., Ferrara, N., Fyfe, G., Rogers, B.,

Ross, R., and Kabbinavar, F. (2004). Bevacizumab plus irinotecan, fluorouracil, and leucovorin for metastatic colorectal cancer. *The New England journal of medicine*, 350(23):2335–2342.

Hyder, S. M., Nawaz, Z., Chiappetta, C., and Stancel, G. M. (2000). Identification of functional estrogen response elements in the gene coding for the potent angiogenic factor vascular endothelial growth factor. *Cancer research*, 60(12):3183–3190.

Ibusuki, M., Fu, P., Yamamoto, S., Fujiwara, S., Yamamoto, Y., Honda, Y., Iyama, K.-i., and Iwase, H. (2013). Establishment of a standardized gene-expression analysis system using formalin-fixed, paraffin-embedded, breast cancer specimens. *Breast Cancer*, 20(2):159–166.

Ikenouchi, J., Matsuda, M., Furuse, M., and Tsukita, S. (2003). Regulation of tight junctions during the epithelium-mesenchyme transition: direct repression of the gene expression of claudins/occludin by snail. *Journal of cell science*, 116(Pt 10):1959–1967.

Inai, T., Mancuso, M., Hashizume, H., Baffert, F., Haskell, A., Baluk, P., Hu-Lowe, D. D., Shalinsky, D. R., Thurston, G., Yancopoulos, G. D., and McDonald, D. M. (2004). Inhibition of vascular endothelial growth factor (vegf) signaling in cancer causes loss of endothelial fenestrations, regression of tumor vessels, and appearance of basement membrane ghosts. *The American journal of pathology*, 165(1):35–52.

Jain, R. K. (1998). The next frontier of molecular medicine: Delivery of therapeutics. *Nature Medicine*, 4(6):655–657.

Jain, R. K. (2001). Normalizing tumor vasculature with anti-angiogenic therapy: a new paradigm for combination therapy. *Nature medicine*, 7(9):987–989.

Jarzab, M., Rózanowski, P., Kowalska, M., Zebracka, J., Rudnicka, L., Stobiecka, E., Jarzab, B., Stachura, J., and Pawlega, J. (2008). Optimization of the method of rna isolation from paraffin blocks to assess gene expression in breast cancer. *Polish journal of pathology : official journal of the Polish Society of Pathologists*, 59(2):85–91.

Jordan, V. C. (2003). Tamoxifen: a most unlikely pioneering medicine. *Nature reviews. Drug discovery*, 2(3):205–213.

Kakodkar, N. C., Peddinti, R. R., Tian, Y., Guerrero, L. J., Chlenski, A., Yang, Q., Salwen, H. R., Maitland, M. L., and Cohn, S. L. (2012). Sorafenib inhibits neuroblastoma cell proliferation and signaling, blocks angiogenesis, and impairs tumor growth. *Pediatric blood & cancer*, 59(4):642–647.

Kalluri, R. and Weinberg, R. A. (2009). The basics of epithelial-mesenchymal transition. *The Journal of clinical investigation*, 119(6):1420–1428.

Kalluri, R. and Zeisberg, M. (2006). Fibroblasts in cancer. *Nature reviews. Cancer*, 6(5):392–401.

Kaneko, T., Okiji, T., Kaneko, R., Suda, H., and Noer, J. E. (2009). Gene expression analysis of immunostained endothelial cells isolated from formaldehyde-fixated paraffin embedded tumors using laser capture microdissection - a technical report. *Microscopy Research and Technique*, 72(12):908–912.

Kelly, B. D., Hackett, S. F., Hirota, K., Oshima, Y., Cai, Z., Berg-Dixon, S., Rowan, A., Yan, Z., Campochiaro, P. A., and Semenza, G. L. (2003). Cell type-specific regulation of angiogenic growth factor gene expression and induction of angiogenesis in nonischemic tissue by a constitutively active form of hypoxia-inducible factor 1. *Circulation Research*, 93(11):1074–1081.

Kim, K. J., Li, B., Winer, J., Armanini, M., Gillett, N., Phillips, H. S., and Ferrara, N. (1993). Inhibition of vascular endothelial growth factor-induced angiogenesis suppresses tumour growth in vivo. *Nature*, 362(6423):841–844.

Klug, F., Prakash, H., Huber, P. E., Seibel, T., Bender, N., Halama, N., Pfirschke, C., Voss, R. H., Timke, C., Umansky, L., Klapproth, K., Schäkel, K., Garbi, N., Jäger, D., Weitz, J., Schmitz-Winnenthal, H., Hämmerling, G. J., and Beckhove, P. (2013). Low-dose irradiation programs macrophage differentiation to an $inos^+$/m1 phenotype that orchestrates effective t cell immunotherapy. *Cancer cell*, 24(5):589–602.

Kokudo, T., Suzuki, Y., Yoshimatsu, Y., Yamazaki, T., Watabe, T., and Miyazono, K. (2008). Snail is required for tgfbeta-induced endothelial-mesenchymal transition of embryonic stem cell-derived endothelial cells. *Journal of cell science*, 121(Pt 20):3317–3324.

Kovacs, E. (2001). The serum levels of il-12 and il-16 in cancer patients. relation to the tumour stage and previous therapy. *Biomedicine & Pharmacotherapy*, 55(2):111–116.

Kraby, M. R., Krüger, K., Opdahl, S., Vatten, L. J., Akslen, L. A., and Bofin, A. M. (2015). Microvascular proliferation in luminal a and basal-like breast cancer subtypes. *Journal of clinical pathology*, 68(11):891–897.

Kukk, E., Lymboussaki, A., Taira, S., Kaipainen, A., Jeltsch, M., Joukov, V., and Alitalo, K. (1996). Vegf-c receptor binding and pattern of expression with vegfr-3 suggests a role in lymphatic vascular development. *Development (Cambridge, England)*, 122(12):3829–3837.

Kümler, I., Christiansen, O. G., and Nielsen, D. L. (2014). A systematic review of bevacizumab efficacy in breast cancer. *Cancer treatment reviews*, 40(8):960–973.

Laginha, K. M., Verwoert, S., Charrois, Gregory J R, and Allen, T. M. (2005). Determination of doxorubicin levels in whole tumor and tumor nuclei in murine breast cancer tumors. *Clinical cancer research : an official journal of the American Association for Cancer Research*, 11(19 Pt 1):6944–6949.

Lamouille, S., Xu, J., and Derynck, R. (2014). Molecular mechanisms of epithelial-mesenchymal transition. *Nature reviews. Molecular cell biology*, 15(3):178–196.

Langer, H. F. and Chavakis, T. (2009). Leukocyte-endothelial interactions in inflammation. *Journal of Cellular and Molecular Medicine*, 13(7):1211–1220.

Lasek, W., Zagożdżon, R., and Jakobisiak, M. (2014). Interleukin 12: still a promising candidate for tumor immunotherapy? *Cancer Immunology, Immunotherapy*, 63(5):419–435.

Lebrin, F., Deckers, M., Bertolino, P., and Tendijke, P. (2005). Tgf-ß receptor function in the endothelium. *Cardiovascular Research*, 65(3):599–608.

Lee, J. M., Dedhar, S., Kalluri, R., and Thompson, E. W. (2006). The epithelial-mesenchymal transition: new insights in signaling, development, and disease. *The Journal of cell biology*, 172(7):973–981.

Lee, S.-W., Won, J.-Y., Kim, W. J., Lee, J., Kim, K.-H., Youn, S.-W., Kim, J.-Y., Lee, E. J., Kim, Y.-J., Kim, K.-W., and Kim, H.-S. (2013). Snail as a potential

target molecule in cardiac fibrosis: paracrine action of endothelial cells on fibroblasts through snail and ctgf axis. *Molecular therapy : the journal of the American Society of Gene Therapy*, 21(9):1767–1777.

Lee, Y. T. (1983). Breast carcinoma: pattern of metastasis at autopsy. *Journal of surgical oncology*, 23(3):175–180.

Lehmann, U. and Kreipe, H. (2001). Real-time pcr analysis of dna and rna extracted from formalin-fixed and paraffin-embedded biopsies. *Methods*, 25(4):409–418.

Leung, D. W., Cachianes, G., Kuang, W. J., Goeddel, D. V., and Ferrara, N. (1989). Vascular endothelial growth factor is a secreted angiogenic mitogen. *Science (New York, N.Y.)*, 246(4935):1306–1309.

Li, X. and Eriksson, U. (2003). Novel pdgf family members: Pdgf-c and pdgf-d. *Cytokine & Growth Factor Reviews*, 14(2):91–98.

Lindahl, P., Johansson, B. R., Levéen, P., and Betsholtz, C. (1997). Pericyte loss and microaneurysm formation in pdgf-b-deficient mice. *Science*, 277(5323):242–245.

Linderholm, B., Bergqvist, J., Hellborg, H., Johansson, U., Linderholm, M., Schoultz, E. v., Elmberger, G., Skoog, L., and Bergh, J. (2009). Shorter survival-times following adjuvant endocrine therapy in oestrogen- and progesterone-receptor positive breast cancer overexpressing her2 and/or with an increased expression of vascular endothelial growth factor. *Medical oncology (Northwood, London, England)*, 26(4):480–490.

Liu, Y., Tamimi, R. M., Collins, L. C., Schnitt, S. J., Gilmore, H. L., Connolly, J. L., and Colditz, G. A. (2011). The association between vascular endothelial growth factor expression in invasive breast cancer and survival varies with intrinsic subtypes and use of adjuvant systemic therapy: results from the nurses' health study. *Breast cancer research and treatment*, 129(1):175–184.

Lyden, D., Hattori, K., Dias, S., Costa, C., Blaikie, P., Butros, L., Chadburn, A., Heissig, B., Marks, W., Witte, L., Wu, Y., Hicklin, D., Zhu, Z., Hackett, N. R., Crystal, R. G., Moore, M. A., Hajjar, K. A., Manova, K., Benezra, R., and Rafii, S. (2001). Impaired recruitment of bone-marrow-derived endothelial and hematopoietic

precursor cells blocks tumor angiogenesis and growth. *Nature medicine*, 7(11):1194–1201.

Lyden, D., Young, A. Z., Zagzag, D., Yan, W., Gerald, W., O'Reilly, R., Bader, B. L., Hynes, R. O., Zhuang, Y., Manova, K., and Benezra, R. (1999). Id1 and id3 are required for neurogenesis, angiogenesis and vascularization of tumour xenografts. *Nature*, 401(6754):670–677.

Lyttle, D. J., Fraser, K. M., Fleming, S. B., Mercer, A. A., and Robinson, A. J. (1994). Homologs of vascular endothelial growth factor are encoded by the poxvirus orf virus. *Journal of virology*, 68(1):84–92.

Maniotis, A. J., Folberg, R., Hess, A., Seftor, E. A., Gardner, L. M., Pe'er, J., Trent, J. M., Meltzer, P. S., and Hendrix, M. J. (1999). Vascular channel formation by human melanoma cells in vivo and in vitro: Vasculogenic mimicry. *The American Journal of Pathology*, 155(3):739–752.

Markwald, R. R., Fitzharris, T. P., and Manasek, F. J. (1977). Structural development of endocardial cushions. *The American journal of anatomy*, 148(1):85–119.

Martin, T. A., Goyal, A., Watkins, G., and Jiang, W. G. (2005). Expression of the transcription factors snail, slug, and twist and their clinical significance in human breast cancer. *Annals of surgical oncology*, 12(6):488–496.

Masuda, N., Ohnishi, T., Kawamoto, S., Monden, M., and Okubo, K. (1999). Analysis of chemical modification of rna from formalin-fixed samples and optimization of molecular biology applications for such samples. *Nucleic acids research*, 27(22):4436–4443.

Mauhin, V., Lutz, Y., Dennefeld, C., and Alberga, A. (1993). Definition of the dna-binding site repertoire for the drosophila transcription factor snail. *Nucleic acids research*, 21(17):3951–3957.

Mazzieri, R., Pucci, F., Moi, D., Zonari, E., Ranghetti, A., Berti, A., Politi, L. S., Gentner, B., Brown, J. L., Naldini, L., and De Palma, M. (2011). Targeting the ang2/tie2 axis inhibits tumor growth and metastasis by impairing angiogenesis and disabling rebounds of proangiogenic myeloid cells. *Cancer cell*, 19(4):512–526.

McClelland, M. R., Carskadon, S. L., Zhao, L., White, E. S., Beer, D. G., Orringer, M. B., Pickens, A., Chang, A. C., and Arenberg, D. A. (2007). Diversity of the angiogenic phenotype in non-small cell lung cancer. *American journal of respiratory cell and molecular biology*, 36(3):343–350.

Medici, D., Potenta, S., and Kalluri, R. (2011). Transforming growth factor-beta2 promotes snail-mediated endothelial-mesenchymal transition through convergence of smad-dependent and smad-independent signalling. *The Biochemical journal*, 437(3):515–520.

Merendino, R. A., Gangemi, S., Misefari, A., Arena, A., Capozza, A. B., Chillemi, S., and Purello D'Ambrosio, F. (1999). Interleukin-12 and interleukin-10 production by mononuclear phagocytic cells from breast cancer patients. *Immunology Letters*, 68(2-3):355–358.

Meyer, M., Clauss, M., Lepple-Wienhues, A., Waltenberger, J., Augustin, H. G., Ziche, M., Lanz, C., Büttner, M., Rziha, H. J., and Dehio, C. (1999). A novel vascular endothelial growth factor encoded by orf virus, vegf-e, mediates angiogenesis via signalling through vegfr-2 (kdr) but not vegfr-1 (flt-1) receptor tyrosine kinases. *The EMBO journal*, 18(2):363–374.

Miller, K., Wang, M., Gralow, J., Dickler, M., Cobleigh, M., Perez, E. A., Shenkier, T., Cella, D., and Davidson, N. E. (2007). Paclitaxel plus bevacizumab versus paclitaxel alone for metastatic breast cancer. *The New England journal of medicine*, 357(26):2666–2676.

Miller, K. D., Chap, L. I., Holmes, F. A., Cobleigh, M. A., Marcom, P. K., Fehrenbacher, L., Dickler, M., Overmoyer, B. A., Reimann, J. D., Sing, A. P., Langmuir, V., and Rugo, H. S. (2005). Randomized phase iii trial of capecitabine compared with bevacizumab plus capecitabine in patients with previously treated metastatic breast cancer. *Journal of clinical oncology : official journal of the American Society of Clinical Oncology*, 23(4):792–799.

Mironchik, Y., Winnard, P. T., Vesuna, F., Kato, Y., Wildes, F., Pathak, A. P., Kominsky, S., Artemov, D., Bhujwalla, Z., van Diest, P., Burger, H., Glackin, C., and Raman, V. (2005). Twist overexpression induces in vivo angiogenesis and correlates with chromosomal instability in breast cancer. *Cancer research*, 65(23):10801–10809.

Molina-Ortiz, P., Villarejo, A., MacPherson, M., Santos, V., Montes, A., Souchelnytskyi, S., Portillo, F., and Cano, A. (2012). Characterization of the snag and slug domains of snail2 in the repression of e-cadherin and emt induction: modulation by serine 4 phosphorylation. *PloS one*, 7(5):e36132.

Morikawa, S., Baluk, P., Kaidoh, T., Haskell, A., Jain, R. K., and McDonald, D. M. (2002). Abnormalities in pericytes on blood vessels and endothelial sprouts in tumors. *The American Journal of Pathology*, 160(3):985–1000.

Moschetta, M., Mishima, Y., Sahin, I., Manier, S., Glavey, S., Vacca, A., Roccaro, A. M., and Ghobrial, I. M. (2014). Role of endothelial progenitor cells in cancer progression. *Biochimica et biophysica acta*, 1846(1):26–39.

Nagy, A. (2000). Cre recombinase: the universal reagent for genome tailoring. *Genesis (New York, N.Y. : 2000)*, 26(2):99–109.

Nastala, C. L., Edington, H. D., McKinney, T. G., Tahara, H., Nalesnik, M. A., Brunda, M. J., Gately, M. K., Wolf, S. F., Schreiber, R. D., and Storkus, W. J. (1994). Recombinant il-12 administration induces tumor regression in association with ifn-gamma production. *Journal of immunology (Baltimore, Md. : 1950)*, 153(4):1697–1706.

Nielsen, J. S. and McNagny, K. M. (2008). Novel functions of the cd34 family. *Journal of cell science*, 121(Pt 22):3683–3692.

Nieto, M. A. (2002). The snail superfamily of zinc-finger transcription factors. *Nature reviews. Molecular cell biology*, 3(3):155–166.

Ohkubo, T. and Ozawa, M. (2004). The transcription factor snail downregulates the tight junction components independently of e-cadherin downregulation. *Journal of cell science*, 117(Pt 9):1675–1685.

Olofsson, B., Korpelainen, E., Pepper, M. S., Mandriota, S. J., Aase, K., Kumar, V., Gunji, Y., Jeltsch, M. M., Shibuya, M., Alitalo, K., and Eriksson, U. (1998). Vascular endothelial growth factor b (vegf-b) binds to vegf receptor-1 and regulates plasminogen activator activity in endothelial cells. *Proceedings of the National Academy of Sciences of the United States of America*, 95(20):11709–11714.

Onoue, T., Uchida, D., Begum, N., Tomizuka, Y., Yoshida, H., and Sato, M. (2006). Epithelial-mesenchymal transition induced by the stromal cell-derived factor-1/cxcr4 system in oral squamous cell carcinoma cells. *International Journal of Oncology*.

O'Reilly, M. S., Boehm, T., Shing, Y., Fukai, N., Vasios, G., Lane, W. S., Flynn, E., Birkhead, J. R., Olsen, B. R., and Folkman, J. (1997). Endostatin: an endogenous inhibitor of angiogenesis and tumor growth. *Cell*, 88(2):277–285.

O'Reilly, M. S., Holmgren, L., Shing, Y., Chen, C., Rosenthal, R. A., Moses, M., Lane, W. S., Cao, Y., Sage, E. H., and Folkman, J. (1994). Angiostatin: a novel angiogenesis inhibitor that mediates the suppression of metastases by a lewis lung carcinoma. *Cell*, 79(2):315–328.

Osborne, C. K. (1998). Tamoxifen in the treatment of breast cancer. *The New England journal of medicine*, 339(22):1609–1618.

Ozaki, H., Yu, A. Y., Della, N., Ozaki, K., Luna, J. D., Yamada, H., Hackett, S. F., Okamoto, N., Zack, D. J., Semenza, G. L., and Campochiaro, P. A. (1999). Hypoxia inducible factor-1alpha is increased in ischemic retina: temporal and spatial correlation with vegf expression. *Investigative ophthalmology & visual science*, 40(1):182–189.

Paku, S., Dezső, K., Bugyik, E., Tóvári, J., Tímár, J., Nagy, P., Laszlo, V., Klepetko, W., and Döme, B. (2011). A new mechanism for pillar formation during tumor-induced intussusceptive angiogenesis: Inverse sprouting. *The American Journal of Pathology*, 179(3):1573–1585.

Park, J. and Schwarzbauer, J. E. (2014). Mammary epithelial cell interactions with fibronectin stimulate epithelial-mesenchymal transition. *Oncogene*, 33(13):1649–1657.

Park, J. E., Chen, H. H., Winer, J., Houck, K. A., and Ferrara, N. (1994). Placenta growth factor. potentiation of vascular endothelial growth factor bioactivity, in vitro and in vivo, and high affinity binding to flt-1 but not to flk-1/kdr. *The Journal of biological chemistry*, 269(41):25646–25654.

Parker, B. S., Argani, P., Cook, B. P., Liangfeng, H., Chartrand, S. D., Zhang, M., Saha, S., Bardelli, A., Jiang, Y., St Martin, Thia B, Nacht, M., Teicher, B. A.,

Klinger, K. W., Sukumar, S., and Madden, S. L. (2004). Alterations in vascular gene expression in invasive breast carcinoma. *Cancer research*, 64(21):7857–7866.

Parwaresch, M. R., Radzun, H. J., Kreipe, H., Hansmann, M. L., and Barth, J. (1986). Monocyte/macrophage-reactive monoclonal antibody ki-m6 recognizes an intracytoplasmic antigen. *The American Journal of Pathology*, 125(1):141–151.

Patenaude, A., Parker, J., and Karsan, A. (2010). Involvement of endothelial progenitor cells in tumor vascularization. *Microvascular research*, 79(3):217–223.

Peinado, H., Olmeda, D., and Cano, A. (2007). Snail, zeb and bhlh factors in tumour progression: an alliance against the epithelial phenotype? *Nature reviews. Cancer*, 7(6):415–428.

Peinado, H., Quintanilla, M., and Cano, A. (2003). Transforming growth factor beta-1 induces snail transcription factor in epithelial cell lines: mechanisms for epithelial mesenchymal transitions. *The Journal of biological chemistry*, 278(23):21113–21123.

Penland, S. K., Keku, T. O., Torrice, C., He, X., Krishnamurthy, J., Hoadley, K. A., Woosley, J. T., Thomas, N. E., Perou, C. M., Sandler, R. S., and Sharpless, N. E. (2007). Rna expression analysis of formalin-fixed paraffin-embedded tumors. *Laboratory investigation; a journal of technical methods and pathology*, 87(4):383–391.

Pepin, F., Bertos, N., Laferrière, J., Sadekova, S., Souleimanova, M., Zhao, H., Finak, G., Meterissian, S., Hallett, M. T., and Park, M. (2012). Gene-expression profiling of microdissected breast cancer microvasculature identifies distinct tumor vascular subtypes. *Breast cancer research : BCR*, 14(4):R120.

Perou, C. M. and Børresen-Dale, A.-L. (2011). Systems biology and genomics of breast cancer. *Cold Spring Harbor perspectives in biology*, 3(2).

Perou, C. M., Sørlie, T., Eisen, M. B., van de Rijn, M, Jeffrey, S. S., Rees, C. A., Pollack, J. R., Ross, D. T., Johnsen, H., Akslen, L. A., Fluge, O., Pergamenschikov, A., Williams, C., Zhu, S. X., Lønning, P. E., Børresen-Dale, A. L., Brown, P. O., and Botstein, D. (2000). Molecular portraits of human breast tumours. *Nature*, 406(6797):747–752.

Popescu, M. R., Zugun, F. E., Cojocaru, E., Tocan, L., Folescu, R., and Zamfir, C. L. (2013). Morphometric study of aortic wall parameters evolution in newborn and child. *Romanian journal of morphology and embryology = Revue roumaine de morphologie et embryologie*, 54(2):399–404.

Potenta, S., Zeisberg, E., and Kalluri, R. (2008). The role of endothelial-to-mesenchymal transition in cancer progression. *British journal of cancer*, 99(9):1375–1379.

Rabinowitz, S. S. and Gordon, S. (1991). Macrosialin, a macrophage-restricted membrane sialoprotein differentially glycosylated in response to inflammatory stimuli. *The Journal of experimental medicine*, 174(4):827–836.

Rai, A. J., Kamath, R. M., Gerald, W., and Fleisher, M. (2009). Analytical validation of the gexp analyzer and design of a workflow for cancer-biomarker discovery using multiplexed gene-expression profiling. *Analytical and bioanalytical chemistry*, 393(5):1505–1511.

Rajantie, I., Ilmonen, M., Alminaite, A., Ozerdem, U., Alitalo, K., and Salven, P. (2004). Adult bone marrow-derived cells recruited during angiogenesis comprise precursors for periendothelial vascular mural cells. *Blood*, 104(7):2084–2086.

Raymond, W. A. and Leong, A. S. (1989). Vimentin–a new prognostic parameter in breast carcinoma? *The Journal of pathology*, 158(2):107–114.

Remmele, W. and Stegner, H. E. (1987). Vorschlag zur einheitlichen definition eines immunreaktiven score (irs) für den immunhistochemischen ostrogenrezeptor-nachweis (er-ica) im mammakarzinomgewebe. *Der Pathologe*, 8(3):138–140.

Ribatti, D. (2004). The involvement of endothelial progenitor cells in tumor angiogenesis. *Journal of Cellular and Molecular Medicine*, 8(3):294–300.

Ribatti, D., Nico, B., Crivellato, E., Roccaro, A. M., and Vacca, A. (2006). The history of the angiogenic switch concept. *Leukemia*, 21(1):44–52.

Robertson, J. F., Nicholson, R. I., Bundred, N. J., Anderson, E., Rayter, Z., Dowsett, M., Fox, J. N., Gee, J. M., Webster, A., Wakeling, A. E., Morris, C., and Dixon,

M. (2001). Comparison of the short-term biological effects of 7alpha-[9-(4,4,5,5,5-pentafluoropentylsulfinyl)-nonyl]estra-1,3,5, (10)-triene-3,17beta-diol (faslodex) versus tamoxifen in postmenopausal women with primary breast cancer. *Cancer research*, 61(18):6739–6746.

Romano, L. A. and Runyan, R. B. (1999). Slug is a mediator of epithelial-mesenchymal cell transformation in the developing chicken heart. *Developmental biology*, 212(1):243–254.

Romano, L. A. and Runyan, R. B. (2000). Slug is an essential target of tgfbeta2 signaling in the developing chicken heart. *Developmental biology*, 223(1):91–102.

Rugo, H. S. (2004). Bevacizumab in the treatment of breast cancer: rationale and current data. *The oncologist*, 9 Suppl 1:43–49.

Seaman, S., Stevens, J., Yang, M. Y., Logsdon, D., Graff-Cherry, C., and St Croix, B. (2007). Genes that distinguish physiological and pathological angiogenesis. *Cancer cell*, 11(6):539–554.

Seftor, R. E., Hess, A. R., Seftor, E. A., Kirschmann, D. A., Hardy, K. M., Margaryan, N. V., and Hendrix, M. J. (2012). Tumor cell vasculogenic mimicry. *The American Journal of Pathology*, 181(4):1115–1125.

Shweiki, D., Itin, A., Soffer, D., and Keshet, E. (1992). Vascular endothelial growth factor induced by hypoxia may mediate hypoxia-initiated angiogenesis. *Nature*, 359(6398):843–845.

Siekmann, A. F. and Lawson, N. D. (2007). Notch signalling limits angiogenic cell behaviour in developing zebrafish arteries. *Nature*, 445(7129):781–784.

Singletary, S. E., Allred, C., Ashley, P., Bassett, L. W., Berry, D., Bland, K. I., Borgen, P. I., Clark, G., Edge, S. B., Hayes, D. F., Hughes, L. L., Hutter, Robert V P, Morrow, M., Page, D. L., Recht, A., Theriault, R. L., Thor, A., Weaver, D. L., Wieand, H. S., and Greene, F. L. (2002). Revision of the american joint committee on cancer staging system for breast cancer. *Journal of clinical oncology : official journal of the American Society of Clinical Oncology*, 20(17):3628–3636.

Sirirattanakul, S., Wannakrairot, P., Tencomnao, T., and Santiyanont, R. (2015). Gene expression profile in breast cancer comprising predictive markers for metastatic risk. *Genetics and molecular research : GMR*, 14(3):10929–10936.

Slamon, D. J., Clark, G. M., Wong, S. G., Levin, W. J., Ullrich, A., and McGuire, W. L. (1987). Human breast cancer: correlation of relapse and survival with amplification of the her-2/neu oncogene. *Science (New York, N.Y.)*, 235(4785):177–182.

Sørlie, T., Perou, C. M., Tibshirani, R., Aas, T., Geisler, S., Johnsen, H., Hastie, T., Eisen, M. B., van de Rijn, M, Jeffrey, S. S., Thorsen, T., Quist, H., Matese, J. C., Brown, P. O., Botstein, D., Lønning, P. E., and Børresen-Dale, A. L. (2001). Gene expression patterns of breast carcinomas distinguish tumor subclasses with clinical implications. *Proceedings of the National Academy of Sciences of the United States of America*, 98(19):10869–10874.

St Croix, B., Rago, C., Velculescu, V., Traverso, G., Romans, K. E., Montgomery, E., Lal, A., Riggins, G. J., Lengauer, C., Vogelstein, B., and Kinzler, K. W. (2000). Genes expressed in human tumor endothelium. *Science (New York, N.Y.)*, 289(5482):1197–1202.

Tarin, D. (2006). New insights into the pathogenesis of breast cancer metastasis. *Breast disease*, 26:13–25.

Terman, B. I., Dougher-Vermazen, M., Carrion, M. E., Dimitrov, D., Armellino, D. C., Gospodarowicz, D., and Böhlen, P. (1992). Identification of the kdr tyrosine kinase as a receptor for vascular endothelial cell growth factor. *Biochemical and Biophysical Research Communications*, 187(3):1579–1586.

Thompson, E. W., Paik, S., Brünner, N., Sommers, C. L., Zugmaier, G., Clarke, R., Shima, T. B., Torri, J., Donahue, S., and Lippman, M. E. (1992). Association of increased basement membrane invasiveness with absence of estrogen receptor and expression of vimentin in human breast cancer cell lines. *Journal of cellular physiology*, 150(3):534–544.

Timmerman, L. A., Grego-Bessa, J., Raya, A., Bertrán, E., Pérez-Pomares, J. M., Díez, J., Aranda, S., Palomo, S., McCormick, F., Izpisúa-Belmonte, J. C., and de la Pompa, José Luis (2004). Notch promotes epithelial-mesenchymal transition during

cardiac development and oncogenic transformation. *Genes & Development*, 18(1):99–115.

Toi, M., Gion, M., Saji, H., Asano, M., Dittadi, R., Gilberti, S., Locopo, N., and Gasparini, G. (1999). Endogenous interleukin-12: relationship with angiogenic factors, hormone receptors and nodal status in human breast carcinoma. *International journal of oncology*, 15(6):1169–1175.

Toi, M., Kondo, S., Suzuki, H., Yamamoto, Y., Inada, K., Imazawa, T., Taniguchi, T., and Tominaga, T. (1996). Quantitative analysis of vascular endothelial growth factor in primary breast cancer. *Cancer*, 77(6):1101–1106.

Urbich, C. and Dimmeler, S. (2004). Endothelial progenitor cells: characterization and role in vascular biology. *Circulation Research*, 95(4):343–353.

Valdimarsdottir, G., Goumans, M.-J., Itoh, F., Itoh, S., Heldin, C.-H., and Dijke, P. (2006). Smad7 and protein phosphatase 1alpha are critical determinants in the duration of tgf-beta/alk1 signaling in endothelial cells. *BMC Cell Biology*, 7(1):16.

Vesuna, F., van Diest, P., Chen, J. H., and Raman, V. (2008). Twist is a transcriptional repressor of e-cadherin gene expression in breast cancer. *Biochemical and Biophysical Research Communications*, 367(2):235–241.

Voest, E. E., Kenyon, B. M., O'Reilly, M. S., Truitt, G., D'Amato, R. J., and Folkman, J. (1995). Inhibition of angiogenesis in vivo by interleukin 12. *Journal Of The National Cancer Institute*, 87(8):581–586.

Vries, C. d., Escobedo, J. A., Ueno, H., Houck, K., Ferrara, N., and Williams, L. T. (1992). The fms-like tyrosine kinase, a receptor for vascular endothelial growth factor. *Science (New York, N.Y.)*, 255(5047):989–991.

Vu, T. and Claret, F. X. (2012). Trastuzumab: updated mechanisms of action and resistance in breast cancer. *Frontiers in oncology*, 2:62.

Wakeling, A. E., Dukes, M., and Bowler, J. (1991). A potent specific pure antiestrogen with clinical potential. *Cancer research*, 51(15):3867–3873.

Weigel, M. T., Ghazoui, Z., Dunbier, A., Pancholi, S., Dowsett, M., and Martin, L.-A. (2012). Preclinical and clinical studies of estrogen deprivation support the pdgf/abl

pathway as a novel therapeutic target for overcoming endocrine resistance in breast cancer. *Breast cancer research : BCR*, 14(3):R78.

Weigelt, B., Peterse, J. L., and van 't Veer, Laura J (2005). Breast cancer metastasis: markers and models. *Nature reviews. Cancer*, 5(8):591–602.

Welch-Reardon, K. M., Ehsan, S. M., Wang, K., Wu, N., Newman, A. C., Romero-Lopez, M., Fong, A. H., George, S. C., Edwards, R. A., and Hughes, Christopher C W (2014). Angiogenic sprouting is regulated by endothelial cell expression of slug. *Journal of cell science*, 127(Pt 9):2017–2028.

Winkler, F., Kozin, S. V., Tong, R. T., Chae, S.-S., Booth, M. F., Garkavtsev, I., Xu, L., Hicklin, D. J., Fukumura, D., Di Tomaso, E., Munn, L. L., and Jain, R. K. (2004). Kinetics of vascular normalization by vegfr2 blockade governs brain tumor response to radiation: role of oxygenation, angiopoietin-1, and matrix metalloproteinases. *Cancer cell*, 6(6):553–563.

Wise, L. M., Veikkola, T., Mercer, A. A., Savory, L. J., Fleming, S. B., Caesar, C., Vitali, A., Makinen, T., Alitalo, K., and Stacker, S. A. (1999). Vascular endothelial growth factor (vegf)-like protein from orf virus nz2 binds to vegfr2 and neuropilin-1. *Proceedings of the National Academy of Sciences*, 96(6):3071–3076.

Wu, Z.-Q., Rowe, R. G., Lim, K.-C., Lin, Y., Willis, A., Tang, Y., Li, X.-Y., Nor, J. E., Maillard, I., and Weiss, S. J. (2014). A snail1/notch1 signalling axis controls embryonic vascular development. *Nature Communications*, 5.

Wykoff, C. C., Beasley, N. J., Watson, P. H., Turner, K. J., Pastorek, J., Sibtain, A., Wilson, G. D., Turley, H., Talks, K. L., Maxwell, P. H., Pugh, C. W., Ratcliffe, P. J., and Harris, A. L. (2000). Hypoxia-inducible expression of tumor-associated carbonic anhydrases. *Cancer research*, 60(24):7075–7083.

Xue, C., Plieth, D., Venkov, C., Xu, C., and Neilson, E. G. (2003). The gatekeeper effect of epithelial-mesenchymal transition regulates the frequency of breast cancer metastasis. *Cancer research*, 63(12):3386–3394.

Yang, A. D., Camp, E., Fan, F., Shen, L., Gray, M. J., Liu, W., Somcio, R., Bauer, T. W., Wu, Y., Hicklin, D. J., and Ellis, L. M. (2006). Vascular endothelial growth

factor receptor-1 activation mediates epithelial to mesenchymal transition in human pancreatic carcinoma cells. *Cancer research*, 66(1):46–51.

Yang, J., Mani, S. A., Donaher, J. L., Ramaswamy, S., Itzykson, R. A., Come, C., Savagner, P., Gitelman, I., Richardson, A., and Weinberg, R. A. (2004). Twist, a master regulator of morphogenesis, plays an essential role in tumor metastasis. *Cell*, 117(7):927–939.

Yook, J. I., Li, X.-Y., Ota, I., Fearon, E. R., and Weiss, S. J. (2005). Wnt-dependent regulation of the e-cadherin repressor snail. *The Journal of biological chemistry*, 280(12):11740–11748.

Yuan, F., Chen, Y., Dellian, M., Safabakhsh, N., Ferrara, N., and Jain, R. K. (1996). Time-dependent vascular regression and permeability changes in established human tumor xenografts induced by an anti-vascular endothelial growth factor/vascular permeability factor antibody. *Proceedings of the National Academy of Sciences of the United States of America*, 93(25):14765–14770.

Zeisberg, E. M., Potenta, S., Xie, L., Zeisberg, M., and Kalluri, R. (2007a). Discovery of endothelial to mesenchymal transition as a source for carcinoma-associated fibroblasts. *Cancer research*, 67(21):10123–10128.

Zeisberg, E. M., Tarnavski, O., Zeisberg, M., Dorfman, A. L., McMullen, J. R., Gustafsson, E., Chandraker, A., Yuan, X., Pu, W. T., Roberts, A. B., Neilson, E. G., Sayegh, M. H., Izumo, S., and Kalluri, R. (2007b). Endothelial-to-mesenchymal transition contributes to cardiac fibrosis. *Nature medicine*, 13(8):952–961.

Zeisberg, M. and Neilson, E. G. (2009). Biomarkers for epithelial-mesenchymal transitions. *The Journal of clinical investigation*, 119(6):1429–1437.

Zeisberg, M., Yang, C., Martino, M., Duncan, M. B., Rieder, F., Tanjore, H., and Kalluri, R. (2007c). Fibroblasts derive from hepatocytes in liver fibrosis via epithelial to mesenchymal transition. *The Journal of biological chemistry*, 282(32):23337–23347.

Zhou, B. P., Deng, J., Xia, W., Xu, J., Li, Y. M., Gunduz, M., and Hung, M.-C. (2004). Dual regulation of snail by gsk-3beta-mediated phosphorylation in control of epithelial-mesenchymal transition. *Nature cell biology*, 6(10):931–940.

List of Publications

Florian Röhrig, Sandra Vorlova, **Helene Hoffmann**, Martin Wartenberg, Freddy Escorcia, Sabrina Keller, Michel Tenspolde, Isabel Weigand, Sabine Gätzner, Katia Manova, Olaf Penack, David Scheinberg, Andreas Rosenwald, and Zvi Granot and Erik Henke

"VEGF-Ablation Therapy Reduces Drug Delivery and Therapeutic Response in ECM-dense tumors"

Oncogene, accepted

Danksagung

An dieser Stelle möchte ich mich besonders bei Dr. Erik Henke bedanken, der mir die Durchführung dieser Arbeit ermöglicht hat, mich in dieser Zeit vielseitig unterstützt hat und mir jederzeit mit Rat und Hilfe zur Seite stand.

Bei Prof. Dr. Manfred Gessler und Prof. Dr. Alexander Buchberger bedanke ich mich für die Bereitschaft, die Betreuung für diese Doktorarbeit zu übernehmen.

Prof. Dr. Thomas Hünig möchte ich für die Übernahme des Prüfungsvorsitz danken.

Prof. Dr. Ulrich Walter sowie Prof. Dr. Elke Butt danke ich für die Bereitstellung der Mittel zur Dürchführung dieser Arbeit. Die Arbeitsatmosphäre im Institut für Klinische Biochemie und Pathobiochemie war einmalig und immer angenehm.

Prof. Dr. Süleyman Ergün sowie den Mitarbeitern des Instituts für Anatomie und Zellbiologie möchte ich für die freundliche Aufnahme unserer Arbeitsguppe danken.

Mein Besonderer Dank gilt Prof. Dr. Andreas Rosenwald für die Bereitstellung der Mammakarzinome. Dr. Martin Wartenberg danke ich für die Hilfe bei der Auswahl der Mammakarzinome sowie deren Färbung und seine Unterstützung bei der Etablierung der RNA Isolation.

Des Weiteren möchte ich mich bei Dr. Daniel Murphy und seiner Arbeitsgruppe für die Einarbeitung in das Leica LMD6500 und die erhaltene Hilfestellung bedanken.

Prof. Dr. Leane Lehmann danke ich für den Zugang zum Leica LMD6500. Ihrer Arbeitsgruppe, insbesondere Dr. Katja Schmalbach, danke ich für die freundliche Aufnahme und die praktische Unterstützung.

Ein großer Dank geht an die AG Herterich für die Bereitstellung des Sequencers und die Einweisung in Methodik des GeXP. Zudem fand ich hier immer Rat und Unterstützung

bei sämtlichen Fragen zum Thema PCR, Western Blot sowie Pufferherstellung. Besonders möchte ich hier Sabine Gätzner für ihre tatkräftige Hilfe und ihre moralische Unterstützung danken.

Für die Einführung in die Immunhistochemie und die vielen hilfreichen Tipps bedanke ich mich herzlich bei Frau Erna Kleinschroth.

Ich danke all den Doktoranden und Diplomanden, die ich während meiner Zeit in Auvera kennengelernt habe. Besonders Florian Röhrig, der mit mir die Höhen und Tiefen der Doktorarbeit durchgestanden hat und immer ein offenes Ohr für mich hatte. Desweiteren danke ich meiner Master Studentin Franziska Karl die mich sehr bei der Durchführung der Tierexperimente unterstützt hat und mit der ich sehr viel Spaß im Laboralltag hatte. Gleiches gilt für Carolin Kastner, der ich unter anderem für die aufbauenden Gespräche danke. Für die angenehme Atmosphäre im Doktorandenzimmer danke ich zudem Katharina Hubertus, Sabrina Mihlan, Amelie Hailer sowie Semjon Willier und Anjana Vaman.

Ein besonderer Dank geht an meinen Freund Mathias, der mich während der Promotion in jeder erdenklichen Hinsicht unterstützt hat. Er hat mich in schwierigen Phasen aufgebaut und jederzeit zu mir gehalten. Meinen Eltern danke ich für Ihre vielfältige Unterstützung während meines Studiums und der Promotion.

Diese Arbeit wurde durch die Deutsche Forschungsgemeinschaft und das Interdisziplinäre Zentrum für Klinische Forschung der Universität Würzburg finanziell unterstützt.

Affidavit

I hereby confirm that my thesis entitled Identifying Regulators of Tumor Vascular Morphology is the result of my own work. I did not receive any help or support from commercial consultants. All sources and / or materials applied are listed and specified in the thesis.
Furthermore, I confirm that this thesis has not yet been submitted as part of another examination process neither in identical nor in similar form.

....
(Place, Date) (Signature)

Eidesstattliche Erklärung

Hiermit erkläre ich an Eides statt, die Dissertation Identifying Regulators of Tumor Vascular Morphology eigenständig, d.h. insbesondere selbständig und ohne Hilfe eines kommerziellen Promotionsberaters, angefertigt und keine anderen als die von mir angegebenen Quellen und Hilfsmittel verwendet zu haben.
Ich erkläre außerdem, dass die Dissertation weder in gleicher noch in ähnlicher Form bereits in einem anderen Prüfungsverfahren vorgelegen hat.

....
(Ort, Datum) (Unterschrift)